DISCLAIMER:

This document does not meet the
current format guidelines of
the Graduate School at
The University of Texas at Austin.

It has been published for
informational use only.

The Dissertation Committee for Binyan Yan Certifies that this is the approved version of the following dissertation:

Understanding Responses of Amazon Forests to Seasonal and Inter-annual Water Stress Based on Modeling Studies and Satellite Observations

Committee:

Robert E. Dickinson, Supervisor

Rong Fu

Luc Lavier

Zong-Liang Yang

Kenneth Young

Michael Young

Understanding Responses of Amazon Forests to Seasonal and Inter-annual Water Stress Based on Modeling Studies and Satellite Observations

by

Binyan Yan, B.S.; M.S.

Dissertation

Presented to the Faculty of the Graduate School of

The University of Texas at Austin

in Partial Fulfillment

of the Requirements

for the Degree of

Doctor of Philosophy

The University of Texas at Austin

December 2016

Acknowledgements

Upon the completion of my PhD studies, I want to give my appreciations to all the people who have helped, supported, and encouraged me.

First and foremost, I would like to express my sincere appreciation to my advisor, Dr. Robert Dickinson, for his guidance, motivation, and inspiration throughout the course of my research and studies. I could not have completed this study without his support. Besides Dr. Robert Dickinson, I would also like to thank the rest of my committee members, Dr. Rong Fu, Dr. Luc Lavier, Dr. Zong-Liang Yang, Dr. Kenneth Young, and Dr. Michael Young for their insightful suggestions and comments that really help to refine this thesis. Additional gratitude is given to Dr. Jiafu Mao and Dr. Lianhong Gu at Oak Ridge National Laboratory for their guidance, inspiration, and encouragement and also for hosting my visits to ORNL. In addition, I would like to thank Dr. Muhammad Shaikh for his tremendous help in setting up model environments and resolving technical issues.

I would like to thank all my previous and current group members for all the discussions we have and ideas they share with me. I also appreciate the substantial help from the coauthors and reviewers for my papers and manuscripts.

My special thanks to my parents for supporting me throughout writing this thesis and my life in general. It would be impossible for me to reach this point without their help.

Understanding Responses of Amazon Forests to Seasonal and Inter-annual Water Stress Based on Modeling Studies and Satellite Observations

Binyan Yan, Ph.D.

The University of Texas at Austin, 2016

Supervisor: Robert E. Dickinson

As the largest tropical forest in the world, the Amazon rainforest plays key roles in regulating regional and global carbon and hydrological cycles. Water availability is a major controlling factor in this ecosystem, in terms of shaping the species composition and distribution as well as controlling the seasonal dynamics. Given the large uncertainty in precipitation projections and the consequent debates as to the fate of the forest, there is a pressing need to examine the response of the forest to water availability.

Here, I first consider the role of two mechanisms that buffer plants from impact of water stress, hydraulic redistribution by plant roots and an internal water pool inside tree trunks, both of which are omitted in the National Center for Atmospheric Research (NCAR) Community Land Model (CLM). The former efficiently redistributes soil water to facilitate easier access by plants, and the latter provides a closer-to-leaf water pool that is more readily accessible than the soil water pool. CLM simulations show that the inclusion of both mechanisms helps fix its overestimation of dry-season water stress.

Based on satellite/ground observations and reanalysis data, we also analyze how plant growth responds to El Niño events that result in below-normal precipitation over large areas across the Amazon basin. We find that the influence of El Niño events on

vegetation differs between wet and dry seasons, with the former mainly controlled by radiation and the latter by water availability.

Table of Contents

List of Tables

List of Figures

CHAPTER 1: Introduction

1.1. THE IMPORTANCE OF AMAZON RAINFORESTS

As the largest tropical forest in the world, the Amazon rainforest plays key roles in the Earth climate system through the exchange of energy, momentum, and mass between the atmosphere and land surfaces. For example, the forest functions to regulate local precipitation: 25% - 50% of the precipitation that falls on the Amazon region is produced by the local evapotranspiration (e.g. Salati et al., 1979; Marengo et al., 2006).

The Amazon rainforest accounts for over half of world's rainforests (WWF, 2016). It stores about 86 Pg C (with ±20% uncertainty, Saatchi et al., 2007), corresponding to a third of total carbon storage inside tropical forests (272 ± 23 Pg C, Pan et al., 2011), which would contribute to global warming if released to the atmosphere. The Amazon rainforest is one of the most productive ecosystems in the world (Grace et al., 2001) accounting for about 30% of global productivity (Roy et al., 2001).

The Amazon rainforest has long been recognized as a repository for preserving species diversity with up to 25% of global biodiversity (Groombridge and Jenkins, 2003). For example, lowland Amazonia harbors 3.9×10^{11} trees belonging to 16,000 species (ter Steege et al., 2013). It also provides many other ecosystem services that range from improving air quality to sustaining local cultures.

1.2. MOISTURE AS A CONTROLLING FACTOR

Moisture, i.e., water availability, is a major controlling factor in this ecosystem in terms of shaping the species composition and distribution as well as controlling the seasonal dynamics.

The mean climate over the Amazon basin is characterized by decreasing precipitation from northwest to southeast (e.g. Davidson et al., 2012). Along this precipitation gradient, the annual dry season (i.e., the period with mean daily precipitation not exceeding 2 mm) increases from 0 month to 6 months.

Precipitation patterns are responsible for shaping the species distributions of tropical trees. For example, precipitation among all environmental factors was found to be a dominant driver for influencing species assemblies in the Panamanian forest (Pyke et al., 2001). The climatic gradient is largely coincident with land use changes, with more conversion to agriculture on the southern and eastern edges where the lowest precipitation and longest dry season occurs (Davidson et al., 2012).

The dry season length has been found to impose even stronger impacts on the spatial variations of forest structure and properties. For example, Saatchi et al. (2007) showed a significant negative correlation between the aboveground live biomass and the length of the dry season across the Amazon basin. The wet western Amazonia has a biomass ranging from 150 to 300 Mg/ha, while the drier southern edge with seasonal and transitional forests has a biomass from 100 to 200 Mg/ha. A large scale study based on remote sensing techniques and observational networks (Saatchi et al., 2009) revealed that many forest parameters, including basal area, fraction of large trees, aboveground biomass, and wood productivity are significantly and negatively correlated with dry season length. From a field experiment, Engelbrecht et al. (2007) further established that drought tolerance shapes the species distribution of tropical trees.

Guan et al. (2015) found that water availability imposes a first-order control on the seasonality of canopy photosynthesis and greenness in tropical forests globally. In tropical forests where annual accumulated precipitation exceeds a threshold of about

2000 mm, intensified photosynthesis and increased canopy greenness are observed in the dry season, and the opposite is seen elsewhere. This threshold apparently determines whether the supply of water, both from rainfall and from seasonally redistributed underground water, is sufficient to satisfy vegetation demands.

1.3. CLIMATE CHANGE IN TERMS OF PRECIPITATION

The climate over the Amazon region has already changed over the last century, but not as clearly for precipitation as for temperature (e.g. Victoria et al., 1998).

Multi-decadal precipitation variations from 1929 to 1998 have changed in opposite directions in the northern and southern portions of the Amazon basin, with the northern part associated with negative trends and its southern counterpart positive (Marengo, 2004). Overall, a negative precipitation trend is found for the basin as a whole. The wetter tendency over the southern portion is confirmed by another observation that show increased annual precipitation over several stations in southern Brazil Amazonia from 1960 to 2000 (Haylock et al., 2006). A weakening of water transport both into and out of the basin has been observed during the 20 year period from 1976 to 1996 (Costa et al., 1999).

In contrast to the results of the above-mentioned research, the hydrological cycle has intensified during the last few decades over almost the whole Amazon except for the southeast portion (Gloor et al., 2013). The “intensified hydrological cycle” refers to the phenomena that wet-season precipitation has increased and dry-season precipitation has decreased since 1980, leading to an increased frequency of severe drought and flooding. Over the southern Amazon (5ºS - 15ºS, 75ºW - 45ºW), the observed Standard Precipitation Index shows a decreasing trend of 0.32/decade during 1970-1999 (Li et al.,

2008). Over the same region, the dry season length has been detected to have increased over recent decades (Fu et al., 2013).

The direction and magnitude of climate change over Amazonia by the end of this century is still debated. GCMs project a decrease in precipitation in the Amazon during dry months by 2050 (Mitchell et al., 1995). Models included in the International Panel on Climate Change (IPCC) fourth Assessment Report (2007) project a precipitation change in the 2080s ranging from -40% to 10% during dry seasons and -10% to 10% during wet seasons. A 21-model average shows a strong reduction in dry season precipitation over central and eastern Amazonia by the end of this century.

Drought frequencies are also projected to increase in the future. For example, by weighting the 24 GCMs that participated in the Coupled Model Intercomparison Archive Project 3 (CMIP3) according to their abilities to reproduce inter-annual variability in seasonal rainfall, Jupp et al. (2010) found that the risk of drought over most of the Amazon basin (except its northwestern part) increases by the end of this century. Droughts like the one in 2005 are suggested to become increasingly common in the 21st Century (Cox et al., 2008).

A recent evaluation of CMIP5 simulations reveals that both drought and wetness, i.e., extreme events in terms of moisture, will be more likely to happen in the future if the emissions of greenhouse gases continue (Duffy et al., 2014).

Despite the variations of precipitation change signals and the large spread in projections of future precipitation pattern, the observations and numerical simulations both point to an increased drought risk in the next few decades and in the coming century.

1.4. RESPONSE OF THE AMAZON RAINFOREST

Given the close relation between Amazon ecosystem and moisture, climate change potentially threatens the Amazon forests whose decline in turn can alter global climate. Actually, droughts or water stress have already caused declines in tropical forests. Wide-spread tree mortalities as a result of drought and heat have already been observed over the globe (Allen et al., 2010). Tree mortality was observed to reach up to 26% after the very strong 1997/1998 El Niño event in a lowland rainforest in East Kalimantan, Indonesia (van Nieuwstadt and Sheil, 2005). The severe 2005 drought caused a loss of 1.2 - 1.6 Pg biomass carbon across the Amazon basin (Phillips et al., 2009). In the face of climate change, the Amazon rainforest is now undergoing a transition (Davidson et al., 2012).

Simulations from climate models have suggested a potential decline or even a significant shift of the Amazon ecosystem. The study of Cox et al. (2000) predicts a large-scale "dieback" of the Amazon rainforest in the 21st century resulting from the projected drying trend. The dieback scenario is also supported by several other large-scale modeling studies (e.g. White et al., 1999; Jones et al., 2003; Cox et al., 2004). GCM simulations projected a replacement of the evergreen forests by mixed forest, savanna, and grassland in the eastern Amazonia (Cramer et al., 2001; Cramer et al. 2004). However, a probabilistic assessment based on simulations from 24 GCMs suggests it is likely that the Amazon forest will shift to an increased biomass (Rammig et al., 2010).

The large spread in the projections of the future Amazon seen in numerical models, ranging from dieback to even increasing biomass, is a result of many causes. One explanation is their deficiencies in simulating the drought response of tropical forests.

1.5. THE NEEDS OF REVISITING

Given the large uncertainty in precipitation projections and the consequent debates as to the fate of the forests, there is a pressing need to examine the response of the forest to water availability. A recent model comparison reveals large discrepancies in modeling vegetation dynamics and carbon cycles in response to drought (Powell et al., 2013), especially over tropical forests (Sitch et al., 2008).

Climate models are deficient in capturing the correct response of tropical forests to water stress or drought. One widely known bias is their underestimated dry-season evapotranspiration rates. The higher evapotranspiration rates measured at the flux towers (e.g. da Rocha et al., 2009) and increased greenness of satellite images (Huete et al., 2006) during the dry seasons indicate no water limitations in contrast to the conclusions from modeling studies (Zheng and Wang, 2007; Baker et al., 2008). The failure of models to capture the vegetation response to droughts is attributed to their lack of key and necessary hydraulic components and processes, including, for example, root functioning (e.g. Baker et al., 2008), soil-plant-atmosphere continuum (Xu et al., 2013), xylem embolism and refilling (McDowell et al., 2013), and trunk water pool (Goldstein et al., 1998).

1.6. SCIENTIFIC QUESTIONS

The scientific questions addressed in this dissertation are:

(1) Can the inclusion of hydraulic redistribution by roots into CLM4.0 improve the simulation of its vegetation response to different types of droughts, including seasonal dry spells and droughts of long duration?

(2) Can the inclusion of trunk water pool into the soil-plant-atmosphere continuum within CLM4.0 improve the simulation of energy and water fluxes on both seasonal and diurnal time scales?

(3) How do El Niño events modulate the influences of precipitation on vegetation growth? How does the impact of El Niño events vary seasonally?

To answer the above scientific questions, we first consider two mechanisms that buffer plants from impact of water stress, hydraulic redistribution by plant roots (Chapter 2, Yan and Dickinson, 2014) and an internal water pool inside tree trunks (Chapter 3) into CLM 4.0. The former efficiently redistributes soil water to facilitate easier access by plants, and the latter provides a closer-to-leaf water pool which is more readily accessible than the soil water pool. Based on satellite/ground observations and reanalysis data, we then analyze in Chapter 4 how plant growth responds to El Niño events that result in below-normal precipitation over large areas across the Amazon basin. Finally, we summarize the main findings and discuss possible future work in Chapter 5.

CHAPTER 2: Modeling hydraulic redistribution and ecosystem response to droughts over the Amazon basin using Community Land Model 4.0 (CLM4.0)[1]

2.1. ABSTRACT

Hydraulic redistribution is the process of soil water transport through the low-resistance pathway provided by plant roots. It has been observed in field studies and proposed to be one of the processes that enable the Amazon rainforest to resist periodical dry spells without experiencing water limitations. How and to what extent hydraulic redistribution may increase vegetation resistance to different types of droughts, including seasonal dry spells and prolonged droughts, is the focus of this study. The artificially prolonged drought produced by a rainfall exclusion experiment is used as an example of long drought. The parameterization of hydraulic redistribution proposed by Ryel et al. (2002) was incorporated into the Community Land Model version 4 (CLM4). Two paired numerical experiments were conducted, one set using the default model (CTL) and the other using the model with hydraulic redistribution (HR) incorporated. Results show that the vegetation response (in terms of surface energy flux and biomass) to dryness is better captured with hydraulic redistribution considered. Plants are more resistant to dryness when hydraulic redistribution increases plant water availability and thus facilitate their growth as is the case in seasonal dry spells. When a drought is long lasting, the vegetation response to water stress is delayed by hydraulic redistribution. It can be further concluded that, if a drought ends before permanent damage is done, the magnitude of vegetation response will be lowered by this mechanism, i.e., the vegetation will be more resistant to dryness.

[1] I was the primary author of this published material.

2.2. INTRODUCTION

An increase in the dry season length over the Amazon basin has been detected over the recent few decades (Fu et al., 2013) and a future drying trend has been projected by many climate models (IPCC, 2007). This increased dryness would inevitably modify vegetation distributions because species distributions are shaped by drought sensitivities over Amazonia (Engelbrecht et al., 2007). Therefore, a better understanding and consequently representation of the forest response to droughts in ecosystem models and land surface models will lead to improved predictions of vegetation dynamics over the basin and their associated energy, water, and carbon cycles over the whole globe.

The Amazon rainforests have been observed to resist seasonal droughts that last for less than one month in the northwest to up to six months in the southeast. Evidence includes high evapotranspiration (ET) rates measured at flux towers (e.g. da Rocha et al., 2009) and increased canopy greenness from satellite observations (e.g. Huete et al., 2006).

However, the forest response to droughts varies with drought time scales (Vicente-Serrano et al., 2013) and drought intensities. For example, during the severe 2005 drought induced by a warm anomaly in Tropical Atlantic Ocean Sea Surface Temperature (Sena et al., 2012), ecosystem structures and functions were substantially modified by live biomass loss (Phillips et al., 2009), increased wild fires (Arogão et al., 2008), structural changes in forest canopies (Saatchi et al., 2012), and reduction in vegetation water content (Saatchi et al., 2012). The more severe 2010 drought (Lewis et al., 2011) also caused a widespread decline in canopy greenness (Xu et al., 2011). Multi-year rainfall exclusion experiments in eastern Amazonia (Engelbrecht and Kursar, 2003; Romero-Saltos et al., 2005; Brando et al., 2008; da Costa et al., 2010) showed forest

resistance to dryness (during about year 1-3) prior to an increase of tree mortality during their manipulated prolonged dry season.

"Soil banking" is essential for forests to maintain their functioning during droughts in Amazonia especially over regions where the water table is deep. If their soil storage cannot be replenished during the following wet season, forests will experience water stress. As the pathway of water and nutrients from soil to plants, fine roots function in several ways that enable plants to better exploit this soil reservoir during periodic dry spells. For example, plants develop deep root systems to maintain water uptake from deeper and wetter soil layers when the shallower layers have been progressively depleted as drought progresses. Observations show that roots extend to as deep as 18 meters in an Amazonian forest (Canadell et al., 1996). Deep roots are also found in eastern Amazonia (Nepstad et al., 1994; da Rocha et al., 2004) and Tropical Africa (Akkermans et al., 2012).

In addition, plant roots have been found to preferably absorb water from where water is more available. During dry seasons, a small amount of roots in the deep soil helps plants obtain enough water for transpiration, implying that the presence rather than the amount of roots is responsible for water uptake (Green and Clothier, 1995; Green et al., 1997; Huang et al., 1997). Those deep roots are also found to have larger radii and thus higher conductivities (Jackson et al., 2000; McElrone et al., 2004).

Plants also dynamically grow roots to optimize the whole plant benefit, e.g., Net Primary Production (NPP) (Kleidon and Heimann, 1998; Kleidon, 2004) or transpiration for arid ecosystems (van Wijk, 2011). The fact that most of the root biomass is near the surface (Jackson et al., 1996, 1997) is a response to abundant nutrients in the upper soil. When water and nutrients are adequate, more carbon is invested in the aboveground

parts, which is common for human-managed crops. Song (2010) related root growth to soil water abundance. Following her work, Hatzis (2010) also considered nitrogen limitations and described root growth as a compromise between water and nitrogen availability.

In addition to the above mentioned mechanisms, roots also serve as a low-resistance pathway between soil layers at different depths by redistributing water along a water potential gradient, namely "hydraulic redistribution", or "hydraulic lift" when only the upward transport is considered. Sap flow measurements confirm the existence of hydraulic redistribution in many species (e.g. Richard and Caldwell, 1987; Caldwell and Richards, 1989; Lee et al., 2005; Oliveira et al., 2005; Prieto et al., 2010). Roots transfer water from deep to shallow layers during the night to compensate daytime water loss through ET. Roots can also transfer water downward after rainfall (Oliveira et al., 2005) to avoid loss from soil evaporation and access by other species. They also laterally redistribute water to improve plant water status (Brooks et al., 2002). Even dormant plants are able to transport water by hydraulic redistribution (Hultine et al., 2004). Typically, hydraulic redistribution increases dry season ET by 20%-50% (Caldwell and Richards, 1987; Dawson, 1993; Ryel et al., 2002, Lee et al., 2005). In this research, we focus on one of these root functioning mechanisms, the hydraulic redistribution, and study its role for the Amazon forest in maintaining ET during periods of water deficit.

Hydraulic redistribution is not routinely included in climate models, leading to model bias in simulating hydrological cycles and the associated energy balances. For example, one widely-known dry bias of land surface models, the underestimation of dry-season ET over the Amazon rainforest, has been attributed to the lack of root functioning

such as hydraulic redistribution (Zheng and Wang, 2007; Baker et al., 2008; Harper et al., 2010).

Incorporation of hydraulic redistribution in these models has provided the observed vegetation resistance to seasonal drought. For example, Lee et al. (2005) incorporated the hydraulic redistribution parameterization proposed by Ryel et al. (2002) into the National Center for Atmospheric Research (NCAR) Community Atmospheric Model version 3 (CAM3) and obtained increased transpiration and photosynthesis over the globe. Zheng and Wang (2007) also incorporated the same hydraulic redistribution parameterization (Ryel et al., 2002) into the NCAR Community Land Model version 3 (CLM3) and the Integrated Biosphere Simulator (IBIS2). A comparison of the simulation and observations at the ABRACOS Reserva Jaru site in Amazonia showed that the simulation of dry-season latent heat flux is improved for both models by incorporating hydraulic redistribution. Baker et al. (2008) also incorporated hydraulic redistribution with a combination of other factors including deep soil column and roots into the Simple Biosphere model (SiB3) and tested the model at the Tapajos KM83 site in Amazonia. Results showed that the simulation of seasonal cycles in both water and carbon fluxes were improved. Wang et al. (2011) have demonstrated the effect of hydraulic redistribution on Amazon vegetation distribution.

As a summary, previous modeling works have mainly focused on the vegetation response to dryness on seasonal time scales. The incorporation of hydraulic redistribution has been shown to solve the underestimation problem by providing more water to plants. However, is has not provided much understanding as to how and to what extent hydraulic redistribution can increase vegetation resistance to other drought types, especially longer

droughts, and so projections of the future vegetation distribution over Amazonia have remained uncertain (Huntingford et al., 2008).

The aim of this research is to answer the scientific question implied above: how and to what extent can hydraulic redistribution increase vegetation resistance to seasonal dry spells and longer droughts? We use a rainfall exclusion experiment as an example of a longer drought. Section 2.3 describes the model, experimental design, and data used. Results are given in Section 2.4, followed by conclusions and discussions in Section 2.5.

2.3. METHOD

2.3.1. Model and parameterizations

The Community Land Model version 4 (CLM4) (Oleson et al., 2010) is the land surface component of Community Earth System Model (CESM) version 1.0. It provides the option to run with prescribed satellite phenology (CLMSP) or with interactive carbon nitrogen cycles (CN) (Thornton et al., 2007). Land cover is fixed in CN. In CLM4, the smallest unit for energy and hydrology calculations is the PFT (plant functional type). Every grid, except for lake and river grids, consists of up to 16 PFTs. Evapotranspiration is calculated at PFT levels and then aggregated to the grid level according to the specific fractional area of each PFT. Vegetation ecological and physical parameters are PFT specific. CLM4 calculates soil hydrology using the Richards equation. It contains 10 hydrologically active soil layers up to 3.4 m deep (layer thicknesses are 1.75 cm, 2.76 cm, 4.51 cm, 7.5 cm, 12.4 cm, 20.4 cm, 33.6 cm, 55.4 cm, 91.3 cm, and 114 cm from top to bottom). Infiltration and subsurface drainage serve as the upper and lower boundary conditions. Only the first layer is responsible for soil evaporation. Transpiration is regulated by stomata, which are the pathway for water to diffuse from inside the leaf to

the outside leaf boundary layer. Plants physiologically adjust the opening and closing of stomata to regulate their use of natural resources including water. At a certain soil depth, water availability, with a scale factor from 0 to 1 that describes to what extent soil water is available for plant transpiration, is derived considering limiting values: soil saturation level, soil moisture amount when stomata start to close and the wilting point. This water uptake by plant roots for transpiration is treated as a sink term in the Richards Equation.

The parameterization of hydraulic redistribution proposed by Ryel et al. (2002) is incorporated in the model. According to Ryel et al. (2002), the net water movement into layer *i* from other layers (*j*) is expressed as:

$$H_i = C_{RT} \sum_j (\Psi_j - \Psi_i) max(c_i, c_j) \frac{R_i R_j}{1 - R_x} D_{tran},$$

here C_{RT} is the maximum radial soil-root conductance of the entire active root system for water (cm·MPa^{-1}h^{-1}), c_i is a factor as a function of Ψ_i, R_i is the active root fraction in layer i, R_x can be R_i or R_j depending the relative abundance of soil moisture of the two layers, and D_{tran} is set to be 1 during the nighttime and 0 during the daytime since this parameterization assumes that hydraulic redistribution only takes place when plants are not transpiring. Though this on/off switch prohibits hydraulic redistribution when daytime transpiration is small, we keep it for simplicity. The values of these parameters used are given in Ryel et al. (2002) and Zheng and Wang (2007). We assume that the transfer of water from or to the top layer is zero since shallow roots easily die in very dry soils. According to this parameterization, water transfer between two layers is driven by soil water potential gradient and is proportional to root fractions of the two layers. Hydraulic redistribution is an efficient form of water diffusion since non-adjacent layers are also able to exchange water. The implementation scheme in CLM4 follows that of

Zheng and Wang (2007) and we also keep the assumption that all PFTs are able to conduct hydraulic redistribution.

2.3.2. Experiment design and data

Two paired experiments were conducted in order to study the effect of root functioning on vegetation response to seasonal droughts (Section 2.4.1) and artificially prolonged droughts (Section 2.4.2). For each experiment, two offline simulations, both with nitrogen and carbon cycling, are conducted, namely simulations using the default model (control run, CTL) and the model with hydraulic redistribution (hydraulic redistribution run, HR). Initial conditions are 800-year spun-up results for site-level simulations. These two simulations of each experiment share the same initial conditions in order to eliminate changes other than those from root functioning.

The Large Scale Biosphere-Atmosphere (LBA) Experiment in Amazonia (Avissar et al., 2002) monitored water, energy, and carbon exchange between ecosystems and the atmosphere. Its sites span across different climates, soil properties, and PFTs. All nine such sites (Table 2.1, Figure 2.1) available in Amazonia are used in this study, namely FNS, RJA, K34, K67, K77, K83, CAX, PDG, and BAN. The dry season length increases from northwestern to southeastern Amazonia, along with a transition from evergreen broadleaf forests to deciduous broadleaf forests and C4 grasses. Surface micrometeorological variables, including rainfall, 2 m air temperature, specific humidity, air pressure, wind speed, and incident solar and longwave radiation are measured at an interval of 30 minutes (Saleska et al., 2009). Although the K83 site is a partially-logged evergreen forest, its moisture and energy fluxes as well as NPP had a negligible change from pre-log periods (Miller et al., 2011). The soil moisture profile at the K83 site (Goulden et al., 2010) confirms the existence of hydraulic redistribution (not shown).

During the LBA Experiment, a rainfall exclusion experiment was conducted from 1999 to 2004 4.5 km south of the K67 site to study the forest response to long droughts. About 60% of the throughfall was removed in the treatment plot from 2000 to 2004 during wet seasons. More details on the experiment are given in Nepstad et al. (2002). Soil moisture (Davidson et al., 2012) and LAI (Nepstad and Mountinho, 2008) were reported for both the control and treatment plots. Through the experiment, substantial impact of drought was found to start after two years of rainfall exclusion. The second pair of numerical experiments was conducted at this site from Jan. 1, 1999 to Dec. 12, 2004. For the treatment plot, in order to mimic the experiment, 40% of the throughfall is retained in the model and the remaining 60% is added to surface runoff during wet seasons from January to July during 2000-2004. In accordance with the simulation period, we combined meteorological data measured at the K67 site (from 2002 to 2004) with that extracted from the Qian reanalysis data (Qian et al., 2006) (from 1999 to 2001) to force the offline simulations. The extracted data (from 1999 to 2004) was first rescaled according to the three years overlapping with the measurements (from 2002 to 2004) and then the first three years (from 1999 to 2001) were combined with the measurements to cover the whole six-year length.

2.4. RESULTS

2.4.1. Response to seasonal droughts

Figures 2.2 and 2.3 compare the simulated (CTL and HR) and measured monthly mean latent and sensible heat fluxes at each site respectively. The default model generally produces reasonable flux patterns compared with measurements except for the K77 site, at which site the seasonality of the CTL simulation deviates substantially from

measurements. A comparison of the prescribed LAI annual cycle at this site with that of the other two savanna sites, FNS and PDG, indicates that its smaller seasonal variation of LAI may explain its lack of seasonality in simulated energy fluxes (not shown).

Figures 2.2 and 2.3 also show that during some dry seasons when precipitation is relatively low (i.e., the dry seasons of 2001 and 2002 at the K83 site, 2001 at the FNS site, and 2005 at the BAN site), the resistance of vegetation to seasonal drought indicated from measurements cannot be captured by the default model without hydraulic redistribution. Hydraulic redistribution decreases dry season Bowen ratio at six sites, K83, CAX, RJA, FNS, BAN, and PDG, with the effect more pronounced at the K83, CAX, and BAN sites, which are selected for further analysis. A comparison with precipitation climatology (Figure 2.1) shows that the three sites chosen are associated with a negative precipitation anomaly during most of the months when measurements are available.

At the K83 site, latent heat flux from HR is lower than that from CTL and measured values in 2003, due to an over-use of deep water earlier in 2002. Even though precipitation in 2003 was abundant relative to previous years, it had not yet recharged the soil storage. The precipitation forcing data may be underestimated since it is 15% lower than the Global Precipitation Climatology Product (GPCP) during 2001-2003 (Adler et al., 2003). A comparison of precipitation between the three adjacent sites, K83, K67, and K77, also reveals that the wet-season rainfall is relatively low at the K83 site (Figure 2.1). To understand the underestimation of latent heat flux in 2003 from HR, two more simulations are conducted at the K83 site and they are forced by a 15% higher wet-season (January to July) precipitation. Results show that the large reduction of latent heat flux in 2003 for the HR simulation is removed if the wet-season rainfall is increased by 15%

(Figure 2.4). Thus the case with a 15% increase in wet-season rainfall over that observed is used for the following analysis.

The unrealistically low latent heat flux during dry seasons produced by the default model is due to its underestimation of plant water availability provided by the soil column, as shown by the "beta factor" in the model. This term is a scale factor ranging from 0 to 1 with larger values indicating higher water availability. Stomatal conductance is linearly related to this factor in the model. Thus an underestimation of the "beta factor" directly reduces the plant transpiration rate, i.e., a major component of evapotranspiration over the Amazon basin.

During dry seasons, roots redistribute water from deeper soil layers to shallower layers (typically above 60 cm) during nights by hydraulic redistribution as shown in Figures 2.5 and 2.6. At the K83 site, the amount of water redistributed upward by HR is up to 1.79 mm per night in dry seasons (August to October) with the average of 1.51 mm per night. Compared with the steady rate of upward redistribution at the K83 site, the BAN site shows a gradually increasing rate as the dry season (June to September) progresses with the average rate of 0.81 mm/day and the maximum of 1.25 mm/day. The different magnitude and pattern at the two sites is primarily owing to the different rate of ET as shown in Figure 2.2. The higher ET rate at the K83 site leads to a steeper soil moisture profile that favors the water potential-driven redistribution. The simulation results are within the range (0.1-3.2 mm/day for upward and/or downward redistribution) from other modeling studies, but are larger than that estimated (0.04-1.3 mm/day) from empirical data across ecosystems summarized by Neumann and Gardon (2012). This upward transport of water compensates for daytime evaporative loss and thus increases plant water availability for the following day, contributing 45.0% of daily transpiration at

the K83 site on average during the dry season, with the maximum contribution up to 61.2%, within the wide range of previous research (Neumann and Gardon, 2012).

Note that hydraulic redistribution is bi-directional. Roots also transport water downward following rainy events during wet seasons (Figure 2.5) and save that water from direct soil evaporation. At the K83 site, hydraulic redistribution transfers 0.05 mm water downward every day on average during the wet seasons (January to June). The downward transfer can be large occasionally following strong precipitation events, reaching 1.25 mm/day. Figure 2.7 demonstrates that more water would be lost from ground evaporation if only upward water transport were to occur by hydraulic redistribution, i.e., "hydraulic lifting". At the BAN site, the downward flux is very small during wet seasons (December to April), approximately zero.

2.4.2. Response to the artificially prolonged drought

Since the rainfall exclusion treatment directly reduces soil moisture, it is used here as an indicator of the timing of drought response. A comparison of soil moisture between the control and treatment plots reveals that an obvious response to the drought started in 2001 and that CTL and HR in the treatment plot started to differ in 2002 (not shown). Therefore, soil moisture is averaged over the last three years (from 2002 to 2004) as shown in Figure 2.8.

In the control plot, hydraulic redistribution produces a lower soil moisture in deeper layers and higher soil moisture in shallower layers compared with CTL, where hydraulic redistribution is not considered, as is more consistent with observations (top panel of Figure 2.8). In the treatment plot, soil moisture is lower for the HR run than the CTL especially in deeper layers (bottom panel of Figure 2.8), where water has been transported to shallower layers for easier access by plant roots. As in the control plot, soil

moisture in HR is also more consistent with the observations in the treatment plot. The total soil water amount of HR is lower than that of CTL, a result due to the hydraulic-redistribution induced increase in plant water uptake.

The effect of rainfall exclusion is demonstrated in Figure 2.9 by the difference of soil moisture between the control and the treatment plots. The magnitude of soil moisture reduction increases with soil depth for both CTL and HR, implying that the location where plants extract water deepens as the experiment proceeds and shallow water storage has been depleted. Compared with CTL, HR shows a more rapid reduction rate in soil moisture in deeper soil layers, because the deeper water storage is more accessible when roots hydraulically redistribute it to shallower layers where fine roots are more abundant. The magnitude of soil moisture reduction increases with soil depth for HR, a pattern that differs from that observed. The observed difference between the two plots decreases from the surface to 4 m. However, below 5 m, the difference increases with depth.

This inconsistency between HR and observations suggests that hydraulic redistribution is not the only mechanism that needs to be considered. Apparently, the disagreement partly resulted from the different soil depth of the model versus reality as well as from the consequently different loses and gains of hydraulically redistributed water. The soil depth, also rooting depth, is 3.4 m in CLM, but it is at least 11 m in field observations. Rooting depth defines the soil domain where water can be accessed by plant roots and thus it sets a limit for the maximum water available to plants. In reality, soil depth varies due to many factors such as different weathering rates (Pelletier and Rasmussen, 2009). Gochis et al. (2010) showed that surface flux simulations in Noah land surface model can be improved by considering the variation in soil depth in several

semi-arid regions. Here we also show that soil depth is a key factor in eco-hydrological modeling over Amazonia rainforest.

Another source of the discrepancy between HR and observations comes from the uncertainty of root fractional distribution. In addition, the uptake and hydraulic redistribution of water are assumed to be linearly proportional to root fractions. In CLM, the vertical profile of root fractions are estimated from the field investigation of maximum rooting depth, fine root biomass, and density for major terrestrial biomes at many sites over the globe (Jackson et al., 1996, 1997) as described by Zeng (2001). Within species, variations can be large (Jackson et al., 1996, 1997), but such variations are omitted in the model.

Water availability limits carbon fixation from photosynthesis, leading to a lower live above-ground biomass (LAGB) in CTL compared with that of HR for both the control and treatment plots (Figure 2.10). Figure 2.10(a) shows the change of LAGB compared with the previous year. LAGB in the control plot always increases from the previous year when hydraulic redistribution is considered; this rate of increase is less in 2003 than in 2002. LAGB decreases for these two years when hydraulic redistribution is not accounted for, due to the reduction of precipitation induced by the 2002/2003 ENSO warm event. At the treatment plot, the reduction of biomass started in 2002, the third year of the experiment, but the reduction rate varies between CTL and HR. A rapid decrease of LAGB occurs in 2002 for CTL but one year later for HR, indicating that biomass response is delayed with higher water availability provided by hydraulic redistribution.

Figure 2.11 shows the measured and simulated LAI at both plots. In the control plot, LAI from HR agrees better with observations than that from CTL, especially during the 2002/2003 ENSO events. During this ENSO event, CTL produces a reduction of

about 1.5 m^2/m^2 in LAI from 2001 in response to the precipitation reduction. However, when hydraulic redistribution is considered, LAI is negligibly affected as seen in observations, since additional water is extracted from deeper soil layers to facilitate plant growth. In the treatment plot, both CTL and HR show a substantial reduction of LAI in 2002. The models (both the default and hydraulic redistribution incorporated models) produce a higher response of LAI to rainfall exclusion than observations.

Interestingly, the LAGB and LAI values are quite similar between HR and CTL at the treatment plot in 2004, the year when the rainfall exclusion experiments ended. Apparently, hydraulic redistribution can only delay the onset of vegetation response to drought rather than modify the response magnitude during a long drought. However, it should be noted that for a drought ending earlier than the experiment, the damage to the trees implied by CTL would be more than that by HR.

2.5. CONCLUSIONS AND DISCUSSIONS

An underestimation of dry season evapotranspiration over the Amazon basin by land surface models, primarily due to their lack of many important root water-uptake processes, initiated this study. Hydraulic redistribution is confirmed to be one of the mechanisms that enhance dry-season water uptake by plant roots. We examined how hydraulic redistribution modifies the vegetation response to droughts of various time scales, namely seasonal dry spells and artificially long drought. Results show that observed vegetation resistance to dryness is better captured by the model with hydraulic redistribution considered since this mechanism enables plants to extract more water from the soil during water shortage periods by transporting more water to shallower soil layers where fine roots are more abundant. Moreover, more water has been "banked" during the previous wet season for dry-season use. However, if a drought is long enough, as with the

artificial long drought during a 5-year rainfall exclusion experiment, the impact or damage of drought on the ecosystem is not mitigated by hydraulic redistribution, i.e. an Amazon rainforest dieback (e.g. Cox et al., 2004) may not be avoided by root hydraulic activities if a drying trend is long-lasting as projected by IPCC AR4 (2007).

Besides hydraulic redistribution realized through the low-resistance pathway provided by fine roots, many other root related mechanisms, including deep root systems of up to 18 m (Canadell et al., 1996), dynamic water uptake (Green and Clothier, 1995), and water-tracking fine root growth, may also contribute to dry-season water uptake and consequently drought responses and need further examination in modeling studies. More field observations are also needed to improve our understanding as to how to represent root activities in plant physiological and ecological aspects. In addition, local environmental factors, including soil, geology, climate, and so on, substantially influence plant hydrological behavior and modify plant properties. For example, the dependence of vertical root distribution on soil texture is widely reported both in field experiments (Lutz et al., 1937) and through numerical simulations (van Wijk, 2011). Plants are found to place fewer roots within the layers with more sand and fewer clay particles and vice versa (Lutz et al., 1937). The rooting depth for water-limited systems has also been predicted to be deeper in coarse soils than fine soils (Jackson et al., 2000) and supported by the global root database (Jackson et al., 1996, 1997). In order to take account of these impacts, Laio et al. (2006) developed an analytical model to relate the vertical root distribution to climate and soil properties.

In addition to root functioning, plants develop other methods to endure water shortage. For example, plants store water in their trunks. It has been observed in field studies that plants usually extract water from stem storage first when it is available in the

morning and then water source moves to the soil water pool in the afternoon (Goldstein et al., 1998; Wang et al., 2012). Nighttime sap flow measurements also show that plants refill stem storage during the night (Wang et al., 2012). A variation of trunk radius has been observed as evidence of water flux out of or into this storage (Zweifel et al., 2001). This internal water storage capacity is positively correlated with tree height and sapwood area (Goldstein et al., 1998). Both diurnal (Goldstein et al., 1998) and seasonal (Borchert, 1994) variation patterns in this storage are responsible for trees to maintain transpiration flow. The contribution of stem water storage is 9%-50% daily transpiration (Goldstein et al., 1998; Scholz et al., 2008; Wang et al., 2012; Köcher et al., 2013).

During severe droughts, the water continuum within xylems can break, which is called embolism. Plants can refill the embolized xylems by spending carbon. Thus the choice of whether to repair the embolism in xylems depends on the whole-plant carbon status. In order to push our models closer to reality, a water-carbon interactive point of view is recommended.

Along the pathway of water transfer from soil to plant leaves and other organs, several elements work in series, including the rhizosphere, fine root xylems, and stem xylems, with different hydraulic properties and carbon-water strategies. Therefore, to improve our ability to model vegetation response to droughts, we need to build up a hydraulic architecture from soil to plants taking into account all the resistance along the path.

2.6. ACKNOWLEDGEMENT

We thank the principal investigators at the LAB sites for providing valuable data. Comments and suggestions from two reviewers are greatly appreciated.

Site Name	Short	Location	PFT	Soil Texture	Water Table Depth
Amazonas (Manaus) - ZF2 km 34	K34	2.5ºS, 60.23ºW	Evergreen broadleaf forest	Clay latosol	
Para Western (Santarem) - km 83 Logged Forest Tower Site	K83	3.02ºS, 54.97ºW	Evergreen broadleaf forest	Clay latosol	At least 100 m
Para Western (Santarem) - km 67 Primary Forest Tower Site	K67	3.02ºS, 54.89º W	Evergreen broadleaf forest	Clay latosol	At least 100 m
Para Western (Santarem) - km 77 Pasture Tower Site	K77	3.01ºS, 54.54ºW	Pasture-crops	Clay latosol	
Para Eastern (Belem) - FLONA Caxiuana	CAX	1.7483ºS, 51.4536ºW	Evergreen broadleaf forest	Sandy latosol	Seasonally flooded
Rondonia - Jaru Biological Reserve Tower B	RJA	10.08ºS, 61.93ºW	Evergreen broadleaf forest	Sandy podsol	
Rondonia - FazendaNossaSenhora	FNS	10.76ºS, 62.36ºW	pasture	Sandy podsol	
Tocantins - Ilha do Bananal	BAN	9.82ºS, 50.16ºW	Forest-savanna	Loamy sand	
Sao Pablo - ReservaPe-de-Gigante	PDG	21.62ºS, 47.65ºW	savanna	Silty sand latosol	

Table 2.1. LBA sites

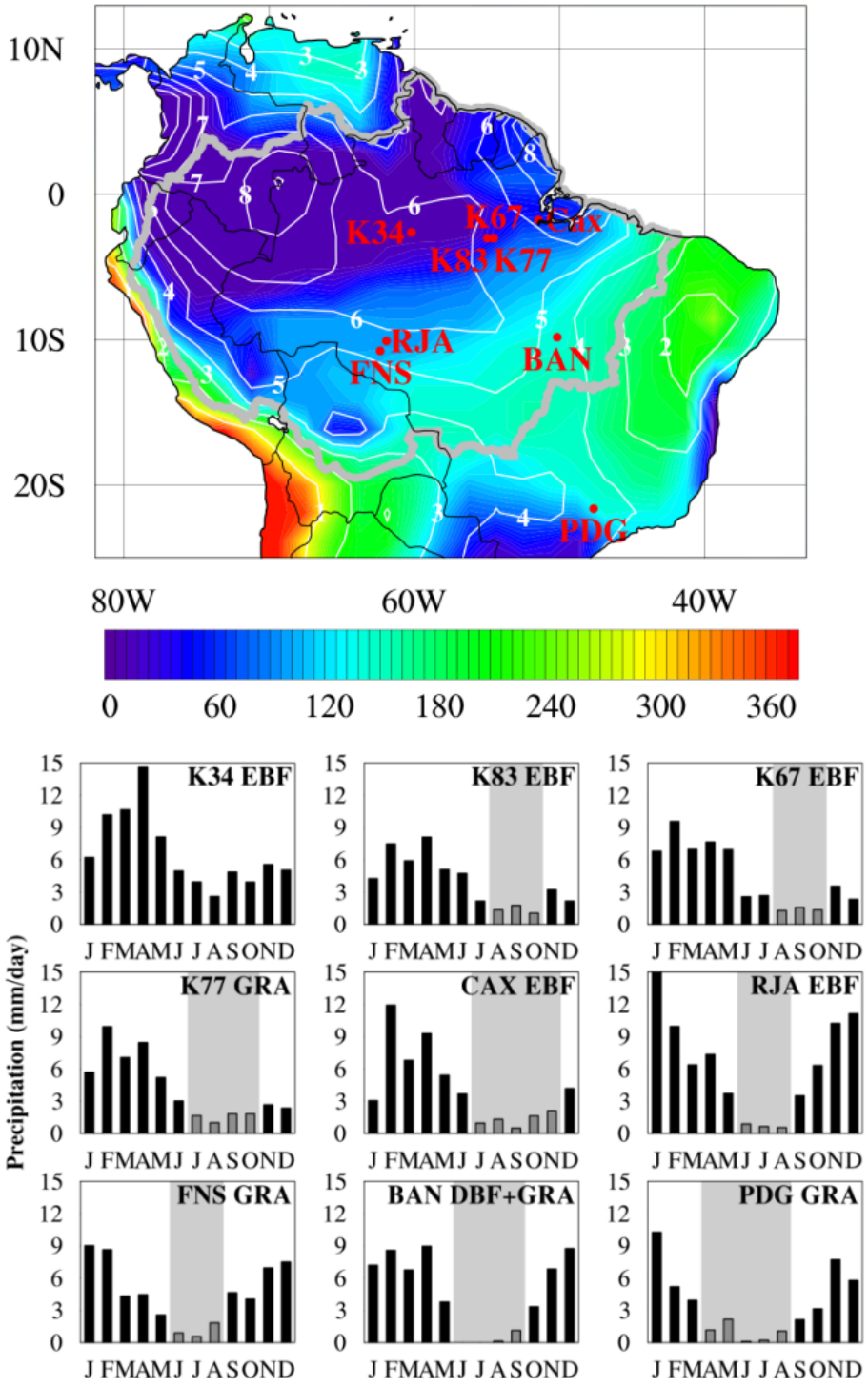

Figure 2.1. Climate gradients and LBA site locations over the Amazon Basin. The top panel shows the geographical distribution of the variables (White lines show the 50-year

climatological annual mean precipitation with units of mm/day; Colors show the number of days when five-day mean precipitation is lower than 2 mm/day; Precipitation climatology is calculated from the Qian et al. (2006) reanalysis data between 1950 and 1999; red points are the LBA sites used in this research; the grey line shows the geographical definition of the Amazon basin). Monthly mean precipitation for the LBA sites is shown in the bottom panel (shaded months are the dry season with monthly mean precipitation lower than 2 mm/day).

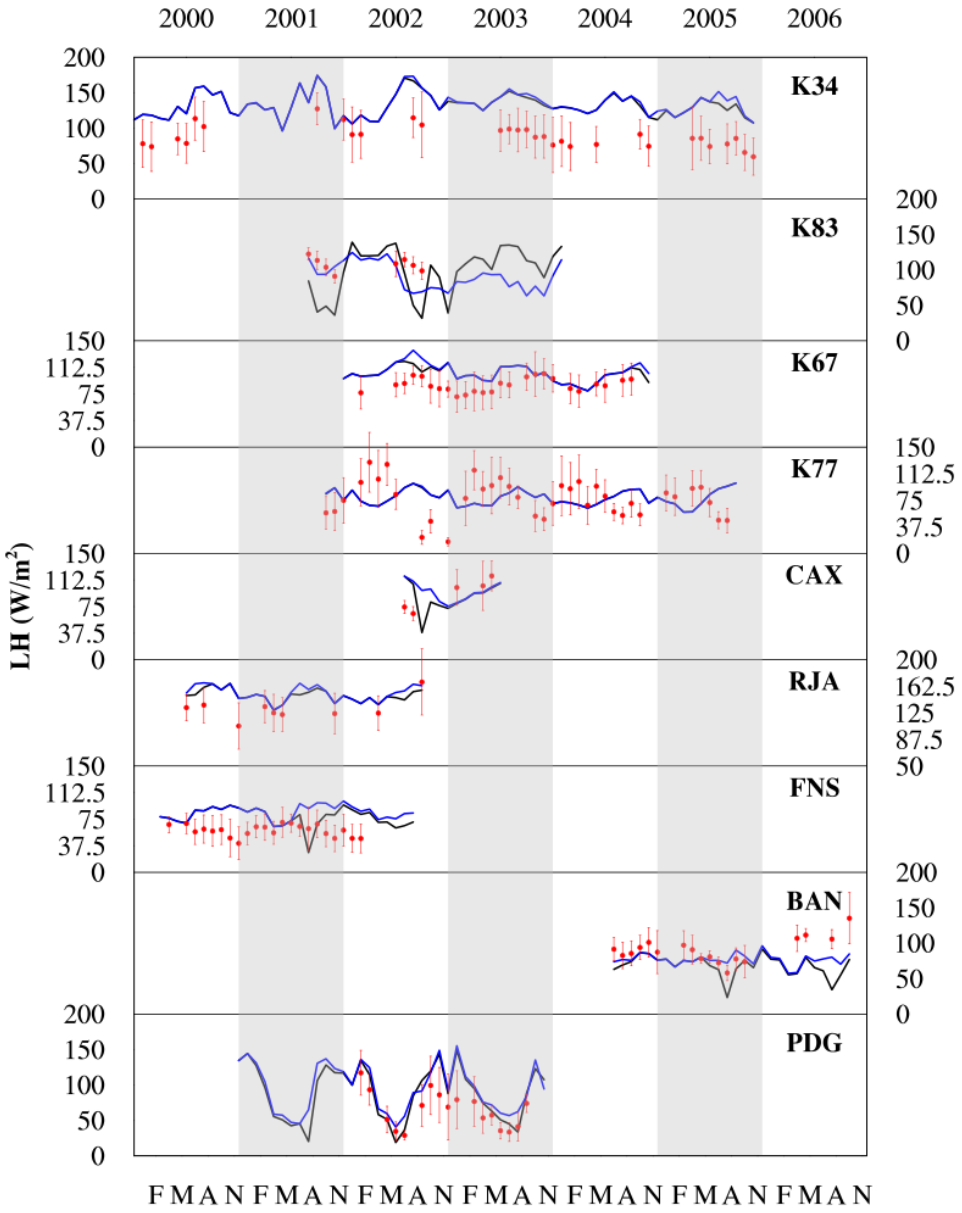

Figure 2.2. Comparisons between simulated (black is CTL and blue is HR) and measured (red) monthly mean latent heat flux.

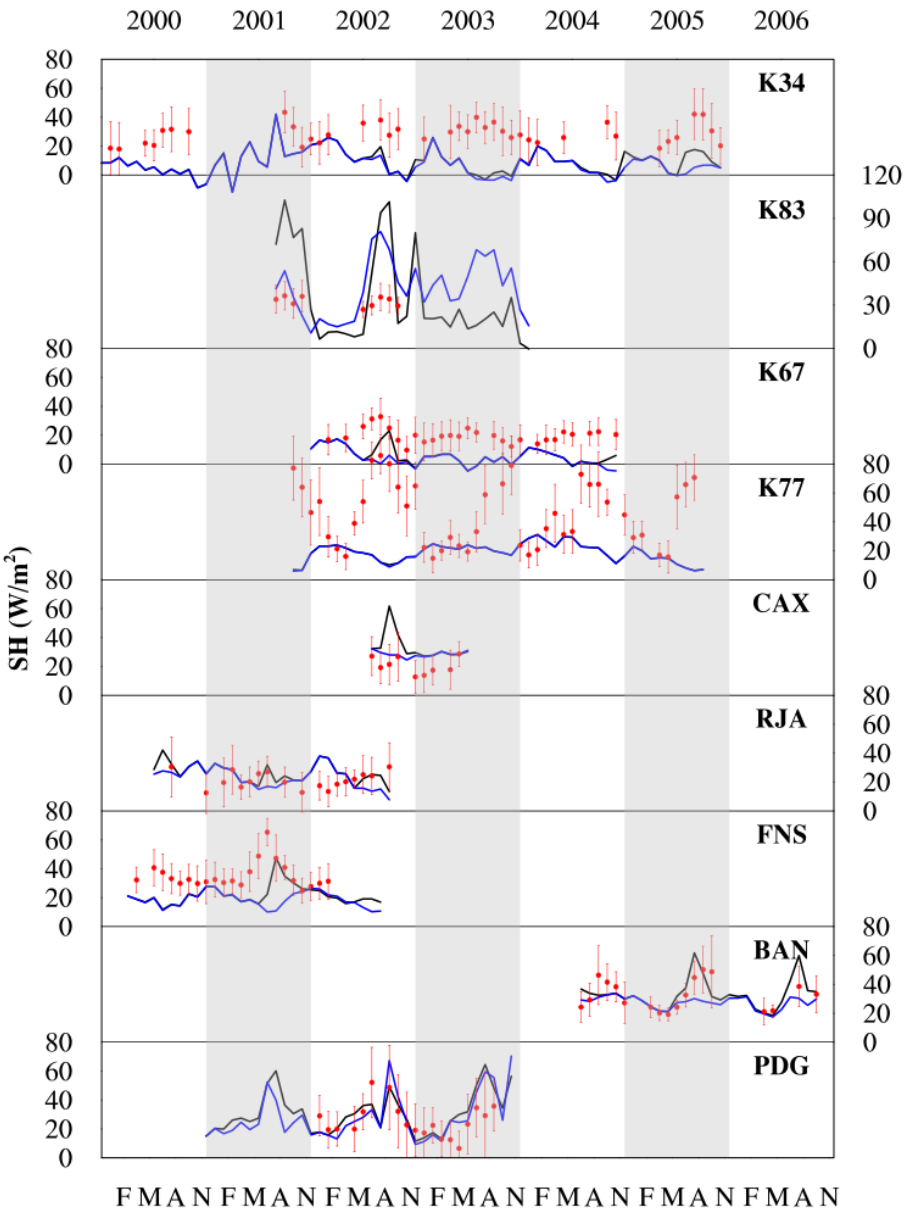

Figure 2.3. Comparisons between simulated (black is CTL and blue is HR) and measured (red) monthly mean sensible heat flux.

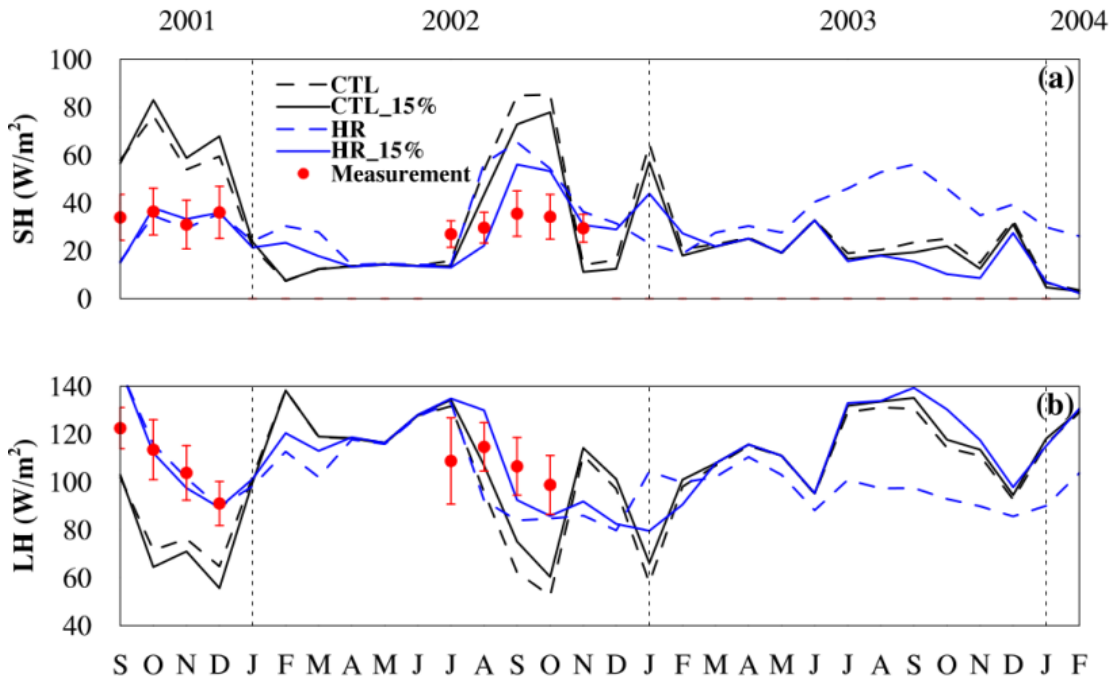

Figure 2.4. Simulated surface energy fluxes at the K83 site forced by original rainfall and by rainfall with 15% increase in wet-season values.

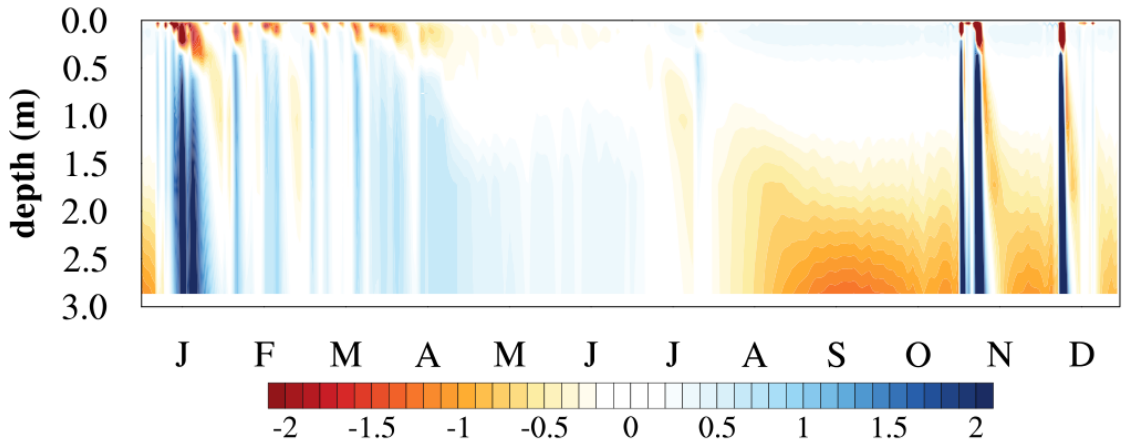

Figure 2.5. The amount of water distributed by HR (mm/day) in 2002 at the K83 site (positive value means gaining water).

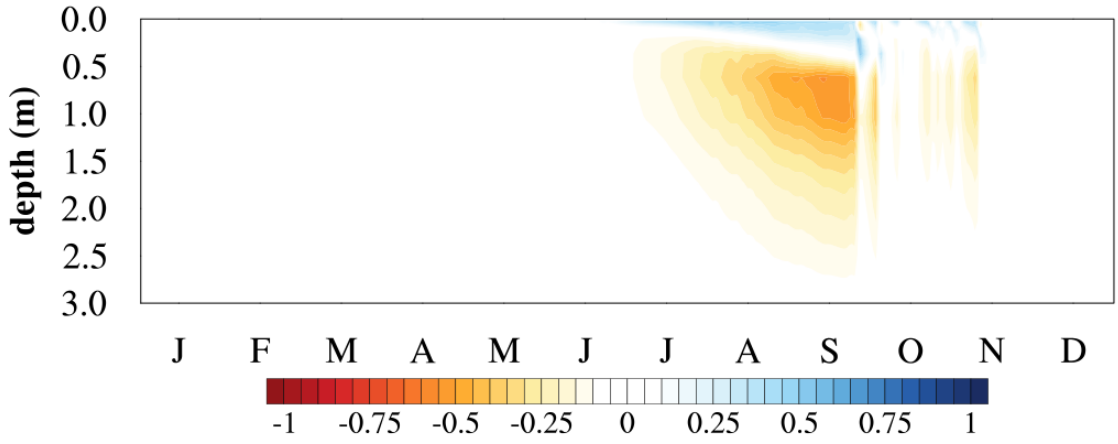

Figure 2.6. The same as Figure 2.5 but at the BAN site and in 2005.

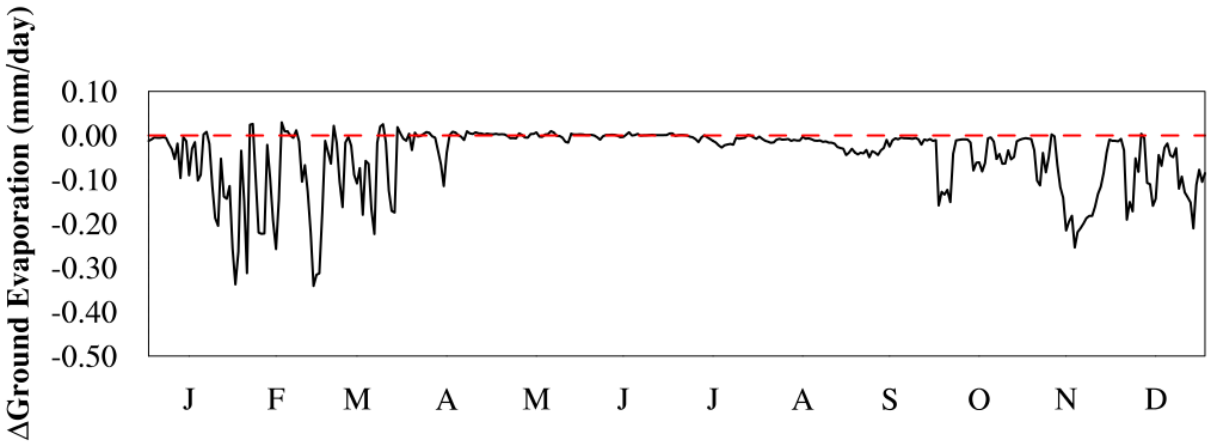

Figure 2.7. The difference of ground evaporation between hydraulic redistribution and hydraulic lifting at the K83 site.

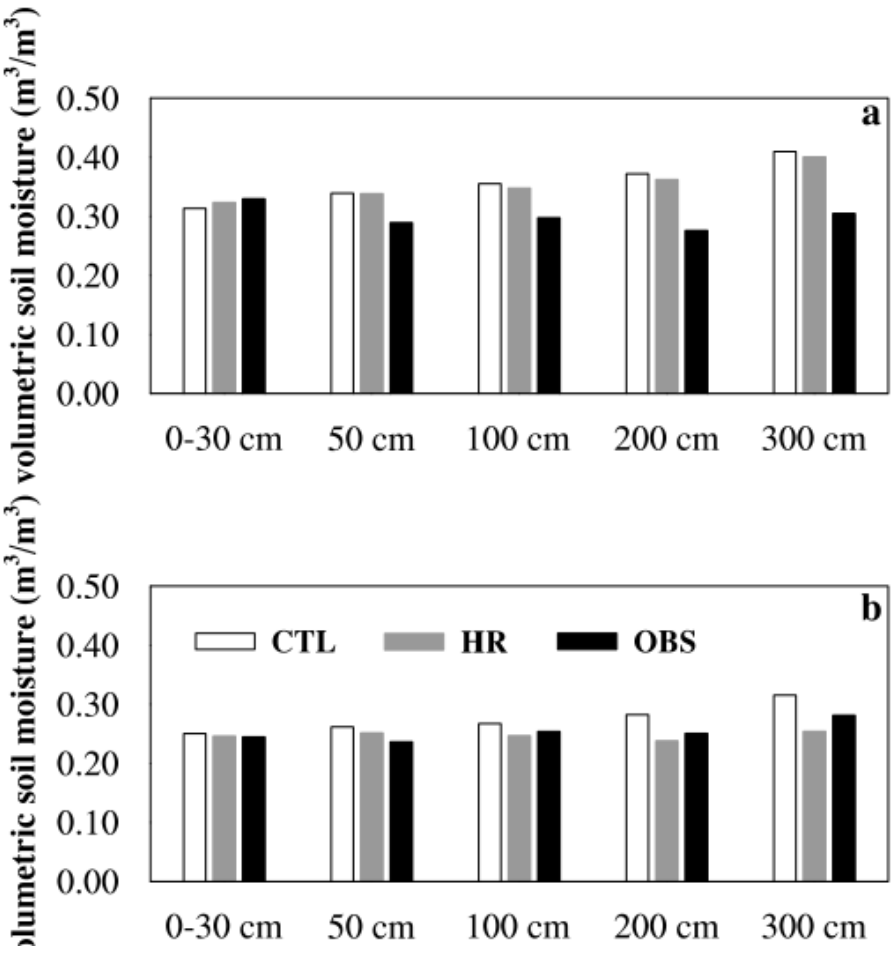

Figure 2.8. Comparisons of 3-year (2002 - 2004) mean volumetric soil moisture (m^3/m^3) between CTL, HR and observations during the rainfall exclusion experiment near the K67 site for control (a) and treatment (b) plots.

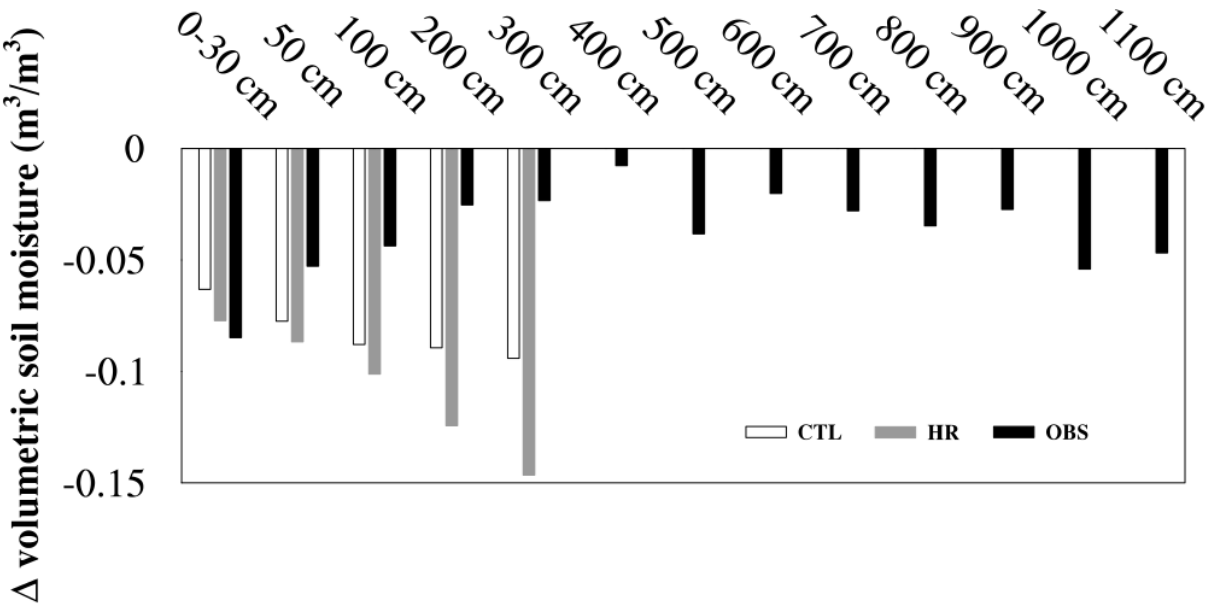

Figure 2.9. Difference in 3-year (2002 - 2004) mean volumetric soil moisture (m^3/m^3) between control plot and treatment plot for CTL, HR and observations during the rainfall exclusion experiment near the K67 site.

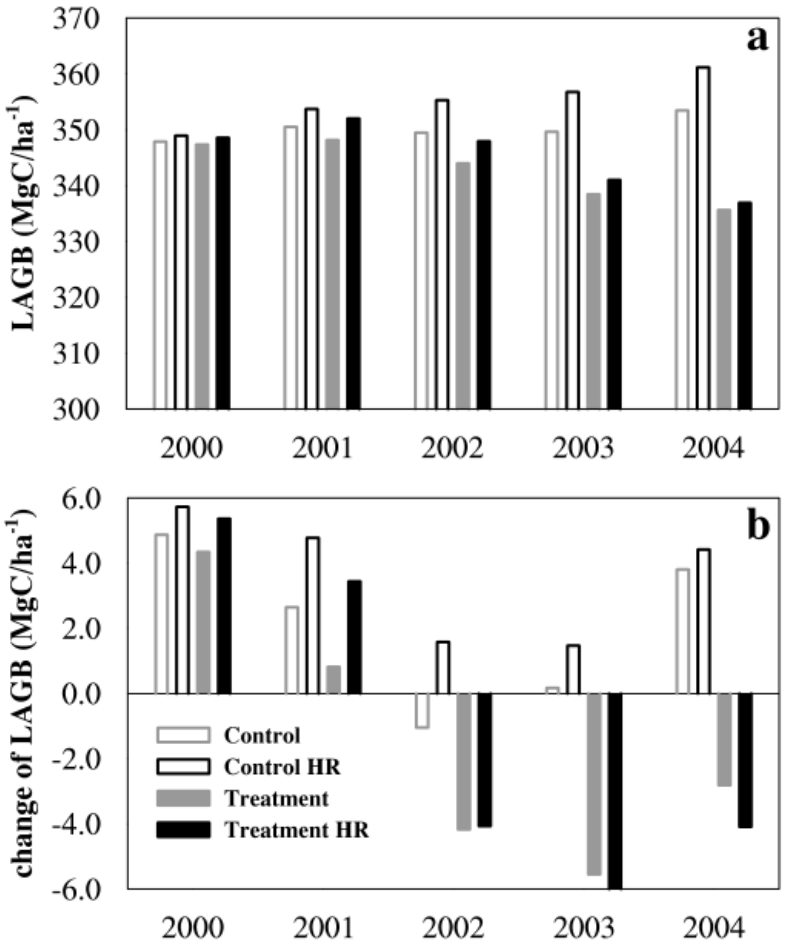

Figure 2.10. Simulated LAGB (a) and the change from the previous year (b) during the rainfall exclusion experiment near the K67 site.

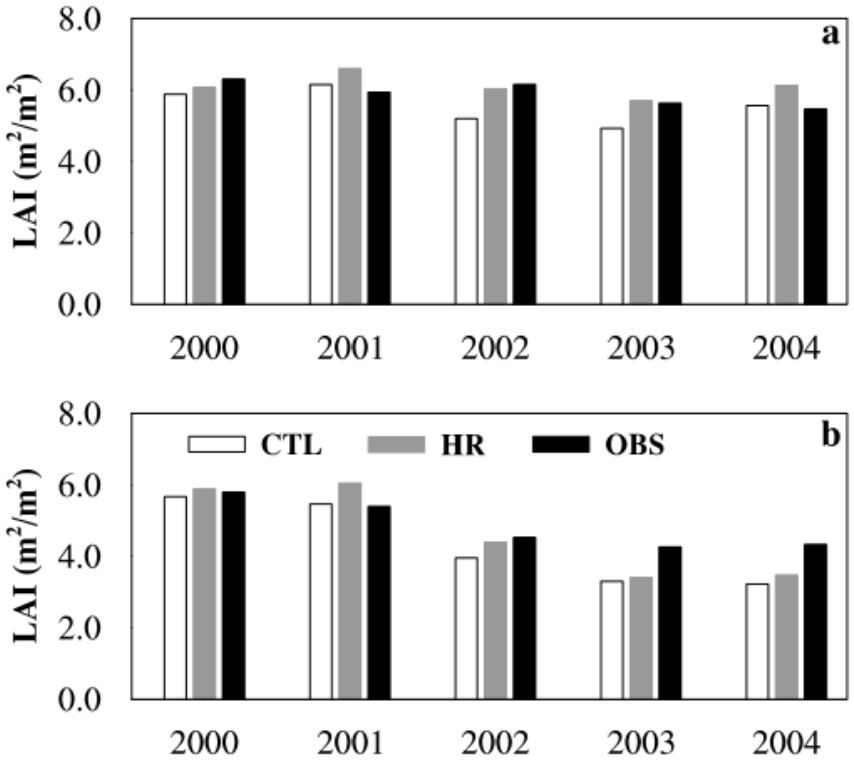

Figure 2.11. Simulated and measured LAI during the rainfall exclusion experiment near the K67 site at control plot (a) and treatment plot (b).

CHAPTER 3: Modeling tree trunk water dynamics over a rainforest site in the Amazon

3.1. ABSTRACT

A trunk water model is proposed to simulate the dynamics of trunk water content and its contribution to daily transpiration. We compare the Community Land Model (CLM) 4.0 without and with this trunk water module at an evergreen rainforest site in Amazonia, i.e., the BR-Sa3 site. With the inclusion of trunk water pool, the model produces dry-season latent heat flux that is higher and closer to observations, facilitated by the higher availability of water and also the easier access to the water source from the trunk. The trunk water content shows seasonal variations, along with the seasonal variations of sap flow rate, following the seasonal pattern of precipitation. Trunk water of a single tree contributes 20-80 kg/day water to transpiration during the wet season and 90-110 kg/day during the dry season. In the morning, trunk water decreases from transpiration and then is refilled by the soil water from the afternoon to the next morning. The recharging and discharging processes are dynamic in response to environmental factors, such as radiation.

3.2. INTRODUCTION

Trees regulate their drought tolerance through storage of water in their trunks. They are observed to extract water from their trunk water pool with the onset of transpiration in the morning with their water extraction moving downward to the soil in the afternoon (Goldstein et al., 1998; Wang et al., 2012). During the night when trees almost stop transpiration, their trunk water pool is refilled by the soil water down a water potential gradient, a phenomenon observed by nighttime sap flow measurements (Wang et al., 2012). A diurnal fluctuation of trunk water content is consequently seen (e.g.

Goldstein et al., 1998) as a response to the diurnal variation of the two processes, i.e., the water extraction from tree trunks for daytime transpiration and their replenishment of water from the soil at night. A resultant variation in tree trunk diameter is also observed on a diurnal time scale. Stem water storage provides 9-50% of daily transpiration (Goldstein et al., 1998; Scholz et al., 2008; Wang et al., 2012; Köcher et al., 2013). This contribution was found to increase after drought, e.g., from 12% of daily transpiration when soil water is abundant to 25% at the end of summer after a drought period (Loustau et al., 1996). During cloudy days, the contribution from the internal pool can be even higher. The long distance between leaves and soil and the high hydraulic resistance limit the immediate use of soil water for transpiration of woody plants. Hence, trees tend to first exploit their internal water storage, i.e., storing and utilizing water inside tree trunks as a solution for the time lag required to access soil water.

This internal storage also dampens the response of xylem to transpiration (Phillips et al., 2004), lowering the risk of xylem embolism and consequent hydraulic failure, thus it is one of the plant drought-coping strategies for many species. On the seasonal time scale, trunk water storage is responsible for trees maintaining transpiration during the dry season (Borchert, 1994). For seasonally deciduous trees, the water inside the trunk provides water that is needed for growing new leaves.

The capacity of a trunk water pool determines how long it can support transpiration. Its diurnal capacity is found to be related to tree allometry. Allometric relationships between tree sizes and sap flow density can be established. For example, Goldstein et al. (1998) found a species-independent linear relationship between the water storing capacity and sapwood area with an increment of 10 kg water per increase of 0.1 m^2 sapwood area. Meinzer et al. (2001) reported the sapwood area as a function of

diameter at breast height (DBH) in the form $y=1.582 \cdot DBH^{1.764}$ ($R^2=0.98$) from a survey of 107 individual trees belonging to 24 species in a tropical forest in Panama. Apparently, the capacity to store water is proportionally related to sapwood volume. Trees with the largest sapwood volumes, such as the evergreen trees in Amazonia, have the highest capability to store water in their trunks.

Drought events and intensities have been projected to increase in the next century over most regions on earth (IPCC, 2007). These increases will inevitably modify vegetation distributions in the future. Wide-spread tree mortalities as a result of drought and heat have already been observed over the globe (Allen et al., 2010). However, a recent model comparison reveals large discrepancies in modeling vegetation dynamics and carbon cycles in response to drought (Powell et al., 2013), especially for tropical forests and these discrepancies are related to the response of tropical vegetation to droughts (Sitch et al., 2008). The largest tropical forest, the Amazon rainforest, is now undergoing a transition (Davidson et al., 2012). An increase in its dry season has been detected (Fu et al., 2013) and future drying in this area has also been projected (e.g. Cox et al., 2004). This increased dryness will inevitably modify vegetation distributions since species distributions are shaped by drought sensitivities (Engelbrecht et al., 2007). A change of vegetation distribution can affect mass and energy exchanges between land surface and the atmosphere. Indirect effects by vegetation feedbacks through its modification of albedo, surface roughness, and other properties will also influence climate. Thus a better understanding of how vegetation distributions respond to climate change is essential for policy makers.

The trunk water pool as a key factor for land surface models in modeling the fundamental hydrological processes and hence plant response to water stresses has been

absent in many such models. This discrepancy between reality and model parameterizations may lead to a bias in drought response simulation, limiting our ability to understand how plants respond to and feedback on water limitations.

The aim of this research is to demonstrate the role of trunk water pool in plant water dynamics. Even though the important role of internal water storage in plant water dynamics and economics has already been addressed in field experiments at a few locations and for specific forest types, knowledge of details as to its dynamics and contributions to plant water consumption on longer time scales and over large spatial ranges are still limited. In particular, we will address the following scientific questions: Can inclusion of a trunk water pool enable a more accurate simulation of Amazon rainforest responses to seasonal drought? How does the trunk water pool vary diurnally and seasonally? How much does the trunk water pool contribute to transpiration? The model used, CLM4.0, is briefly introduced in Section 3.3. The parameterization and implementation of a trunk water pool as well as experimental design are also described there. Section 3.4 gives results. Finally, we present our major findings in Section 3.5.

3.3. MODEL, PARAMETERIZATION, AND EXPERIMENT

We use the Community Land Model version 4 (CLM4) (Oleson et al., 2010), the land surface component of NCAR Community Earth System Model (CESM) version 1.0. It describes hydrological, biophysical, and biochemical processes at scales ranging from the level of PFTs (plant functional types), the smallest unit for energy and hydrology calculations, to atmospheric grid level. The vegetated fraction of a grid consists of up to 16 PFTs. PFT specific processes, for example, transpiration, are calculated at PFT levels and then aggregated to the grid level according to the specific fractional area of each PFT.

CLM4 assumes that only soil (10 layers) and an underground aquifer store water and only the former directly provides water for plant use. The 1D Richards Equation (Equation 3.1) governs water transport with infiltration and subsurface drainage serving as the upper and lower boundary conditions. Only its first layer is responsible for soil evaporation. Plant transpiration is treated as a sink term. It is regulated by stomata, which are the pathway for water to diffuse from inside the leaf to the outside leaf boundary layer. Plants physiologically adjust the opening and closing of stomata to regulate their use of natural resources including water. At each soil layer, water availability, with a scale factor from 0 to 1 describing to what extent soil water is available for plant transpiration, is derived considering some limiting values, i.e., the levels of soil water when stomata starts to close and the wilting point.

The 1D Richards equation is used to describe water diffusion within the soil/trunk system,

$$\partial\theta/\partial t = -\partial q/\partial z - s, \tag{3.1}$$

where θ is the volumetric water content (m^3/m^3), s is the sink term for transpiration loss, t is time and z is depth, and q is the flux out of the depth given by Darcy's law:

$$q = -K[\partial(\varphi + z)/\partial z], \tag{3.2}$$

where K (m/s) and φ (m) are the hydraulic conductivity and water potential of specific elements. The soil hydraulic conductivity and water potential depend on mineral composition and abundance of organic matter (e.g. Clapp and Hornberger, 1978). We assume that the trunk water pool is located in the middle of the tree trunk. Water directly diffuses between adjacent soil layers as well as between each soil layer and the tree trunk. The Richards equation is solved numerically by dividing the soil and stem storage domain into several layers in the vertical direction (10 layers of soil as default in CLM

model and 1 layer of trunk) and then integrating downward over each of the model layers, i.e., for the *i*th layer (either soil or trunk layer), the change of water amount in unit time equals to the difference of net water flux into the layer and the sink term, $\Delta z_i \, \partial\theta_i/\partial t = -\left(q_{i,lower} - q_{i,upper} - e_i\right)$, where $q_{i,lower}$ and $q_{i,upper}$ are the water fluxes across the lower and upper boundary of this layer respectively and e_i is the sink term. We define the upward direction as positive for water fluxes.

The soil-plant hydraulic path can be viewed as a series of electric resistors, with its total hydraulic resistance being the sum of all those along the path, namely the soil-to-root resistance, r_{sr}, and xylem resistance, r_x,

$$r_{tot} = r_{sr} + r_x. \tag{3.3}$$

According to Gardner (1960), the soil-to-root resistance can be estimated by assuming the root system to be a single tube that extracts water from the surrounding soil over a distance,

$$r_{sr} = log\left(R_{cyl}/R_r\right)/2\pi L_v \Delta z K_s, \tag{3.4}$$

where K_s is the soil hydraulic conductivity (m/s), R_r is the root radius (m) and is set as 3×10^{-4} m (Manzoni et al., 2013). Although studies have reported the variation of fine root radius with depth (e.g. Maeght et al., 2015), we use a constant here for simplicity. R_{cyl} (m) is the radius of the soil cylinder to which the root has access to (Newman, 1969),

$$R_{cyl} = 1/(\pi L_v)^{1/2},$$

where L_v is root length density which is approximately 1000 m/m^3 for fine roots (radius <1 mm) in Amazonian soils (Nepstad et al., 1994). Δz is the depth of soil layer (m).

Xylem conductivity is calculated according to the traditional Hagen-Poiseuille equation,

$$r_x = 32\eta S/\pi \sum_{i=1}^{n} {D_i}^2, \tag{3.5}$$

where η is the viscosity of water (1.002 MPa·s at 20°C), S is the length of the xylem tube which is set as the tree height here, n is the number of vessels, and D is the vessel diameter. Zach et al. (2010) measured trunk vessel diameter and vessel density from 51 trees growing in lower montane rainforest in Sulawesi, Indonesia. Vessel diameters range from 69.4 μm to 199.2 μm and vessel density from 2.9 mm^{-2} to 16.3 mm^{-2}. Based on the measurements, we set D to 130 μm and n to 9 mm^{-2}. Sapwood area is needed to calculate the number of vessels. A species-independent empirical relationship between sapwood area (cm^2) and DBH (diameter at breast height, cm) is established as $y=1.582 \cdot DBH^{1.764}$ (Meinzer et al., 2001). A mean DBH measured at our study site is 1.02 m (Figueira et al., 2011). Here we use a constant xylem conductivity that is only dependent on the vascular anatomy for simplicity. Its variations with water amount inside xylem tubes, temperatures, and other factors, e.g. the cavitation and refilling processes, are not considered.

The water potential of trunk is described as a function of its volumetric water content,

$$\varphi = \varphi_{sat}(\theta/\theta_{sat})^{-b}, \tag{3.6}$$

where φ_{sat} is the water potential at saturation, set as -100mm (corresponding to -1000 Pa). b is a constant and set as 2.0 for this study. θ_{sat} is the maximum volumetric water content the trunk can reach. According to Borchert (1994), the saturation water content with respect to dry mass of tree trunk is $WC_{sat} = 100 \cdot \frac{SM-DM}{DM} = 100 \cdot \frac{1-D/1.5}{D}$. SM is the trunk mass at saturation, DM is the dry mass, D is the wood density (g/cm^3). 1.5 g/cm^3 is the approximate species-independent value for wood density excluding open spaces due to the similar composition of wood: cellulose and lignin (Williamson, 1984). WC_{sat} is the same as θ_{sat} after multiplying the latter by ρ_{water}/D. Baker et al. (2004)

measured the wood density near the BR-Sa3 site, the average value among different methods and plots is 0.65 g/cm^3, giving a value of 56.67% for θ_{sat}. We set the minimum stem water potential at -4MPa following Zweifel et al. (2001).

Our "big tree" model simulates hydraulic processes for one virtual tree instead of many individuals separately. Basal area is used to scale stand level moisture amounts to grid level one. The basal area was measured at three plots near our flux tower in the Tapajos forest (3.31ºS, 54.94ºW) in 1995 as 26.89 m^2/ha, 31.31 m^2/ha, 34.39 m^2/ha (Baker et al., 2004). We use the average of the three values, 30.86 m^2/ha, in our modeling study.

Our study site is the km83 Tapajos national forest site, located in the middle of Amazonia (3.0180ºS, 54.9714ºW). It is mainly covered by evergreen broadleaf rainforest with 35 m canopy height. The average daily precipitation is 12 mm. The dry season with daily rainfall lower than 2 mm is from August to October. A tower mounted with measurement equipment was set up at this site. Measurements that include meteorological variables (wind speed, air temperature, air humidity, air pressure precipitation and so on), radiation variables (incoming solar and thermal radiation, outgoing solar and thermal radiation), surface energy fluxes (sensible and latent heat fluxes), and environmental variables (such as soil moisture) were taken at a half hourly time scale from 2000 to 2004. In addition, some biological variables were also measured, such as leaf area index (LAI). The precipitation measurement at the K83 site might be underestimated since it is 15% lower than given by the Global Precipitation Climatology Product (GPCP) during 2001-2003 (Adler et al., 2003). A comparison of the precipitation at the K83 site with that of the other two adjacent evergreen rainforest sites (K67 and k77) reveals an obvious low wet-season precipitation at K83 site. To fix this

underestimation, we increase the rainy season rainfall by 15% following Yan et al. (2014).

To demonstrate the difference of plant water balances with and without trunk water pools, we conduct two numerical experiments, one with trunk water pool (EXP) and one without (CTL), with both these versions taking into account the root and trunk resistance to water flow. We ran offline CLM4.0 simulations at the K83 site. The model is forced by the site measured meteorological variables. Gaps of measurement due to interruption of precipitation or equipment malfunction are first filled before use. The PFT is set to be evergreen broadleaf forest and its coverage is set to be 100%. We use the default soil texture provided in the model. Simulation is from 2000 to 2004 and the time step is half hour.

Water balance is maintained during simulation periods. CLM4.0 checks water balance at each time step to make sure that water balance error is not higher than a threshold (10^{-7} mm). In the new model, water balance is also routinely checked. The PDF of water balance errors (Figure 3.1) shows that the error is far less than the threshold with mean value of 1.01×10^{-12} mm and maximum value of 2.95×10^{-10}.

3.4. RESULTS

3.4.1. Seasonal variations

The comparison of seasonal dynamics in precipitation, surface energy fluxes, and trunk water status between EXP and CTL is shown in Figures 3.2 and 3.3. As shown in Figure 3.2a, the year 2002 had a pronounced dry season from August to October with very low precipitation. Though several strong precipitation events occurred in November and December, the period of most continuously high precipitation (characteristics of the

wet season) did not return until the next January. In contrast, in 2003 it rained moderately from August to October, the climatologically dry season at this location, leading to a lack of a well-developed dry season for this year. Hence the analysis for dry season below is focused on that of 2002.

Figure 3.2b and c present the comparison between simulated and observed daily mean latent and sensible heat flux. These two experiments are in good agreement when there is no water stress. The major discrepancy occurs during the 2001 and 2002 dry seasons, where the default model underestimates/overestimates latent/sensible heat flux due to an underestimation of water availability, a well-known deficiency of CLM4.0 over the Amazon rainforest region (Zheng and Wang, 2007; Baker et al., 2010; Lee et al., 2005). The EXP model fixes this deficient drought response in the 2002 dry season, with good agreement with observations, but overestimates latent heat flux in the less pronounced 2001 dry season. Student's t test results are listed in Table 3.1.

The saturation level of tree trunks exhibits a pronounced seasonal variation following the pattern of precipitation (Figure 3.3a), higher in the wet season than in the dry season, indicating that water storage inside tree trunks is used to support dry-season transpiration. The trunk water amount fluctuates pronouncedly at the beginning of the wet season, becomes more stable for the rest of the wet season, and then decreases gradually during the dry season in response to the loss of trunk water to transpiration (Figure 3.3b). Trunk water contributes around 45% of daily transpiration during the wet season, and the proportion goes up during the dry season when it can reach up to 70%.The higher contribution from trunk water in the dry season is consistent with field observations (Wang et al., 2011), but its magnitude is a little bit higher than the reported values, 9%-50% (Goldstein et al., 1998; Lostau, 1996; Waring, 1979).

The seasonal variation of daytime and nighttime sap flow rates from model simulations are shown in Figure 3.4. Daytime sap flow peaks in the wet season, but nighttime sap flow peaks in the dry season. The lag between the two peaks is also seen in field observations (e.g. Wang et al., 2011). Nighttime sap flow can reach 100 kg/day per single tree in the dry season.

3.4.2. DIURNAL CYCLES

The diurnal cycles of latent and sensible heat fluxes in the three months during the dry season are plotted to examine the performance of the new model (Figure 3.5). In order to remove noise, the diurnal cycles are averaged on a monthly basis. EXP and CTL coincide with each other in terms of latent/sensible heat fluxes in the wet season and agree very well with observations (not shown). All the three dry-season months (August, September, and October) are shown separately in Figure 3.5. Their peak values are compared in Figures 3.6 and 3.7. Latent heat flux from EXP exceeds that from CTL for all the three months, associated with lower sensible heat flux from EXP than that from CTL. Generally, EXP simulations are more in agreement with observations.

The diurnal patterns of trunk saturation (Figure 3.8a) are similar for the three months, and feature three periods: 1) trunk water decreases during 6:30 am - 2 pm (local time) to support transpiration; 2) increases during 2pm-midnight in response to the recharging of trunk water pool by soil water; 3) continues to increase from midnight to 6:30 am with a lower rate of increase. The major difference between the three months lies in the strength of the refilling processes after midnight, which increases from August to October. Through the dry season, the magnitude of diurnal fluctuation in trunk saturation increases, i.e., is more pronounced, when water stress is more severe.

The diurnal pattern of sap flow rates is shown in Figure 3.8b to better illustrate the dynamics in trunk water content. The canopy sap flow is defined as the sap flow across the top boundary of the trunk pool, i.e., very close to the canopy, and is equal to the transpiration rate. Basal sap flow is the accumulated sap flow from each soil layer to the trunk water pool. The canopy sap flow is zero at night, corresponding to the assumption in the CLM that plants stop transpiration during the night. It increases in the morning with the onset of transpiration and reaches its peak around 11am - 12 pm. It remains at its peak value for about 3-5 hours and then starts to decrease in the afternoon. Basal sap flow generally follows the diurnal pattern of canopy sap flow except that nighttime sap flow is positive indicating nighttime refilling of trunk pool by soil water. The growth of basal sap flow starting at sunrise is weaker than its canopy counterpart. It reaches its peak around 2pm-3pm, about 3 hours later than the peak of canopy sap flow.

The time-lag between sap flow at these two elevations increases from early to late dry season. The hysteresis of the two sap flows is demonstrated in Figures 3.9 - 3.11. Basal sap flow decreases from the late afternoon to the night and then decreases more gradually in the night. The magnitude of basal sap flow is generally lower than that of canopy sap flow during most of the day time. Its peak value decreases from early to late dry season, indicating decreasing ability of soil water to recharge trunk water pool. Its peak value is about 90 kg/m^2/30min (August), 50 kg/m^2/30min (September), and 40 kg/m^2/30min (October), corresponding to 40 kg/h, 22.9 kg/h, 18.28 kg/h per single tree after being scaled by the allometric information, well within the range measured from five tropical trees by Goldstein et al. (1998), which is 6 kg/h - 50 kg/h. Another measurement by Gilbert et al. (2006) reported basal sap flow rate for *Populus nigra*at of about 25-50 kg/m^2/30min, similar to our simulation results.

The net change of trunk water is illustrated in Figure 3.8b by the difference between basal and canopy sap flow rates. Positive value means higher basal sap flow rate and lower canopy rate and hence indicates a net recharging process. On the other hand, a negative value represents a net discharging process. Most of the daytime is dominated by a net discharging process. The late afternoon and nighttime are dominated by a net recharging process.

3.4.3. Seasonal evolutions in diurnal cycles of trunk water content

Though sharing similar diurnal patterns over the year, the trunk water amount has large seasonal variations (Figure 3.12a), especially in the timing of the transition from net discharging to net recharging in the afternoon as well as the recharging strength from midnight to the early morning. Trunk water amount peaks at about 6 am after the whole night of refilling by the soil water and it reaches its minimum in the afternoon due to its support of transpiration; thus the difference between the peak and the minimum water amount inside the trunk, defined as discharge magnitude here, can serve as a proxy for the trunk contribution to transpiration per day. Figure 3.12b shows that this contribution is higher in the dry season than in the wet season, consistent with Figure 3.3b. The discharge magnitude is about 20-80 kg/day in the wet season and about 90-110 kg/day in the dry season, higher than measured by Goldstein et al. (1998), which is 4 kg/day - 54 kg/day depending on tree size. The measurement conducted by Goldstein et al. (1998) was during a very wet period with the total precipitation about 250% above normal so the discharge value should be smaller than normal.

3.4.4. The dynamic nature in sap flows: Cloudy versus sunny days

The recharging/discharging processes are dynamic in response to environmental conditions. The relative strength of the two processes hence determines the dynamic variability oftrunk water content. Figure 3.13 compares two consecutive days with the first cloudy and second sunny indicated by the net radiation. The higher peak of net radiation at noon in the cloudy day than in the sunny day is probably owing to the increased downward scattering by clouds. The diurnal evolution of sap flow is quite smooth on the sunny day, while it fluctuates considerably on the cloudy day. The canopy sap flow drops to and stays at zero for a period of time during the afternoon before it peaks again later. This allows the trunk recharge to be quite pronounced during that period, leading to a weaker recharge rate at night than on a sunny day.

The general features shown in Figure 3.13 are further explored by examining more cloudy and sunny days in Figure 3.14. We pick 16 sunny days and 15 cloudy days in the dry season of 2002 by examining the standard deviation between the observed net radiation curve and the climatological fit. It is a sunny day if the standard deviation is smaller than a threshold and vice versa. The comparison between the net radiation curves averaged within each category and the fitted curve from the climatology is shown in Figure 3.14a and b. The net radiation is normalized before the above-mentioned treatment. We can see similar patterns in sap flow rates as in Figure 3.12, i.e., smooth curves for sunny days and fluctuating ones for cloudy days. The recharge magnitude after midnight differs pronouncedly between the two categories.

3.5. CONCLUSIONS

We present a trunk water module based on CLM4.0, the land surface component of NCAR Earth System Model 1.0. Trunk water dynamics and its contribution to daily

transpiration are simulated at a flux tower site in Central Amazonia, BR-Sa3, which is covered mainly by evergreen broadleaf forest. The site experiences a dry season of three months from August to October with mean daily precipitation lower than 2 mm. The well-known underestimation of dry-season water availability at this site, which subsequently results in an underestimation of latent heat flux, is fixed by the inclusion of trunk water module. The ability of the new model to capture the lack of water stress in the dry season is facilitated by the more readily accessibility of trunk water pool than of the soil water and also the storage of water inside the trunk itself. On the seasonal time scale, trunk water amount follows that of precipitation, i.e., higher in the wet season than in the dry season. As the dry season starts, the trunk water decreases to support transpiration. It contributes more to the daily transpiration in the dry season than in the wet season. The diurnal cycle of trunk water amount is featured by three periods, namely the decrease from morning to the afternoon, followed by two increases from afternoon to the next morning, produced by two competing processes, recharging and discharging. The discharge magnitude, defined as the difference between daily maximum and minimum trunk water content, which corresponds to the diurnal water storage in other studies (e.g. Goldstein et al., 1998), is higher in the dry season (90-110 kg/day) than in the wet season (20-80 kg/day). By comparing cloudy and sunny days, we also show that the two competing processes of recharge and discharge are dynamic in nature.

3.6. ACKNOWLEDGEMENT

We would like to thank all data providers and model developers for making this study possible.

	Latent heat flux	Sensible heat flux
CTL and OBS	9.456e-05	1.482e-13
EXP and OBS	0.006934	0.02663
CTL and EXP	<2.2e-16	<2.2e-16

Table 3.1. p-values from *t*-test results comparing latent and sensible heat fluxes from CTL, EXP, and OBS during the 2002 dry season.

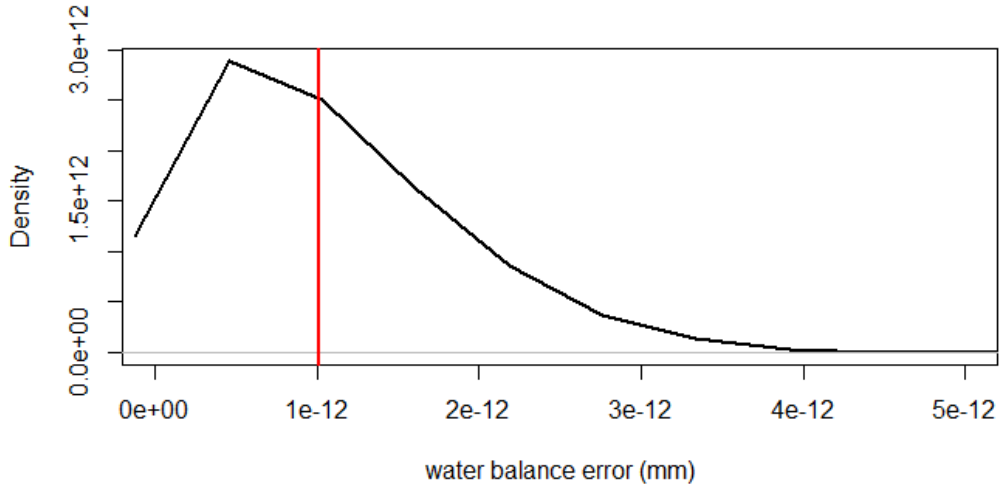

Figure 3.1. Probability density distribution of water balance error for EXP. The red vertical line shows the mean error.

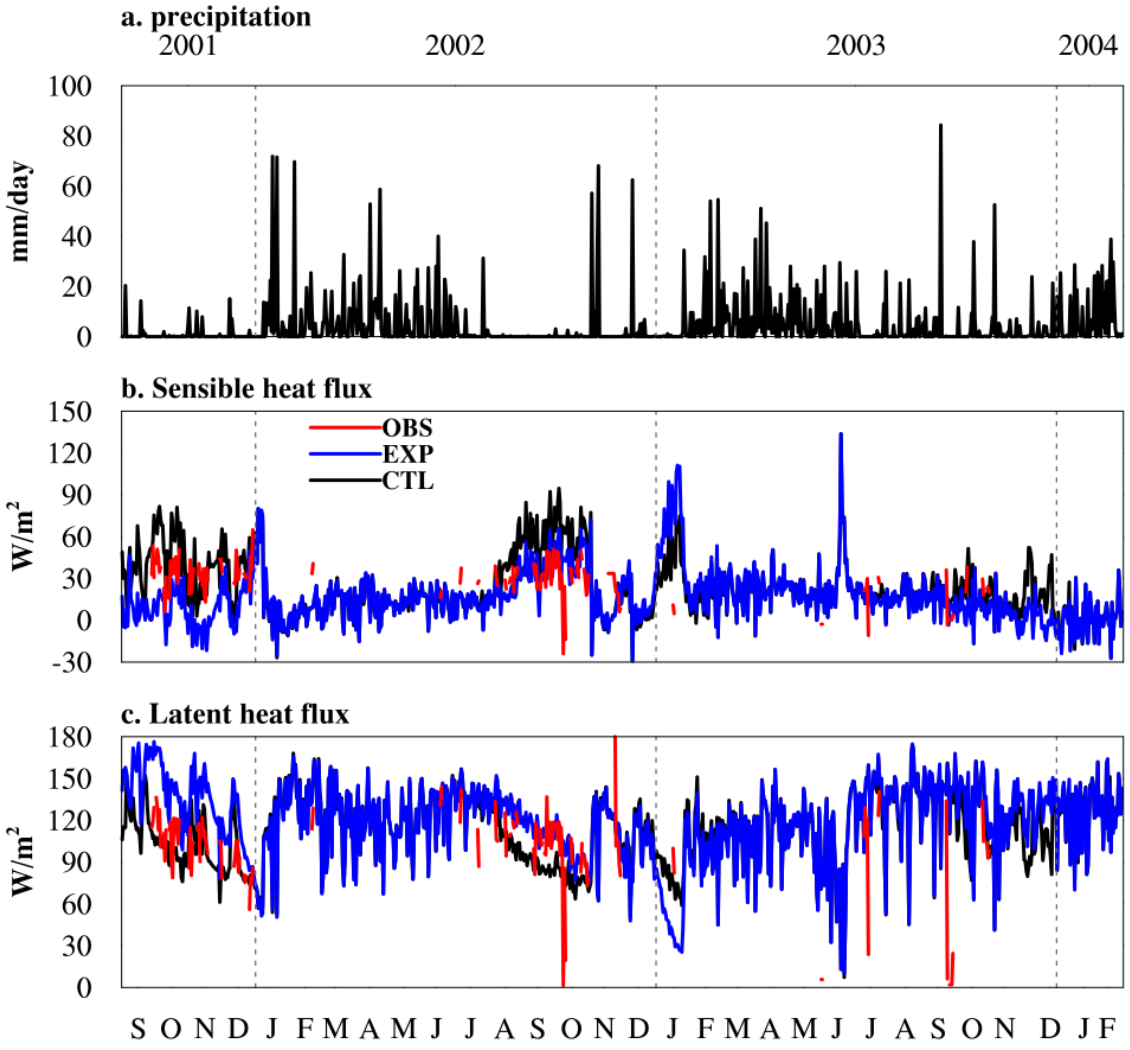

Figure 3.2. Daily averaged model simulations and observations at the BR-Sa3 site during September, 2001 to February, 2004: (a) observed precipitation (mm), (b) a comparison of sensible heat flux among model simulations from CTL, EXP, and observations, (c) the same as (b) but for latent heat flux.

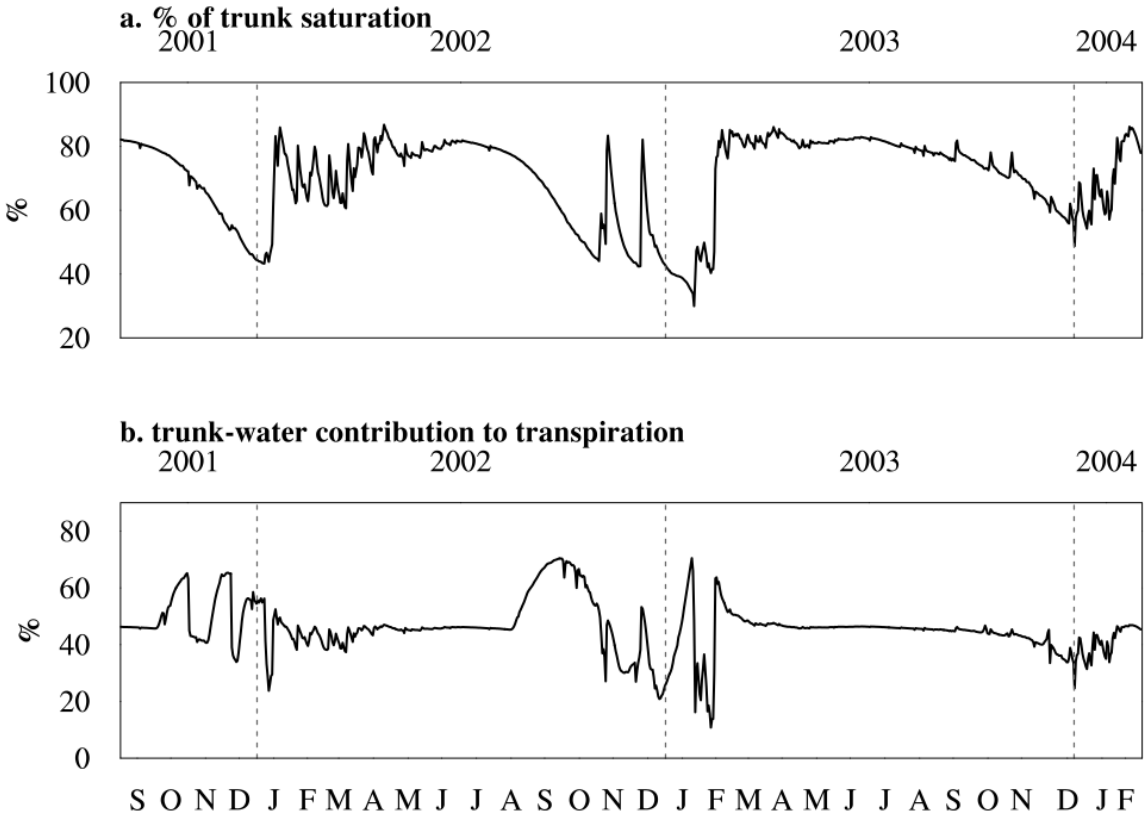

Figure 3.3. Daily averaged model simulations and observations at the BR-Sa3 site during September, 2001 to February, 2004: (a) the percentage of trunk saturation, and (b) trunk water-contribution to transpiration.

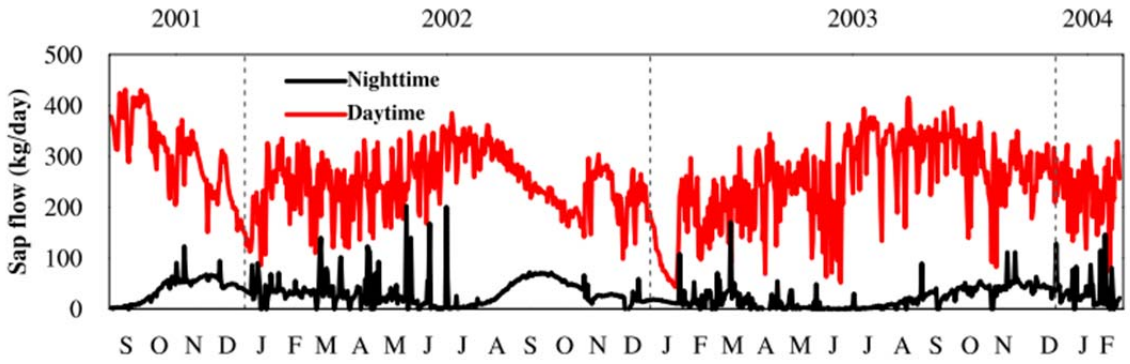

Figure 3.4. Daytime and nighttime sap flow rate for a single tree.

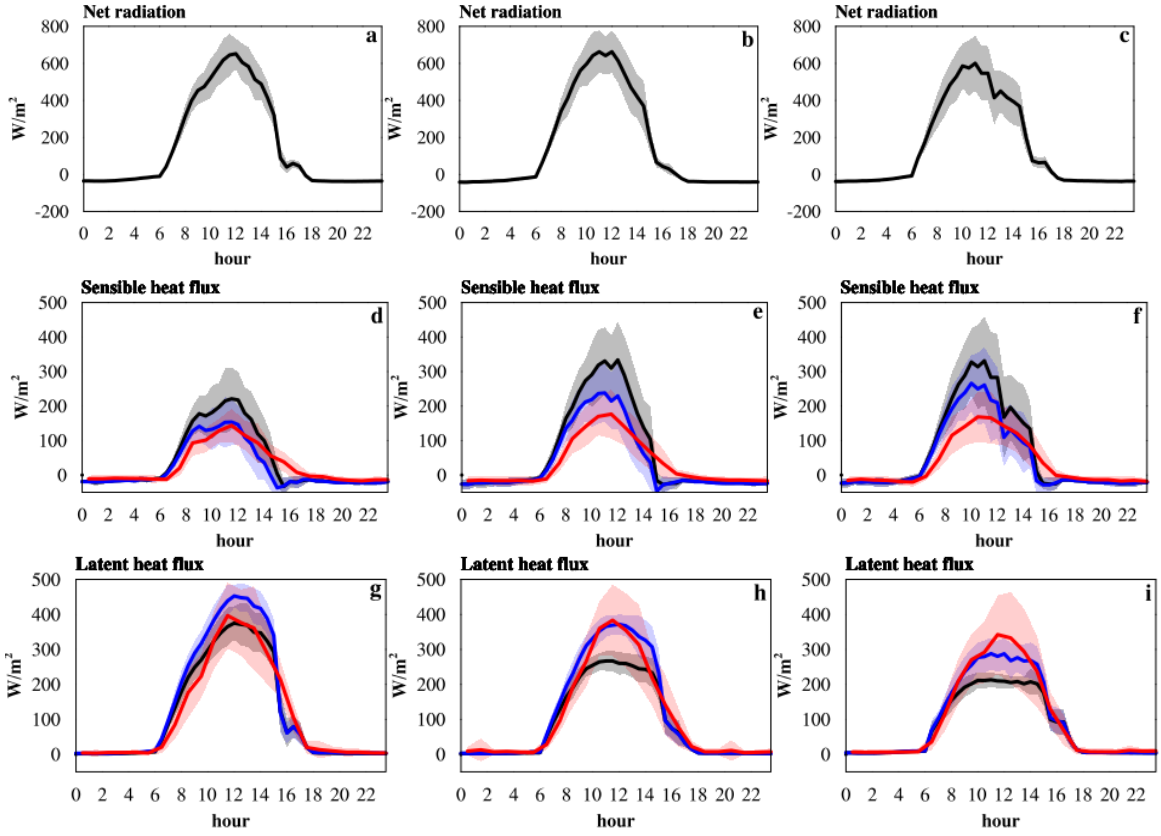

Figure 3.5. Monthly-averaged diurnal cycles of net radiation (a, b, and c), sensible heat flux (d, e, and f), and latent heat flux (g, h, and i) in August (a, d, and g), September (b, e, and h), and October (c, f, and i), 2002. Black, blue, and red colors represent CTL, EXP, and observations respectively. Solid lines are for monthly mean values and shadings are mean values ± standard deviation.

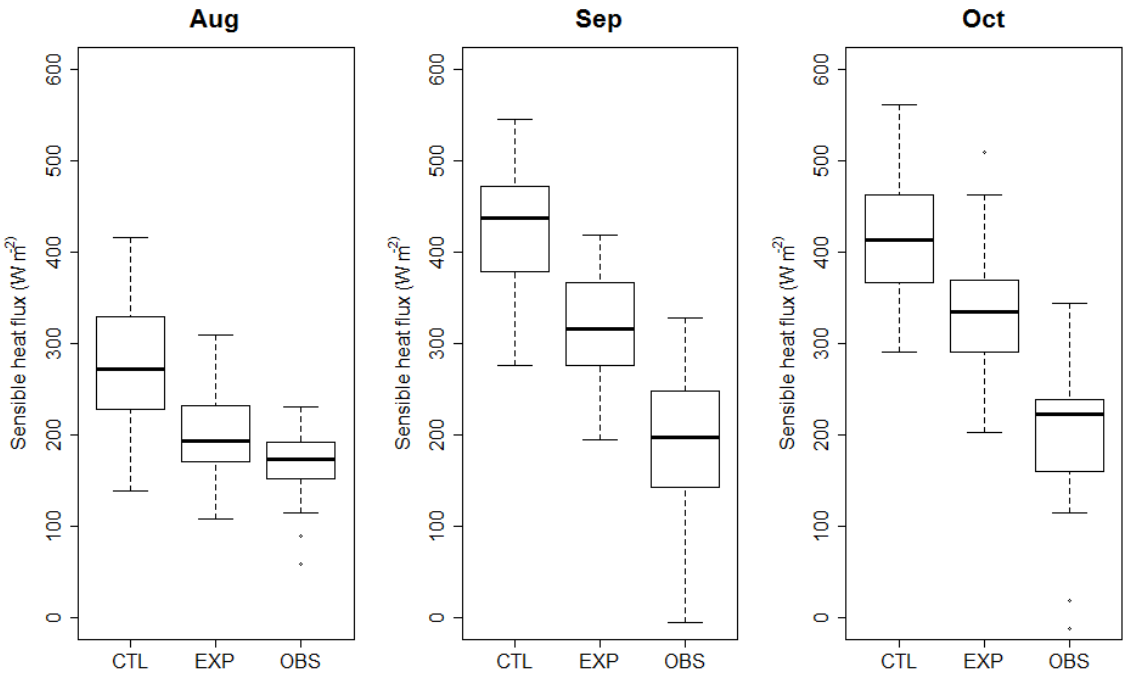

Figure 3.6. Peak values of sensible heat flux on daily basis for the three months in the 2002 dry season. The bottom and top of the box represent lower and upper quartiles (25th and 75th percentile), central bar indicates the median. The two ends of whiskers indicate 95% confident interval.

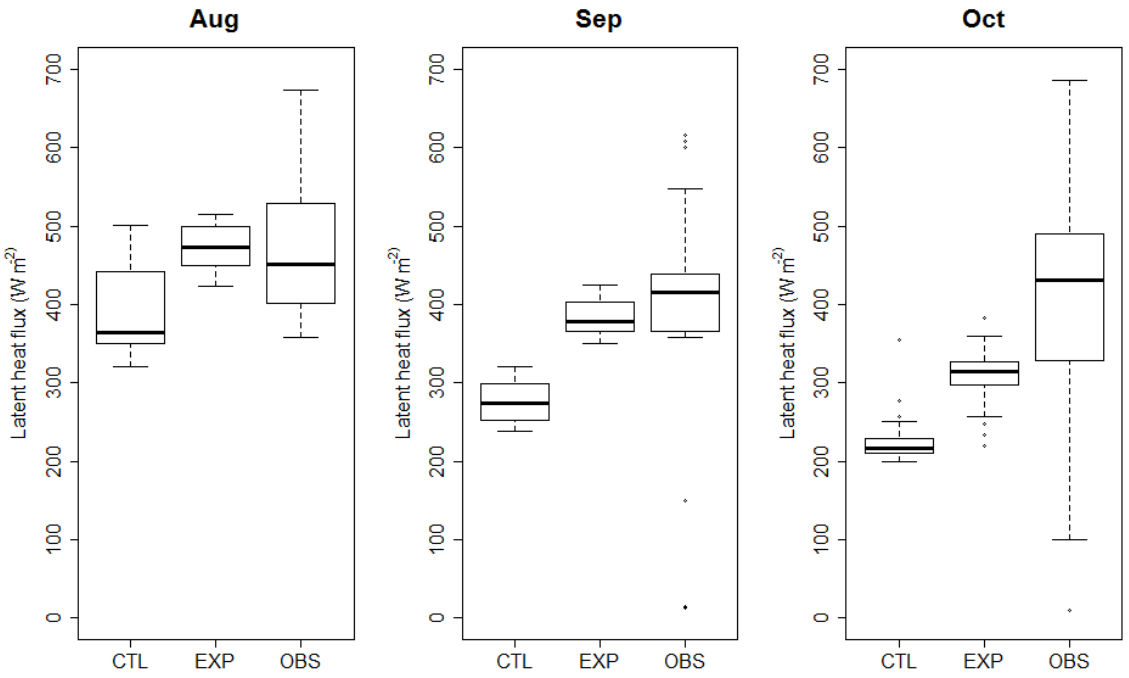

Figure 3.7. The same as Figure 3.6 but for latent heat flux.

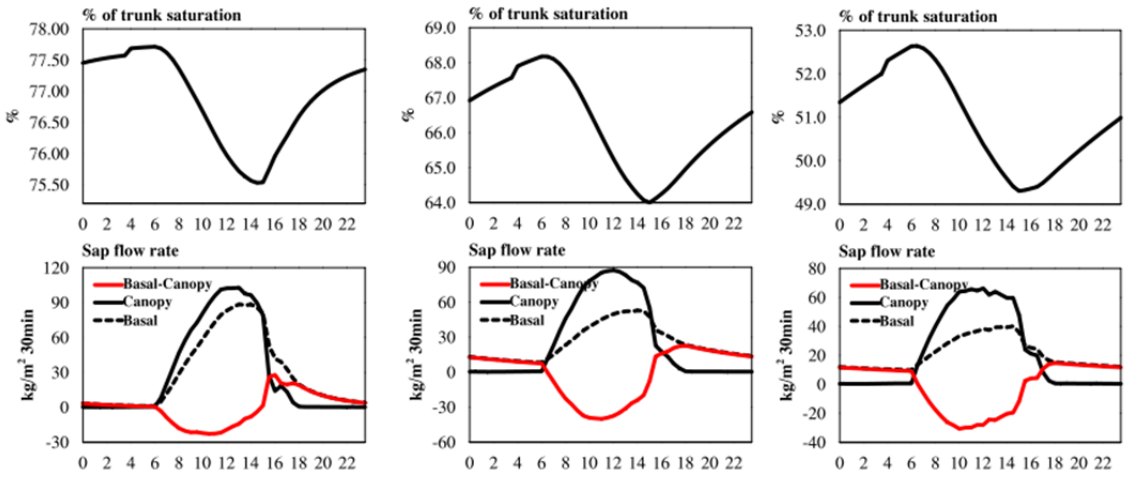

Figure 3.8. Monthly-averaged diurnal cycles of stem water content (top panels) and sap flow rates (bottom panels) from EXP during the dry season of 2002 (the three columns are for August, September, and October from left to right).

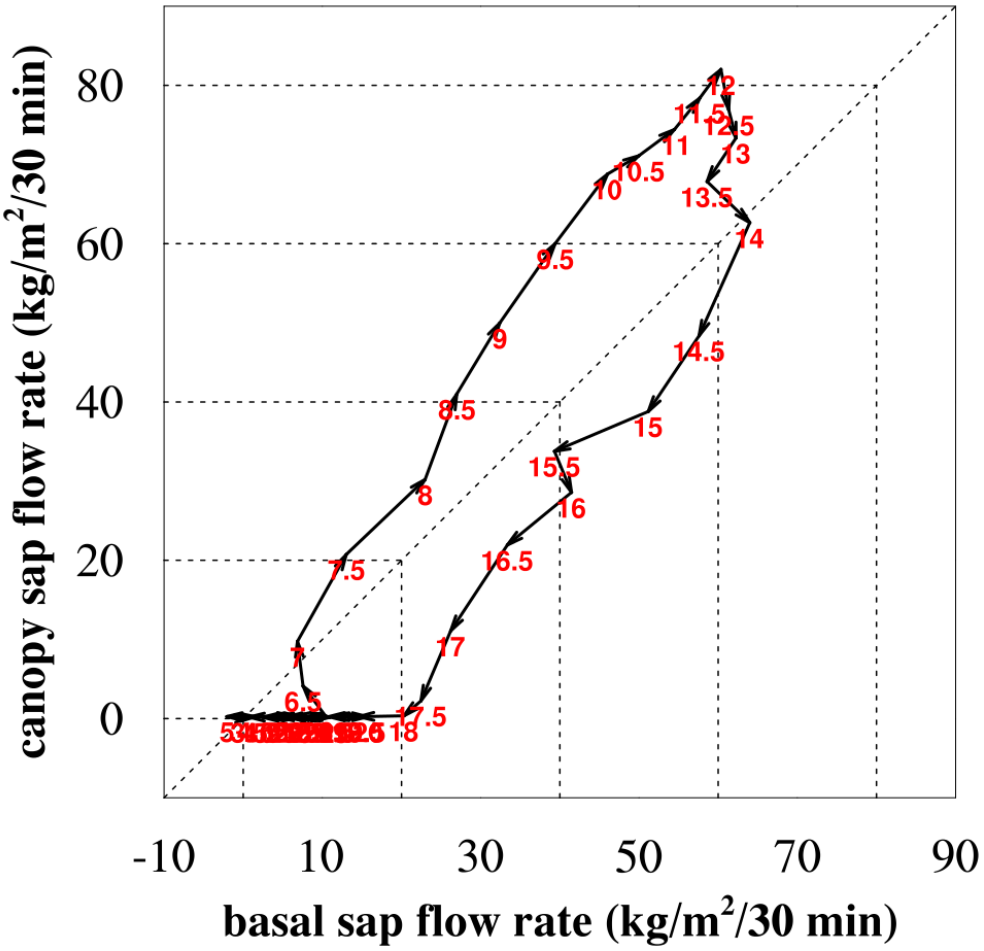

Figure 3.9. The onset and magnitude of the hysteresis between basal and canopy sap flows in August, 2002. Values in the figure are monthly mean.

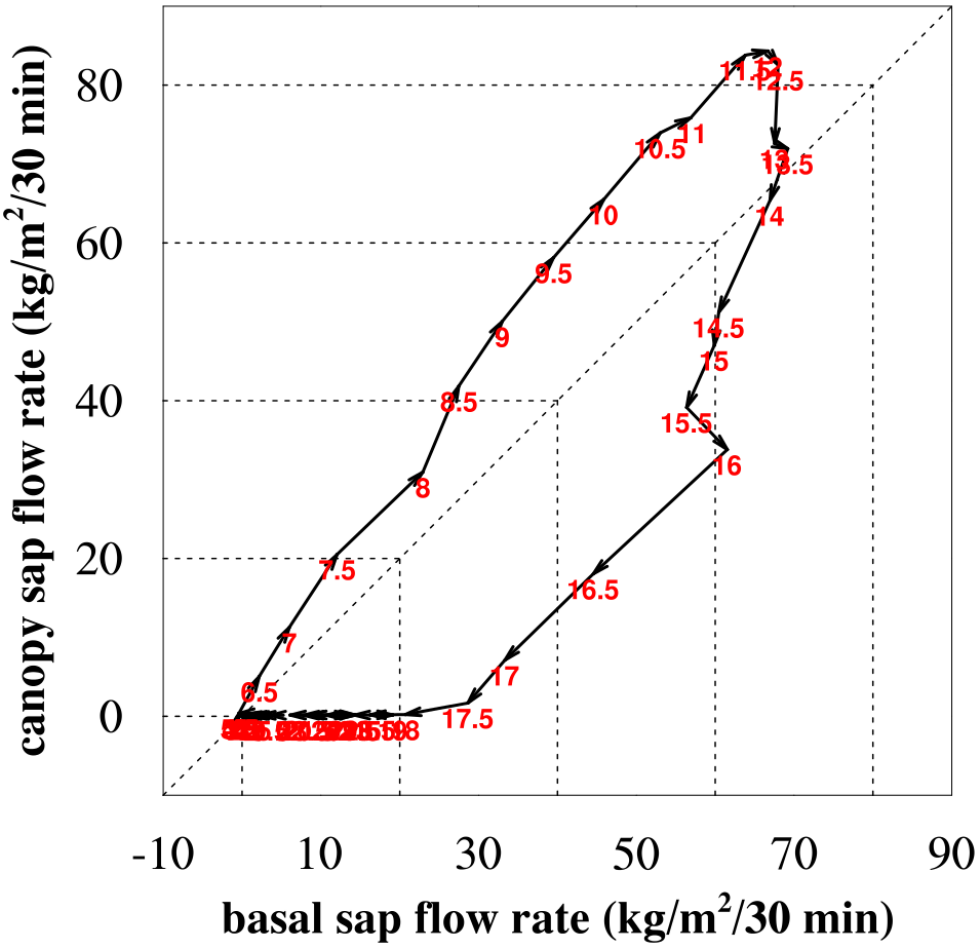

Figure 3.10. The same as Figure 3.9 but for September, 2002.

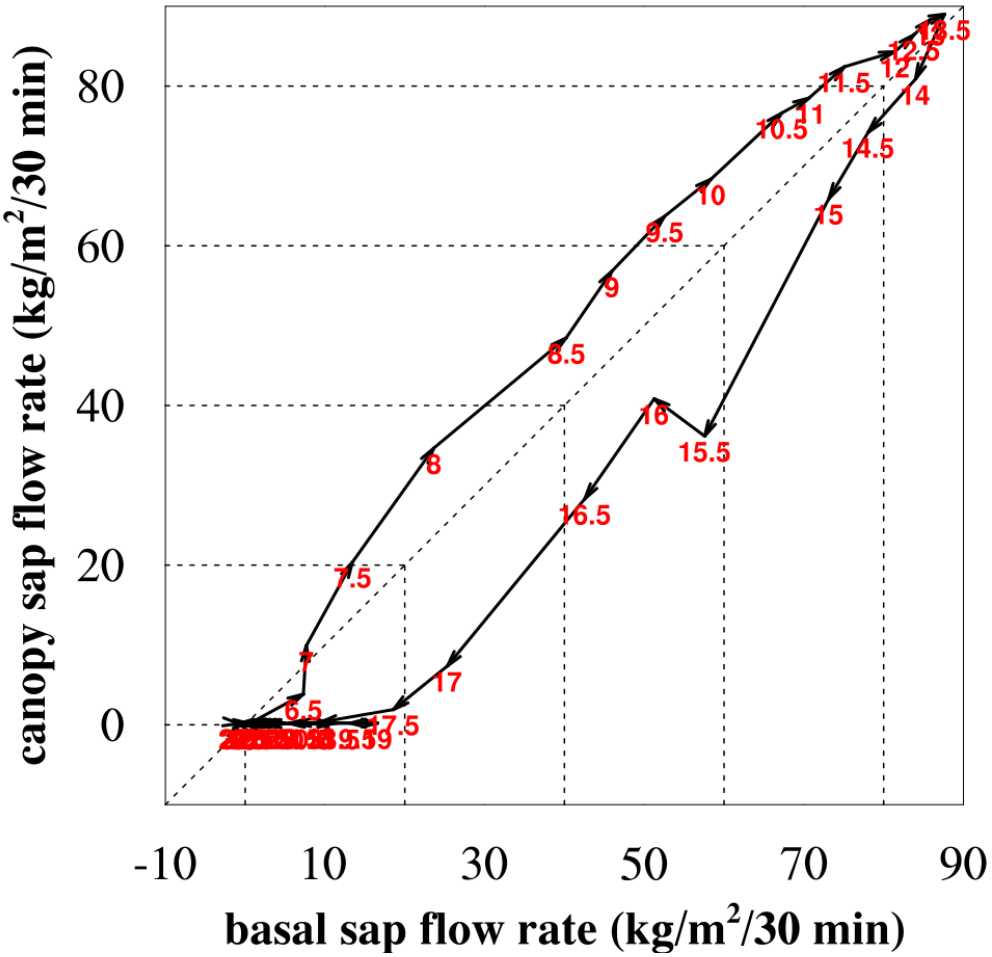

Figure 3.11. The same as Figure 3.9 but for October, 2002.

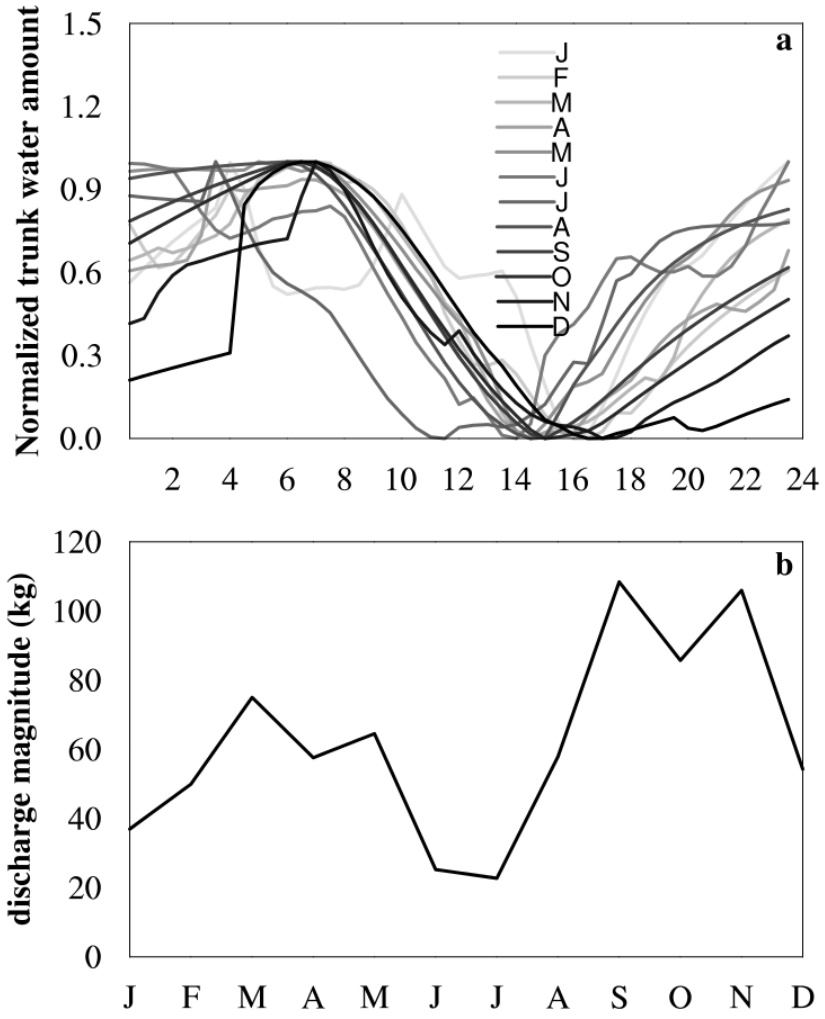

Figure 3.12. The seasonal evolution of diurnal cycles of the normalized trunk water amount (a) and the daily discharge magnitude (b) of a single tree.

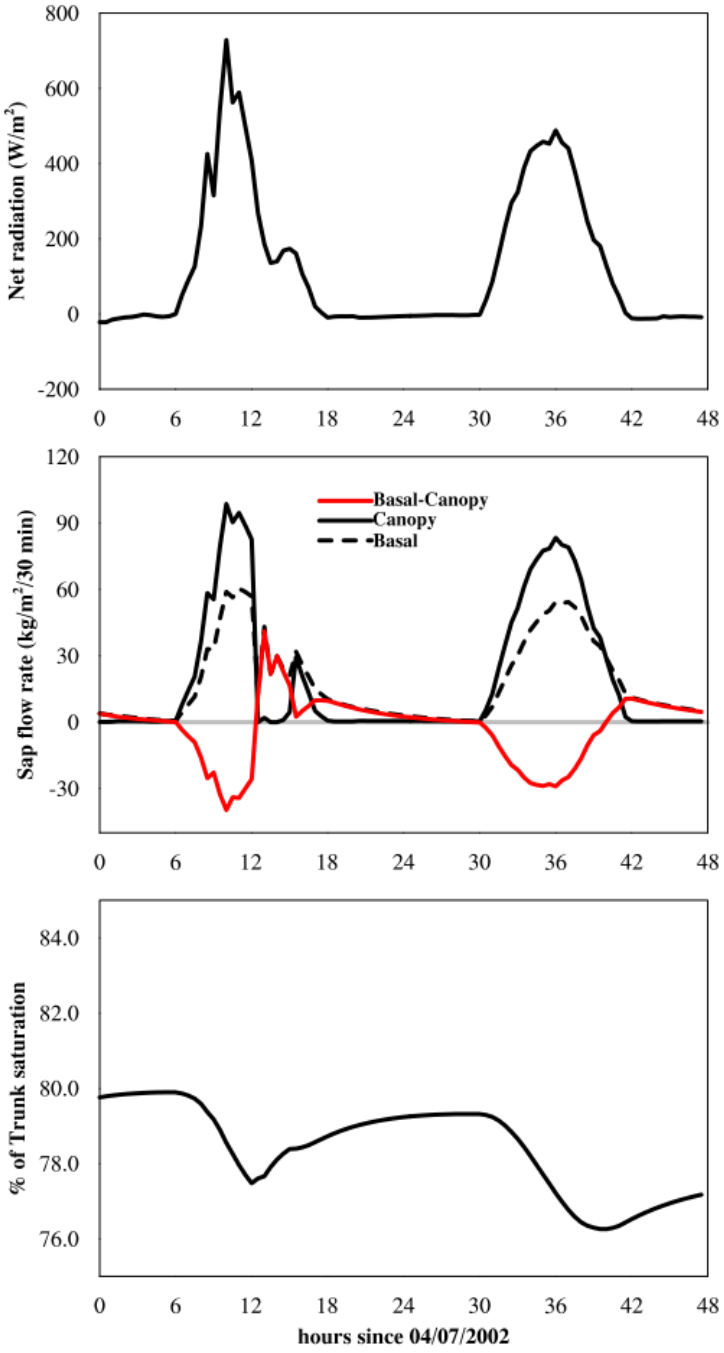

Figure 3.13. A comparison of net radiation (a), sap flow rate (b), and trunk saturation percentage (c) from two consecutive dates with one cloudy and one sunny indicates the dynamic nature of discharge and recharge processes.

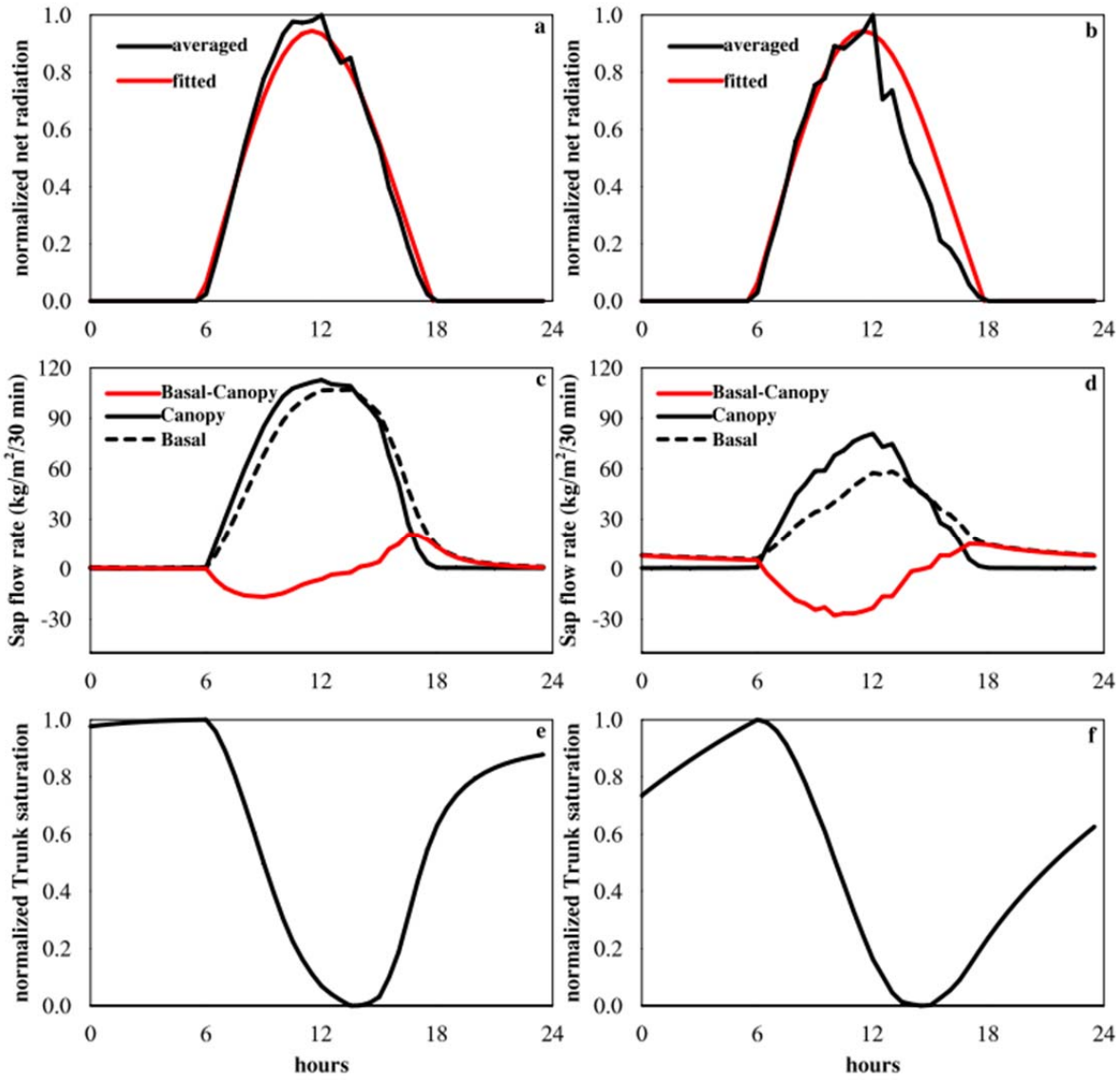

Figure 3.14. The same as Figure 3.13 but from a sample of several sunny (a, c, and e) and cloudy (b, d, and f) days.

CHAPTER 4: Seasonally asymmetric responses of Amazon forests to El Niño

4.1. ABSTRACT

El Niño Southern Oscillation (ENSO) events impose strong inter-annual signals on local climates and terrestrial ecosystem dynamics in many regions especially tropical forests (e.g. Wang et al., 1999; Dai et al., 1997; Prentice and Lloyd, 1998). Using satellite/ground observations and reanalysis data, we analyzed the spatial and temporal patterns of plant growth response to the warm phase of ENSO (i.e., El Niño) that result in below-normal precipitation over a large area across the Amazon basin. A "hotspot" region was identified as the area where ENSO events had the most pronounced influence on precipitation, and we focused our analysis on this region. The major finding is that the influence of El Niño events on vegetation growth differs between wet and dry seasons, with the former mainly controlled by radiation and the latter by water availability. With the on-going debates as to the magnitude and direction of Amazon forests response to drought (e.g. Philips et al., 2009; Salska et al., 2007), this study contributes to our understanding of how water and radiation control vegetation growth in Amazonia.

4.2. INTRODUCTION

As the largest tropical forest in the world, the Amazon rainforest stores about 86 billion tons of carbon (Saatchi et al., 2007), corresponding to a third of the total carbon storage inside tropical forests (Pan et al., 2011). It also plays key roles in the climate system through the exchange of energy, momentum, and mass between the atmosphere and land surfaces. Given its important role in fixing carbon and modulating regional and global climates, the inter-annual variations of the forest have received growing attention,

in terms of its greenness (Hilker et al., 2014), photosynthetic strength (Bastos et al., 2013), and area (Marle et al., 2016), wild fires (Alencar et al., 2006).

The El Niño Southern Oscillation (ENSO) is the strongest signal in the inter-annual variation of the ocean-atmosphere system (Wang et al., 1999). The warm phase of ENSO, also known as El Niño, causes reductions in precipitation over eastern Amazonia through its modifications of the Walker Circulation (Ropelewski and Halpert, 1989; Mason and Goddard, 2001). The strength of El Niño events has been found to be closely and linearly correlated with the spatial extent of drought in the Tropics (Dai et al., 1997; Lyon, 2004; Lyon and Barnston, 2005) and also the magnitude of precipitation anomalies (Gu and Adler, 2011).

Such interannual occurrence of drought has long been recognized to influence the Amazon ecosystem in many ways. It increases vegetation respiration and decreases photosynthesis leading to reduced net ecosystem productivity (Prentice and Lloyd, 1998). In addition, increased fires (Nepstad et al., 1999; Alencar et al., 2006; Page et al., 2008) and tree mortality (Williamson et al., 2000) have been observed, causing the Amazonian ecosystem to change from a carbon sink to carbon source (Prentice and Lloyd, 1998; Tian et al., 1998) and increase atmospheric CO_2 concentrations (Chiodi and Harrison, 2014), further contributing to global warming which could cause changes in El Niño as a feedback (Yeh et al., 2009).

The influence of El Niño on inter-annual changes of canopy greenness on large spatial scales, as detected by satellite observations of vegetation indices (VI), has been reported previously. Myneni et al. (1996) showed that the Normalized Difference Vegetation Index (NDVI) in the northeastern Brazil is negatively correlated with sea surface temperature (SST) anomalies of the Eastern Tropical Pacific (Nino-3 region)

from 1982 to 1990. Los et al. (2001) examined the co-variability of NDVI and precipitation on global scale during the 1980s and also showed negative precipitation and NDVI anomalies associated with positive SST anomalies in the equatorial Pacific Ocean. Poveda et al. (2001) have shown negative NDVI anomalies throughout the entire year during El Niño over almost the entire Amazon basin based on four El Niño events. Hilker et al. (2014) demonstrated a close link between El Niño events and browning areas defined by standardized anomalies in Moderate Resolution Imaging Spectroradiometer (MODIS) Enhanced Vegetation Index (EVI) lower than -1. Asner et al. (2000) found that ENSO events increase the annual amplitude of NDVI over southeastern Amazonia where ENSO events have the most pronounced influence on precipitation.

Those previous studies were limited in their short temporal coverage (about one decade) and consequently small number of El Niño events included in their study periods, inadequate from a statistical sampling viewpoint. Recent emergence of long-term observations of plant growth (e.g., the NDVI3g and FRAR3g, Zhu et al., 2013), however, provides us a unique opportunity to better understand and quantify El Niño impacts on vegetation growth over the Amazon tropical forests. In particular, long time series enable us to establish relations amongst El Niño, precipitation, and vegetation greenness beyond simply identifying some associations.

The seasonal variations of vegetation response to El Niño have been rarely studied. ENSO adds inter-annual signals on top of the dominant and strong seasonal cycle of precipitation. It is reasonable to hypothesize that the impact of ENSO-induced precipitation variation may differ between dry and wet seasons. With long-term remotely sensed vegetation index datasets, as well as observed and reanalysis precipitation data,

we examine the spatial patterns of precipitation and vegetation growth response to El Niño events and how these spatial patterns vary between dry and wet seasons.

4.3. METHOD

To monitor the onset and duration of El Niño events, two primary ENSO indices, the Oceanic Nino Index (ONI) and the Multivariate ENSO Index (MEI), are utilized. The ONI is calculated based on 3-month running mean of ERSST.v4 SST anomalies in the Niño 3.4 region from 1950 to present by National Oceanic and Atmospheric Administration (NOAA). MEI (Wolter et al., 1993) is calculated based on six observed variables including sea surface temperature, surface air temperature, and so on, over the tropical Pacific from 1950 to present. Hanley et al. (2003) evaluated several ENSO indexes including ONI and MEI according to their sensitivity to two phases of ENSO and concluded that MEI can detect ENSO events that are missed by other indexes.

Gridded monthly precipitation data from five different sources were used in this study. The Global Precipitation Climatology Project (GPCP) Version 2.2 combined precipitation dataset (Adler et al., 2003) developed and computed by the NASA/Goddard Space Flight Center's Laboratory provides monthly precipitation that combines observations and satellite data at 2.5×2.5 degree globally from January 1979 to October 2015. The Climatic Research Unit (CRU) Time-Series (TS) Version 3.23 of high resolution (0.5 degree) gridded data provides monthly precipitation from 1901 to 2014 (Harris et al., 2014). Daily precipitation from the WATCH Forcing Data methodology applied to ERA-Interim (WFDEI) reanalysis data (Weedon et al., 2014) was used to derive the monthly accumulated precipitation. A global 50-year near-surface meteorological forcing dataset was developed at Princeton University that combines observations and reanalysis data (Sheffield et al., 2006). We refer in this study to this

dataset as the Princeton forcing. It provides monthly precipitation at 0.5 degree globally from 1948 to 2014 (version 2). The 3-hourly precipitation from the Tropical Rainfall Measurement Mission Project (TRMM) Multi-satellite Precipitation Analysis (TMPA) 3B42V7 (Huffman et al., 2007) is also used here. This data covers 1998 to July 2015 at 0.25 degree resolution.

The downward shortwave radiation at the land surface from the Princeton forcing data (Sheffield et al., 2006) and Global Soil Wetness Project Phase 3 (GSWP3) forcing data were also downloaded.

Dry seasons are defined as the months with precipitation lower than their potential evapotranspiration (PET). We obtained the gridded monthly PET data from CRU TS3.23 (Harris et al., 2014) from 1982 to 2013 to determine Amazon dry seasons at each grid point.

To assess ecosystem dynamics in response to climate variations, we used three long-term satellite vegetation index/photosynthetic proxy observations that cover at least 30 years.

We used the two-band EVI (EVI2) (Jiang et al., 2008; Zhang et al., 2015), a special version of EVI that keeps the advantage of the latter, which is its enhancement of the vegetation signal by minimizing soil and atmospheric influences. However, instead of requiring three bands of surface reflectance, EVI2 uses only two of them, i.e., the blue band is eliminated in the calculation of EVI2 since it does not provide additional biophysical information on vegetation properties. EVI2 is widely used to study the dynamics of tropical ecosystems on the seasonal (e.g. Kim et al., 2007; Yan et al., 2016) and inter-annual (e.g. Zhang et al., 2014) time scales as well as biomass/carbon

estimation (e.g. Eckert, 2012; Mitchard et al., 2013). The EVI2 data we used is at a bi-weekly temporal resolution and 0.5 degree grid from 1982 to 2014.

Recently, a 31-year bi-weekly Global Inventory Modeling and Mapping Studies (GIMMS) normalized difference vegetation index version 3 (NDVI3g), from the Advanced Very High Resolution Radiometer (AVHRR), was published from July, 1981 to December, 2011 at 1/12 degree grids (about 8 km at the equator) (Pinzon and Tucker, 2014). This dataset has been effectively used to study the seasonal (e.g. Silva et al., 2013) and inter-annual (e.g. Erasmi et al., 2014) dynamics of Amazon rainforests.

The GIMMS fraction of absorbed photosynthetic active radiation (FPAR)3g was also produced based on GIMMS NDVI3g (Zhu et al., 2013). FPAR specifies the percentage of photosynthetic active radiation that is absorbed by vegetation. Compared with EVI2 and NDVI that describe the greenness of vegetation canopies, FPAR is more closely related to photosynthetic activity and thus is a proxy of photosynthesis strength. The GIMMS NDVI3g and FPAR3g data are available at http://cliveg.bu.edu/modismisr/lai3g-fpar3g.html.

To evaluate the reliability of these three vegetation index datasets, we compared them with MODIS EVI (collection 5) during their overlapping years (2000-2011). Comparison results are presented in the discussion section. Quite a large number of cross-comparisons between different vegetation indexes including the ones we used here have previously been published (e.g. Fensholt and Proud, 2012; Xu et al., 2013; Marshall et al., 2016).

Tropical evergreen broadleaf forests are identified from the standard MODIS land cover type data product (MCD12Q1) in The International Geosphere–Biosphere Programme (IGBP) Land Cover Type Classification (Friedl et al., 2010; Channan et al.,

2014). This product classifies ecosystems into 17 types at 0.5 degree over land surfaces. It is downloadable at http://glcf.umd.edu/data/lc/.

The above-mentioned datasets are also summarized in Table 4.1.

We first resample all the gridded data to 0.5×0.5 degree accounting for variations in grid areas caused by earth curvature. Grids other than tropical evergreen forest regions are masked based on the IGBP classifications. Unlike the treatment of the climate variables, the three bi-weekly vegetation indexes are converted into monthly means by picking the higher value of the two bi-weekly ones in a given month in order to reduce cloud contamination. We extract a period of 30 years (1982-2011) to match that of plant growth observations (we used only 14 years for TRMM from 1998 to 2011 due to its availability).

Based on the MEI and ONI data, the 30 years (1982-2011) are divided into three categories, El Niño years (10 years), La Niña years (7 years), and non-ENSO years (12 years). The years in each category are listed in Table 4.2. Due to our specific definition of a year, only 29 years are used instead of 30 years. We use the standardized anomalies of each variable, obtained as the difference of the composite means between El Niño years and no ENSO years divided by its standard deviation, in the analysis. We constructed the seasonal-average composites for the dry and wet seasons separately. In order to test the robustness of our results, an alternative anomaly definition is also used, which is based on the all-year climatology rather than non-ENSO-year climatology.

4.4. RESULTS

4.4.1. Spatial-temporal pattern of ENSO impact on precipitation

The correlation of monthly time series of ENSO indices and precipitation is calculated (Figure 4.1) to examine the spatial and temporal response of precipitation to ENSO events. In the computation of correlation, the time series of precipitation is lagged from the ENSO indices to give the maximum absolute correlation value, following previous studies (e.g. Gu and Adler, 2011). The linear trend and annual cycle have been removed from the precipitation time series before the calculation. Consistent with previous studies (e.g. Ropelewski and Halpert, 1989), a "hotspot" region with the highest negative value is identified, which is eastern Amazonia, i.e., precipitation variations in response to ENSO episodes are the strongest over this region, consistent with previous studies. Quantitatively, we further specified the hotspot region as the region where correlation is below a value of -0.3 (corresponding to all the pixels with blue shades in Figure 4.1) and focused on this hotspot region in the following analysis. Besides the highest sensitivity of precipitation over this region, a second reason for focusing our analysis on this region is presented in the discussion section.

Generally, the lag correlation map uses zero lag-month, indicating that the impact of ENSO on precipitation is immediate over the hotspot region. Since El Niño events usually start from June/July and last till the end of this year or even the boreal spring of the next year, and the influence of ENSO on precipitation is immediate over the hotspot region, we define a year as the 12 months from the July of this year to June of the next year. For example, the year 2001 is defined as from July 2001 to June 2002. Previous study has suggested that El Niño impacts on vegetation (implied by changes in atmospheric CO_2 concentration) are mainly from December of year 0 (the year that El

Niño starts) to August of year 1 (Chiodi and Harrison, 2014). Our definition of a year from July of year 0 to June of year 1 should well capture the signal of vegetation dynamics due to El Niño influences.

The spatial pattern of precipitation anomaly varies between dry and wet seasons (Figure 4.2). We observed a reduction in the dry-season precipitation over the entire hotspot region in El Niño years. In contrast, the wet-season precipitation anomaly shows a north/south division over the study region, with its northern portion associated with slight increase and its southern counterpart relatively stronger decrease. Wet-season precipitation is reduced more pronouncedly and less uniformly, consistent with previous studies (Adis and Latif, 1996; Tian et al., 1998; Marengo and Nobre, 2001), and the absolute reduction in monthly precipitation is weak with magnitude not exceeding 50 mm in the mean state. Two types of climatology are employed in the calculation of anomalies. One is the average of all 30 years (1982-2011) and the other is the average of all non-ENSO years. Both these definitions produce similar patterns of precipitation anomalies, but they differ in the magnitude with the latter associated with a stronger response (not shown).

4.4.2. Vegetation response

In the dry season, a negative anomaly is observed over nearly the entire hotspot region. In contrast, the wet-season VI anomaly shows a north-south pattern in opposition to the precipitation anomaly, i.e., a positive VI anomaly is associated with a negative precipitation anomaly and vice versa. The fact that VI varied with precipitation in the same direction in the dry season but opposite in the wet season suggests that different factors control plant growth in different seasons.

As previously stated, the dry season is defined as the months when precipitation is lower than PET, i.e., the period that precipitation cannot satisfy the demand of vegetation growth. Thus water availability is a key limiting factor at this time. Any further decline in the already very low precipitation during the seasonal dry spells should further limit plant growth by imposing even stronger water stress.

In the wet season, however, when precipitation is higher than plant demand, a slight decrease (the case in El Niño events) in precipitation is not sufficient to cause a water shortage for plants. Other factors, like radiation, may be controlling plant growth during this period. We see that the anomalies of shortwave radiation (Figure 4.4) and precipitation (Figure 4.2) are largely opposite in both dry and wet seasons. Over the hotspot region, the high agreement between the radiation anomalies and VI anomalies suggests that radiation limits plant growth in the wet season rather than precipitation. High cloud coverage or low sunlight has long been recognized as responsible for the decline in vegetation greenness in the wet season over the Amazon forests (Graham et al., 2003; Huete et al., 2006), but recently leaf age has been suggested as the cause (Wu et al., 2016; Lopes et al., 2016). The two explanations are reconciled by Brando et al. (2010) who suggested that leaf flushing that usually happens in coincidence with periods of increased radiation (Wright and van Schaik, 1994) could be a plant strategy to synchronize leaf flushing and tree water status.

The substantial cloud contamination may cause biases in satellite observations of VI in the wet season over the Amazon region (Samanta et al., 2012). According to the formulation of the two vegetation indexes, the presence of cloud depresses both NDVI (Huete et al., 2002; Motohka et al., 2011) and EVI2 (Motohka et al., 2011) with the latter less sensitive to cloud than the former (Motohka et al., 2011). It is possible that the

opposite signs of VI anomaly (Figure 4.3) and cloud anomaly (revealed by the negative radiation anomaly; Figure 4.4) noted above is at least in part a product of cloud contamination. In order to reduce cloud influences, we have picked the higher of the two values contained in a given month to generate monthly vegetation index, which is a common practice for this purpose (e.g. Guan et al., 2015). However, we are aware that we cannot fully exclude the possibility that the wet-season pattern we see here is not generated at least in part by this data issue.

These seasonal and spatial variations of limiting factors that control vegetation growth in dry and wet seasons in response to El Niño events are further illustrated in Figures 4.5 and 4.6. In the dry season, the anomalies in vegetation index largely agree with the anomalies in precipitation in terms of signs over the entire hotspot region, indicating the limiting role of precipitation in this season. In the wet season, the signs in anomalies of vegetation index and radiation are generally more agreeable especially over the southern portion hotspot region.

Because many satellite observations of vegetation indexes are obtained from a combination of AVHRR and another satellite sensor (e.g. MODIS) leading to possible mismatching issues around the connecting year, we further look at the sub-periods of 1982-1999 and 2000-2011 separately. These results still hold for the former, but not for the latter. This could be explained by the intensified El Niño events during the 1980s and 1990s (Dai et al., 1998; Schongart et al., 2004) in contrast to 2000-2011 when none of the El Niño events have reached a very strong level.

4.5. CONCLUSION

El Niño generally reduces precipitation over the entire Amazon forests, as is revealed by the significantly negative correlation between monthly precipitation and

ENSO indexes, with the eastern portion influenced the most. This region is defined as the "hotspot" region on which the analysis is focused. Composite analysis shows that the influence of El Niño events on precipitation varies seasonally. We observed a reduction in the dry season precipitation over the entire hotspot region during El Niño events. However, the wet-season precipitation anomaly shows a north/south gradient, with the northern portion associated with slight increase and southern counterpart a stronger decrease. Vegetation indexes correlate positively with precipitation in the dry season, but negatively in the wet season. The anomaly in shortwave radiation suggests that the response of vegetation growth in the wet season may be controlled by radiation rather than moisture. The depressed vegetation index in response to increased cloud fractions (corresponding to decreased radiation to some extent) in the wet season, however, could possibly be a result of cloud contamination. Further analysis is still needed to unravel the true mechanism. In summary, the results indicate a seasonal switch between precipitation and radiation in regulating El Niño impacts on vegetation indices over Amazon forests.

4.6. DISCUSSION

4.6.1. Comparisons of datasets

The persistent presence of both cloud and fire-induced aerosols make it very challenging for satellite sensors to obtain an unbiased signal from the land surface over the Amazon forest region (Samanta et al., 2012), leading to possible discrepancies among individual datasets and limitations in tropical studies.

We compared the three long-term VIs used in the study and MODIS EVI for their overlapping years (2000-2011) in terms of monthly time series, climatologically annual cycles, and annual mean time series. Spearman correlations of monthly time series

between any combinations of two products shown in Figure 4.7 illustrate the high reliability of remotely sensed vegetation index over the hotspot region, which is the second reason for focusing our analysis on this region.

MODIS EVI is a widely-accepted vegetation index in tropical studies (e.g. Guan et al., 2015). It is based on MODIS Terra observations and thus only exists after 2000, which is too short for our study. After 2000, there were only 4 El Niño events, none of which reached the very strong level as defined by the ONI or MEI, except the most recent one starting from 2015 and developing into 2016. However, the 2015/2016 El Niño event is not included in our study due to the lack of most of the data we used.

Five precipitation datasets and two solar radiation datasets are also compared in Figures 4.8 and 4.9. They are quite consistent with each other especially in the hotspot region.

4.6.2. Whether the changes in El Niño years are detectable?

Probability density distributions of GPCP precipitation and EVI2 for El Niño years and non-ENSO years during dry and wet seasons are shown in Figures 4.10 and 4.11. A clear shift of both variables to lower values in El Niño years compared with non-ENSO years are seen in both dry and wet seasons. Student's t test indicates that this shift is significant with a p value lower than 0.01. This shift is also tested for all other precipitation data, vegetation data, and downward shortwave radiation data. Their mean values and p values are listed in Table 4.3. Small p values (<0.01) are seen for all variables from all sources except dry-season TRMM precipitation. TRMM precipitation data is available only after 1998. As mentioned in Section 4.4.2, El Niño events are intensified during the 1980s and 1990s (Dai et al., 1998; Schongart et al., 2004) in

contrast to 2000-2011. During the latter period (2000-2011), none of the El Niño events reached a very strong level.

4.6.3. Robustness

Our results are tested to be robust by including several available products for the same variables, for example, five monthly precipitation datasets are included in the study. They differ in generation approaches (satellite observations, ground measurements, reanalysis data), developing groups, spatial resolutions, and so on. The seasonal variations and spatial patterns of precipitation response to ENSO events agree remarkably well among all these products. Figure 4.12 shows the number of products that agree in the same sign of dry- and wet-season anomalies. In the dry season, regions with at least four products agreeing in the same sign of anomalies covers 65.74% (anomalies based on non-ENSO year climatology) and 67.80% (anomalies based on all-year climatology) of all grids, among which a large proportion is supported by all the five products (40.30% and 43.38% of all grids). The agreement is even higher for the wet-season precipitation anomalies (71.58% and 75.51% of all grids are associated with at least 4 products that agree with each other in the same sign of anomalies based on different types of climatology).

4.7. ACKNOWLEDGEMENT

This work was supported as part of the Next Generation Ecosystem Experiments-Tropics, funded by the U.S. Department of Energy, Office of Science, Office of Biological and Environmental Research. We are grateful to all the data providers for making this study possible. We especially would like to thank Dr. Xiaoyang Zhang from South Dakota State University for preparing the gridded bi-weekly EVI2 data. The help

from Dr. Myneni on obtaining and utilizing GIMMS NDVI3g and FPAR3g data is greatly appreciated. We also would like to thank Dr. Hyungjun Kim from The University of Tokyo for instructions on using GSWP3 forcing data.

Abbreviation	Full Name	Spatial Resolution	Temporal Resolution	Organization	Reference
MEI	Multivariate ENSO Index	NA	3-month running mean		Wolter et al., 1993
ONI	Oceanic Nino Index	NA	3-month running mean	National Oceanic and Atmospheric Administration (NOAA)	
GIMMIS NDVI3g	Global Inventory Modeling and Mapping Studies (GIMMS) normalized difference vegetation index version 3 (NDVI3g)	1/12 degree	Bi-weekly		Pinzon and Tucker, 2014
GIMMIS FPAR3g	GIMMS fraction of absorbed photosynthetic active radiation (FPAR)3g	1/12 degree	Bi-weekly		Zhu et al., 2013
EVI2	two-band Enhanced Vegetation Index (EVI)	0.5 degree	Bi-weekly		Jiang et al., 2008; Zhang et al., 2015
GPCP precipitation	Global Precipitation Climatology Project (GPCP) Version 2.2 combined precipitation dataset	2.5 degree	monthly	NASA/Goddard Space Flight Center's Laboratory	Adler et al., 2003
CRU precipitation	Climatic Research Unit (CRU) Time-Series (TS) Version 3.23 of high resolution gridded data	0.5 degree	monthly	Climatic Research Unit (CRU)	Harris et al., 2014

Table 4.1. A list of data used in this study.

TRMM precipitation	Tropical Rainfall Measurement Mission Project (TRMM) Multi-satellite Precipitation Analysis (TMPA) 3B42V7	0.25 degree	3-hourly	NASA	Huffman et al., 2007
WFDEI precipitation	WATCH Forcing Data methodology applied to ERA-Interim (WFDEI) reanalysis data	0.5 degree	daily	The EU WATCH project	Weedon et al., 2014
Princeton precipitation	a 50-Year High-Resolution Global Dataset of Meteorological Forcings for Land Surface Modeling (version 2)	0.5 degree	monthly	Princeton University	Sheffield et al., 2006
Princeton radiation	a 50-Year High-Resolution Global Dataset of Meteorological Forcings for Land Surface Modeling (version 2)	0.5 degree	monthly	Princeton University	Sheffield et al., 2006
GSWP-3 radiation	Global Soil Wetness Project Phase 3 (GSWP3) forcing data	0.5 degree	monthly	Global Soil Wetness Project Phase 3 (GSWP3)	
CRU PET	Climatic Research Unit (CRU) Time-Series (TS) Version 3.23 of high resolution gridded data	0.5 degree	monthly	Climatic Research Unit (CRU)	Harris et al., 2014
IGBP classification	The International Geosphere–Biosphere Programme (IGBP) Land Cover Type Classification	0.5 degree			Friedl et al., 2010; Channan et al., 2014

Table 4.1 continued.

Category	Years
El Niño	1982, 1986, 1987, 1991, 1994, 1997, 2002, 2004, 2006, 2009
La Niña	1984, 1988, 1995, 1998, 1999, 2007, 2010
Non-ENSO	1983, 1985, 1989, 1990, 1992, 1993, 1996, 2000, 2001, 2003, 2005, 2008

Table 4.2. A list of El Niño years, La Niña years, and non-ENSO years.

	Dry Season			Wet Season		
	El Niño	Non ENSO	p value	El Niño	Non ENSO	p value
GPCP precipitation	61.51 mm	63.86 mm	<0.01	239.3 mm	250.01 mm	<0.01
CRU precipitation	52.27 mm	54.43 mm	<0.01	237.33 mm	246.70 mm	<0.01
WFDEI precipitation	56.51 mm	58.27 mm	<0.01	247.64 mm	257.30 mm	<0.01
Princeton precipitation	52.30 mm	54.42 mm	<0.01	237.41 mm	246.62 mm	<0.01
TRMM precipitation	56.85 mm	57.31 mm	0.169	255.34 mm	261.69 mm	<0.01
Princeton RSDS	217.46 W/m^2	216.15 W/m^2	<0.01	188.76 W/m^2	187.08 W/m^2	<0.01
GSWP3 RSDS	218.61 W/m^2	216.75 W/m^2	<0.01	189.83 W/m^2	186.23 W/m^2	<0.01
EVI2	0.51	0.51	<0.01	0.49	0.50	<0.01
NDVI3g	0.77	0.78	<0.01	0.72	0.72	<0.01
FPAR3g	0.86	0.87	<0.01	0.87	0.87	<0.01

Table 4.3. Mean values in El Niño years and non-ENSO years for each variable.

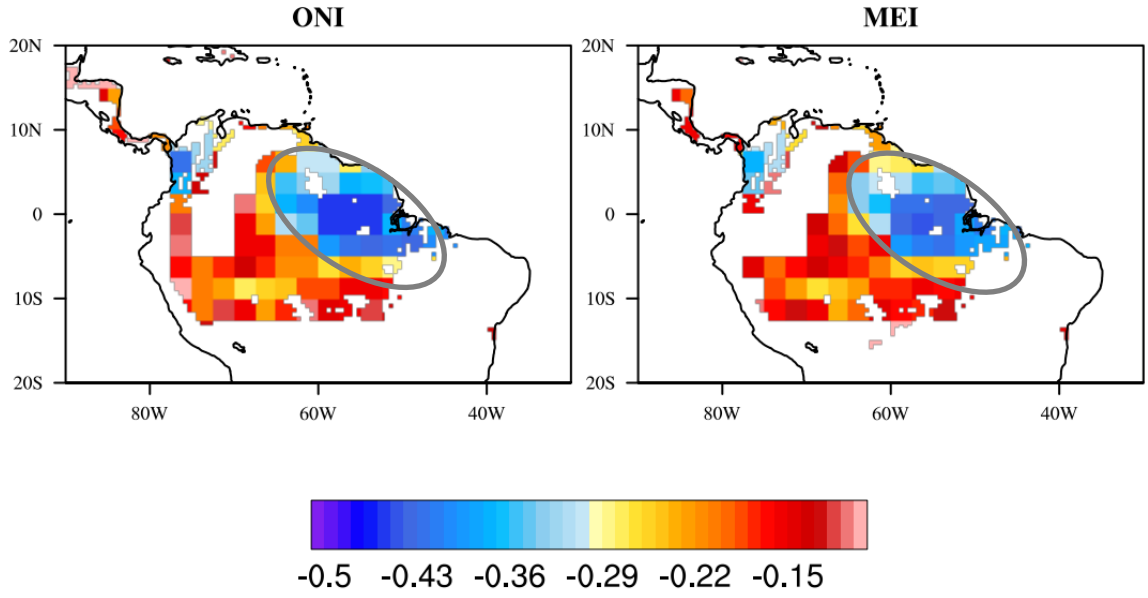

Figure 4.1. Correlations of ENSO indices and precipitation (GPCP precipitation data is used here) on monthly timescale. Values with $p<0.05$ are shown. Blue pixels indicate the hotspot region as highlighted by a grey circle.

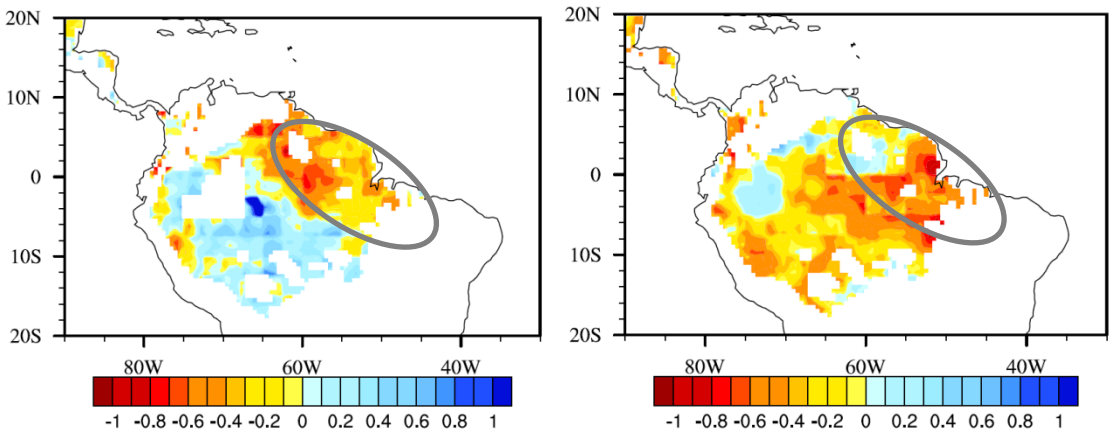

Figure 4.2. Standardized precipitation anomalies during dry (left) and wet (right) seasons (left) in the El Niño years based on climatology of all non-ENSO years. Precipitation anomaly is the mean value of precipitation anomalies from five precipitation datasets. Blank areas in the left panel indicate missing values due to the lack of dry season months. The hotspot region is highlighted by a grey circle.

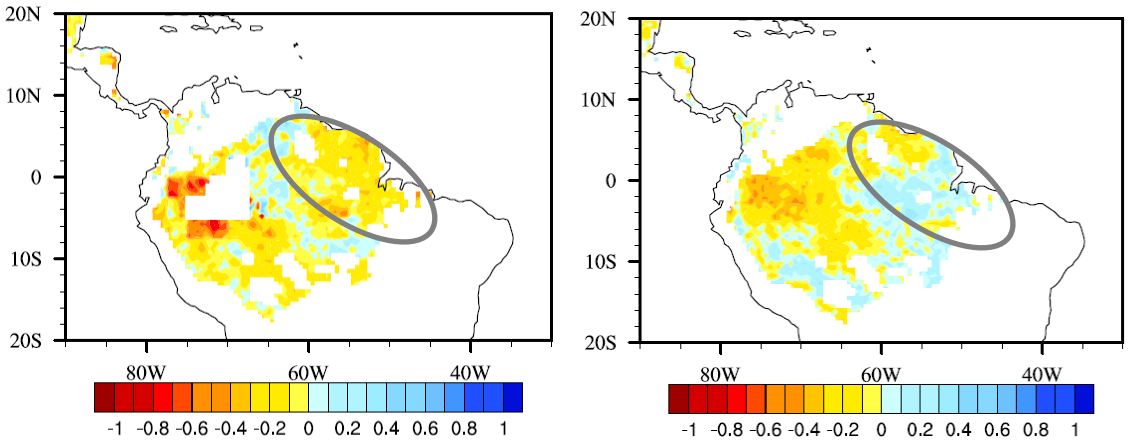

Figure 4.3. Standardized anomaly of VI in the dry (left) and wet (right) seasons during the El Niño years based on climatology of all non-ENSO years. Hotspot region is highlighted by a grey circle.

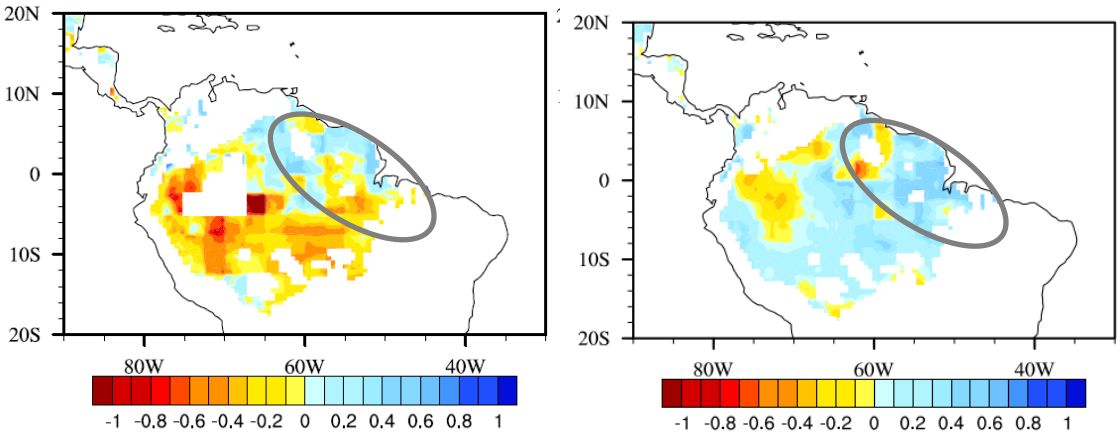

Figure 4.4. Standard anomaly of dry-season (left) and wet-season (right) downward shortwave radiation in El Niño years based on climatology of all non-ENSO years.

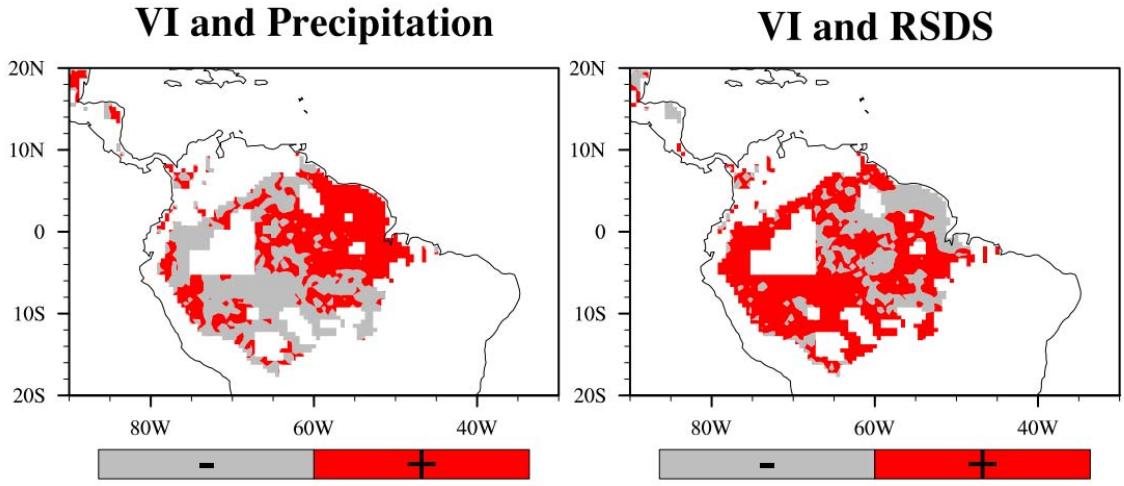

Figure 4.5. The agreement in signs of variable anomalies in the dry season. + and – represent that the signs of the two variables are the same and opposite respectively.

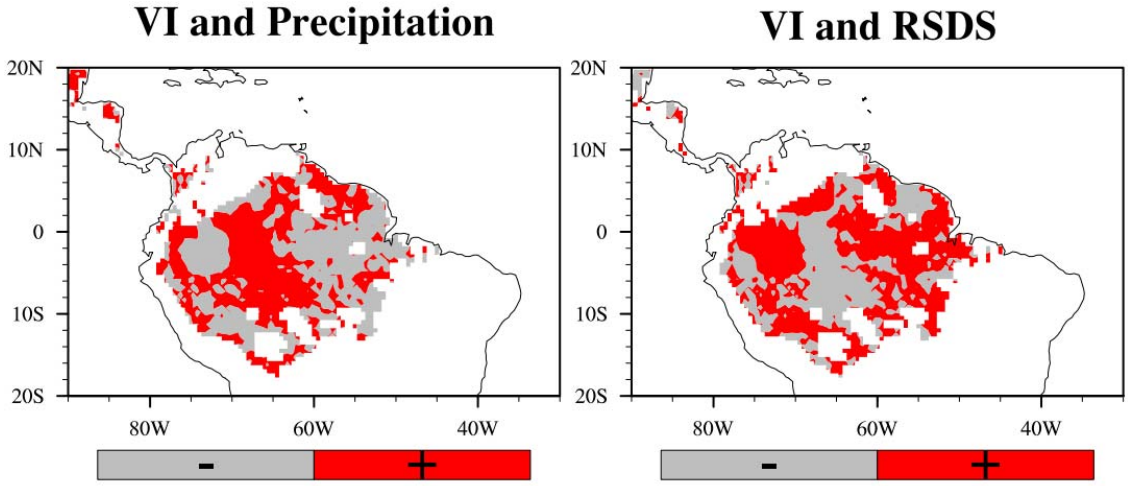

Figure 4.6. The same as Figure 4.5 but for the wet season.

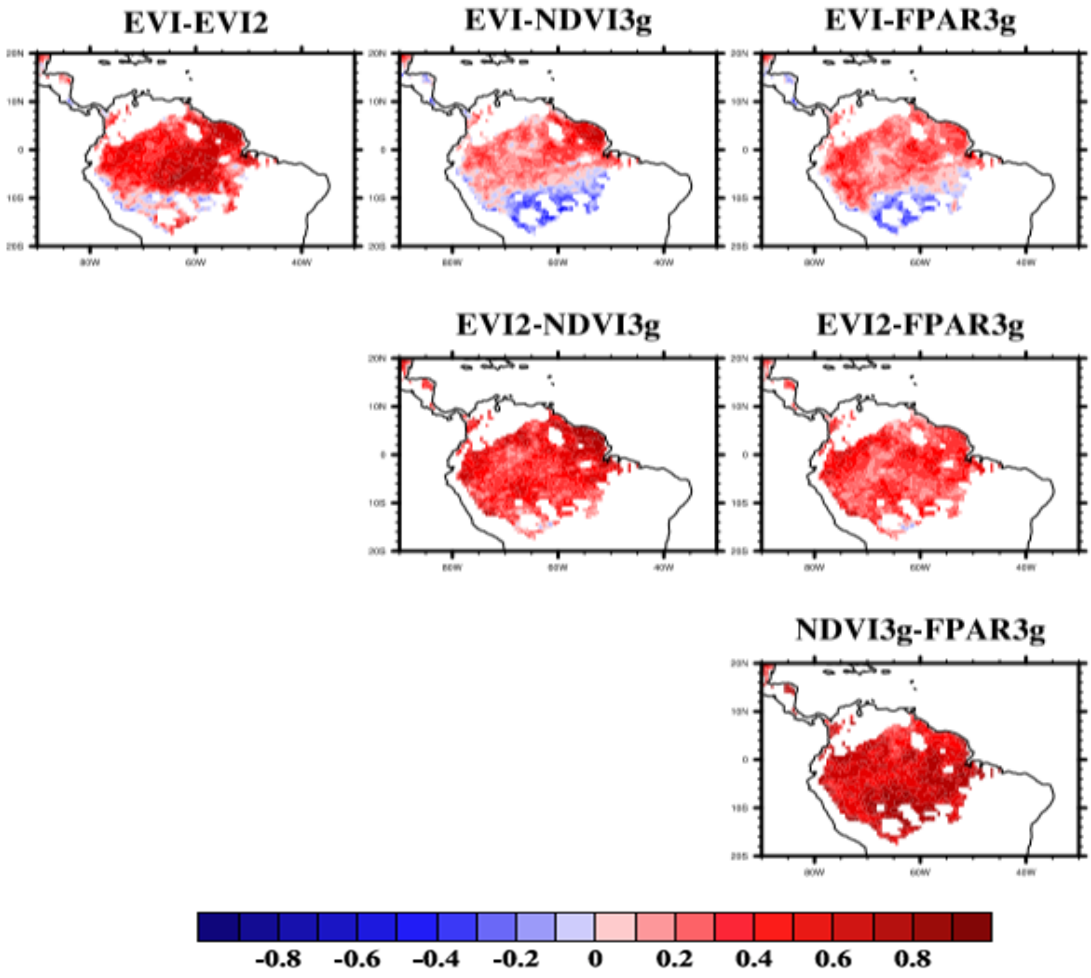

Figure 4.7. Spearman correlations between different satellite observations.

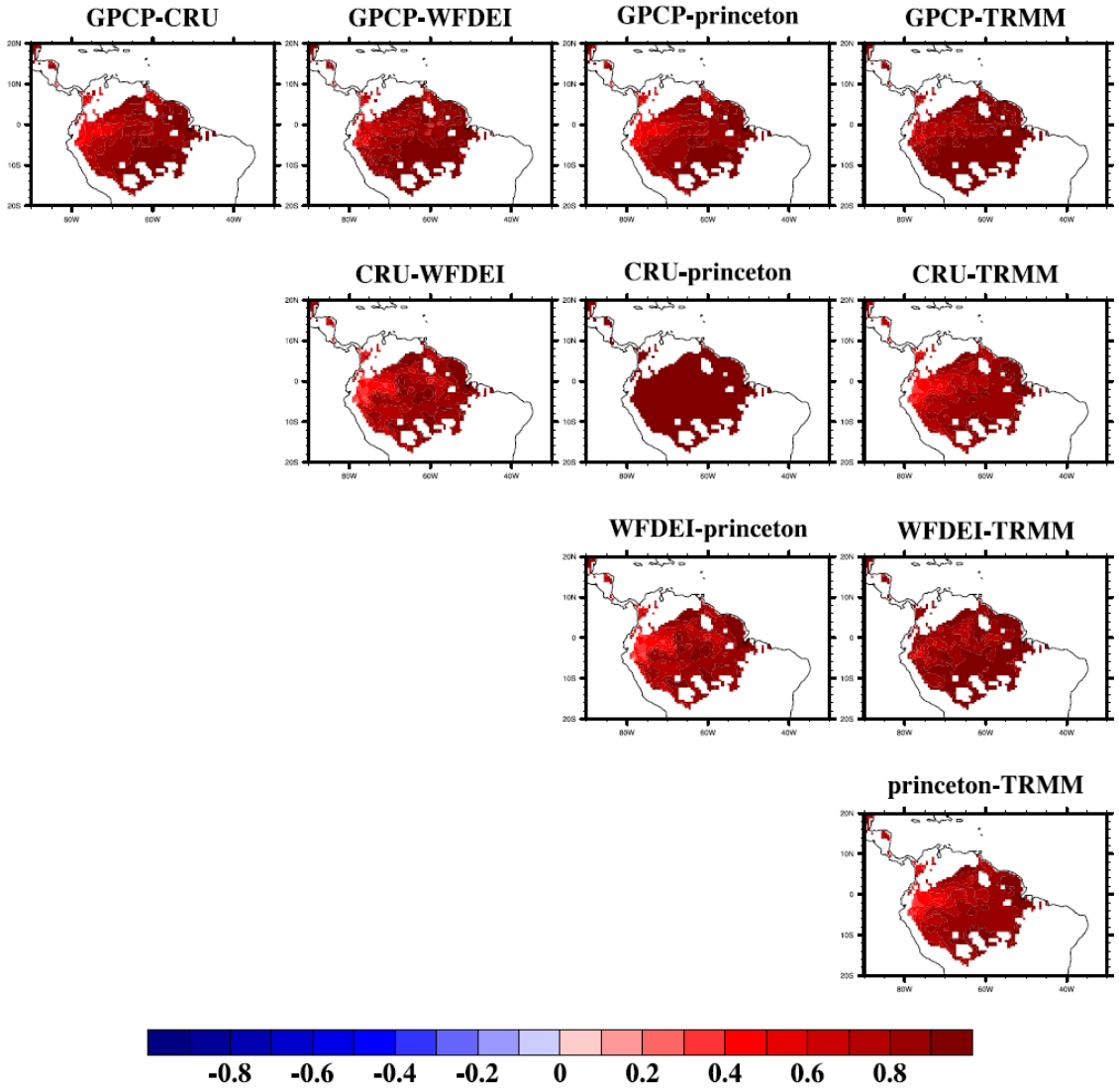

Figure 4.8. Spearman correlations between different precipitation data.

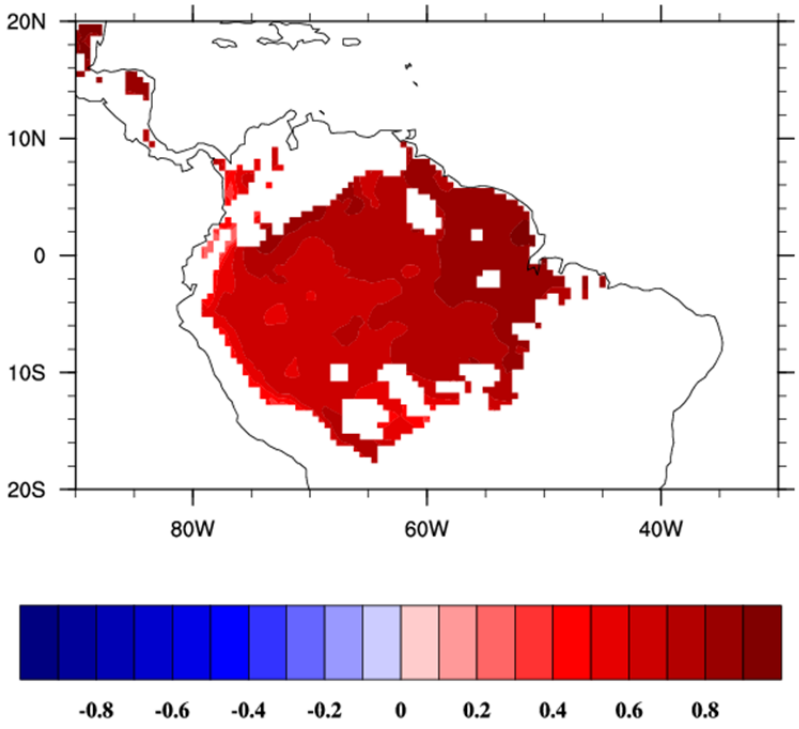

Figure 4.9. Spearman correlation of downward shortwave radiation from Princeton forcing and GSWP3.

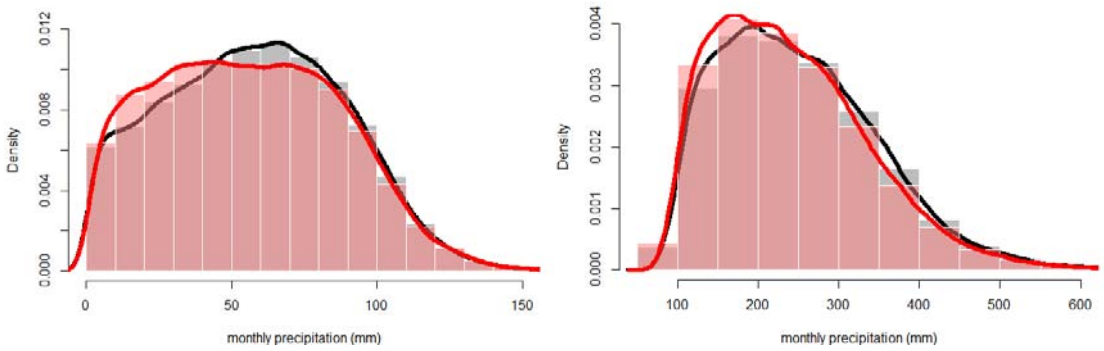

Figure 4.10. Probability density of GPCP precipitation over the whole Amazon forest region for the dry (left) and wet (right) seaons. Red bars and curves represent El Niño years and black non-ENSO years.

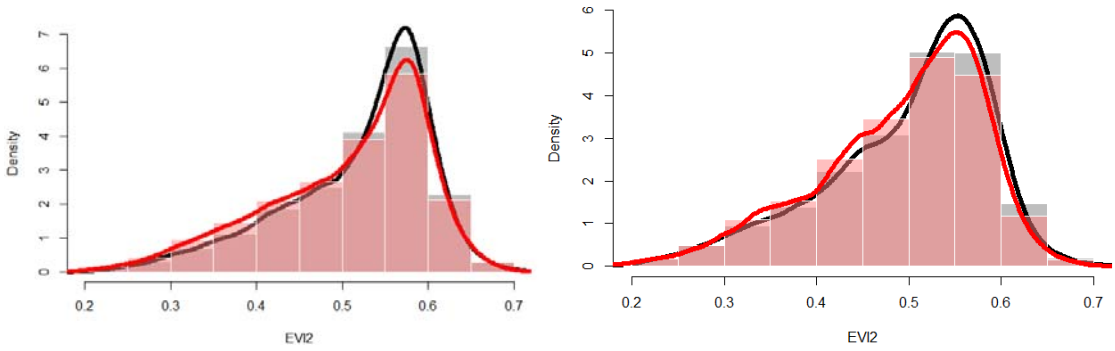

Figure 4.11. The same as Figure 4.10 but for EVI2.

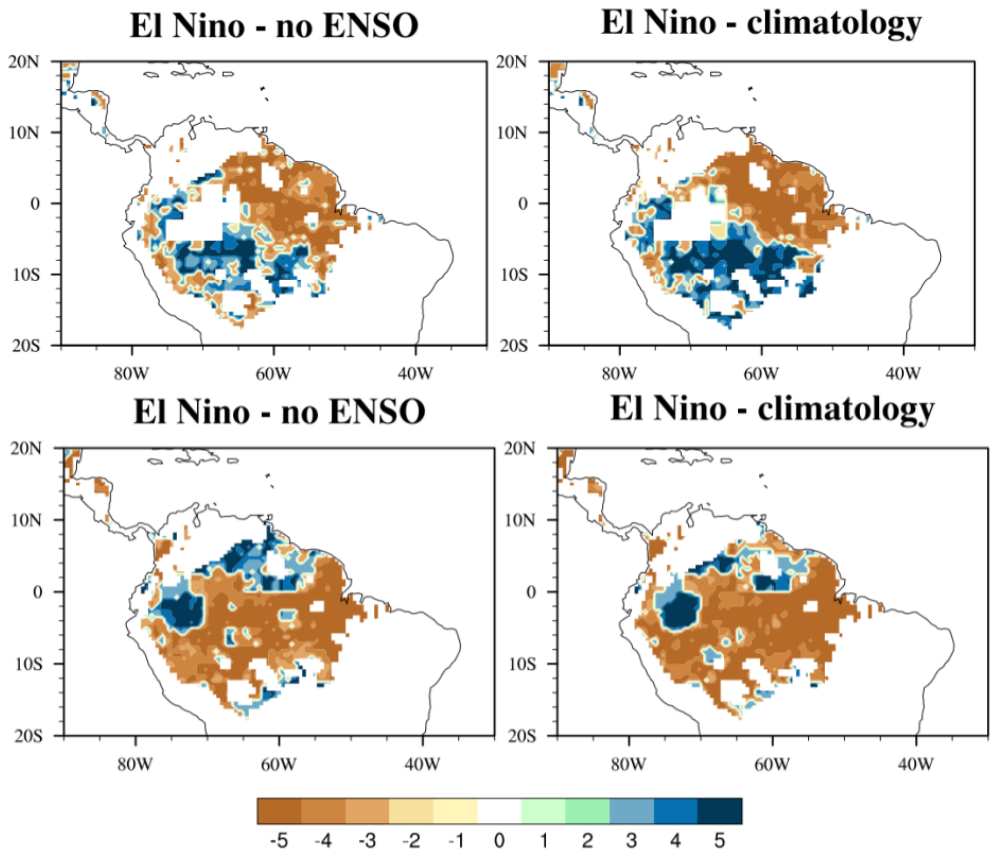

Figure 4.12. The agreement in the sign of dry-season (top panel) and wet-season (bottom panel) precipitation anomaly among five different precipitation datasets. Colors denote the number of products that agree in the same direction of precipitation change based on non-ENSO year climatology (left) and all year climatology (right). Positive/negative value illustrates the number of products that agree in the positive/negative anomaly.

CHAPTER 5: Summary and future work

5.1. SUMMARY

This dissertation is focused on understanding how the Amazon forest responds to water stress both via modeling and analysis of observed and reanalysis data. The seasonal dry spell that lasts1 to 6 months from northwest to southeast of the basin is the first type of water stress considered in this thesis. The first two main chapters (Chapters 2 and 3) are devoted to incorporating well-known drought-coping mechanisms of trees into the Community Land Model (CLM), the land component of NCAR's Community Earth System Model (CESM). We evaluated the performance of the revised model by assessing whether the underestimation of dry-season water and energy fluxes can be corrected. Then Chapter 4 focuses on how the El Niño events, which cause wide-spread below-normal precipitation anomalies over large areas across the basin especially over the eastern portion, influence vegetation growth on the inter-annual time scale. The seasonal difference of ENSO impact has also been studied.

Chapter 2 focuses on the function of fine roots in redistributing water down the water potential gradient between two soil depths. It is a more efficient way of water redistribution than water diffusion directly between two adjacent soil layers since it provides a low-resistance pathway between any two soil layers, even if they are very far away in distance. The parameterization was developed by previous study. We incorporate this mechanism into CLM4.0 and run site-level simulations at several sites in the Amazon basin. The default CLM4.0 model, without the hydraulic redistribution by roots, underestimates dry-season evapotranspiration and latent heat flux, which is a widely known bias. With the new mechanism incorporated, the simulation shows that the observed vegetation resistance to dryness is better captured. Higher plant water

availability is obtained via the ability to extract more water from the soil during water shortage periods. The deep soil layers where more water is available are taken advantage of during dry periods. However, it should be noted that if a drought is long enough, as with the artificial long drought during the 5-year rainfall exclusion experiment (Engelbrecht and Kursar, 2003), the impact or damage of drought on the ecosystem is not mitigated by hydraulic redistribution.

We developed a trunk water pool model and incorporated it into CLM4.0 in Chapter 3. Trunk water dynamics and its contribution to daily transpiration are simulated at a flux tower site in Central Amazonia, BR-Sa3, which is covered mainly by evergreen broadleaf forest. The site experiences a dry season of three months from August to October with mean daily precipitation lower than 2 mm. The dry-season underestimation bias discussed in Chapter 2 is also fixed by the inclusion of trunk water pool. The ability of the new model to capture the lack of water stress in the dry season is facilitated by the more ready accessibility of trunk water pool than of the soil water pool and also the storage of water inside the trunk itself. On the seasonal time scale, trunk water amount follows that of precipitation, i.e. it is higher in the wet season than in the dry season. As the dry season starts, the trunk water decreases to support transpiration. It contributes more to the daily transpiration in the dry season than in the wet season. The diurnal cycle of trunk water amount has three distinct periods, namely the decrease from morning to the afternoon, followed by two periods of increase from afternoon to the next morning, produced by competing recharging and discharging processes. The discharge magnitude, defined as the difference between daily maximum and minimum trunk water content, which corresponds to the diurnal water storage in other studies (e.g. Goldstein et al., 1998), is higher in the dry season (90-110 kg/day) than in the wet season (20-80 kg/day).

By comparing cloudy and sunny days, we also show that the two competing processes of recharge and discharge are dynamic in nature.

The influences of El Niño on vegetation growth over Amazon forests are analyzed in Chapter 4 using satellite observations of vegetation greenness (EVI and NDVI) and photosynthetic proxy (FPAR) as well as observed and reanalysis precipitation and solar radiation data. A hotspot region was identified in eastern Amazonia where monthly precipitation has the most pronounced influence by ENSO as revealed by a correlation between monthly time series of precipitation and ENSO indices. We focused our analysis on this hotspot region not only because this is the region that El Niño leads to a substantial reduction in precipitation, but also due to the high agreement between satellite observations of vegetation growth. Wet-season precipitation reduction shows a north/south pattern with the northern part associated with slight increase and its southern counterpart a more pronounced reduction. Dry-season precipitation is reduced in El Niño years across the whole hotspot region. Anomalies in vegetation growth in wet-season are of opposite sign to those of precipitation anomalies, suggesting that other factors that link radiation may be controlling plant growth in the wet season. Surface radiation data shows a similar patterns as vegetation growth in this season, further confirming our assumption. However, it is suspected that cloud effects could contaminate satellite observation in vegetation growth and our findings based on those data could be misleading. Future work is needed to address this issue. In the dry season, vegetation growth positively responds to precipitation reduction, i.e., we see declines in vegetation growth with precipitation reduction in the El Niño years, which could be explained by stronger limitations by water in the dry season.

5.2. FUTURE WORK

The current modeling scheme for soil-to-leaf water transfer is quite simplified, leaving many important aspects out of consideration. For example, the xylem that functions to store and transport water within plant bodies can influence water-transporting efficiency by changing resistance with water abundance inside the tube. In our current parameterization scheme, only the water-storing function of xylems is taken into account. A constant hydrologic resistance is applied, which is mainly based on the geometric characteristics of the xylem tube. Therefore, further improvement of the basic parameterization scheme toward a more sophisticated and more realistic version is one of the future directions.

The models were run at site levels for both Chapters 2 and 3. Extending to a larger spatial scale is one of the future plans. One difficulty for extending the trunk pool model to the whole basin scale is the collection of ecological and physiological parameters (e.g. tree density, xylem density, trunk radius, and diameters of roots) over large spatial scales. These parameters vary with Plant Functional Types (PFT). They also vary spatially even within a certain PFT. Possible solutions include employment of some empirical relationships, like the one between trunk radius and trunk height with the latter gained from some remote sensing techniques. The problem can also be solved by a large number of simulations using parameters from a reasonable domain. Knowledge can be gained from a statistical analysis of the simulated results.

There are many land surface models and many different versions even of the same model. For example, the CLM model we used to demonstrate the performance of the drought-coping mechanisms now has been updated to the 4.5 version and the 5.0 version

is planned to be released in early 2017. Applying these modeling schemes in other land surface models is also a future plan.

In the study of El Niño impact on vegetation growth, more data can be added to future analyses. For example, a new version of the BRDF-corrected EVI product, referred to as MAIAC EVI, is now under production to correct some known errors in the old MAIAC data. Also the GIMMS group is now working to extend the NDVI3g product to present. They can be added to our analysis in the future, when available. In addition, with more data extending to present, the newly developed very strong 2015/2016 El Niño event can be included in our study. Some ground measurements collected from observational groups and from the literature can also be a data source, with which the conclusions from large-scale analysis can be further validated at the site level.

References

Adis, J. and M. Latif (1996), Amazonian arthropods respond to El Niño, Biotropica, 28(3), 403-407.

Adler, R. F., G. J. Huffman, A. Chang, R. Ferraro, P.-P. Xie, J. Janowiak, B. Rudolf, U. Schneider, S. Curtis, and D. Bolvin (2003), The version-2 global precipitation climatology project (GPCP) monthly precipitation analysis (1979-present), Journal of hydrometeorology, 4(6), 1147-1167.

Akkermans, T., D. Lauwaet, M. Demuzere, G. Vogel, Y. Nouvellon, J. Ardö, B. Caquet, A. De Grandcourt, L. Merbold, and W. Kutsch (2012), Validation and comparison of two soil-vegetation-atmosphere transfer models for tropical Africa, Journal of Geophysical Research: Biogeosciences, 117(G2).

Alencar, A., D. Nepstad, and M. C. V. Diaz (2006), Forest understory fire in the Brazilian Amazon in ENSO and non-ENSO years: area burned and committed carbon emissions, Earth Interactions, 10(6), 1-17.

Allen, C. D., A. K. Macalady, H. Chenchouni, D. Bachelet, N. McDowell, M. Vennetier, T. Kitzberger, A. Rigling, D. D. Breshears, and E. T. Hogg (2010), A global overview of drought and heat-induced tree mortality reveals emerging climate change risks for forests, Forest ecology and management, 259(4), 660-684.

Aragao, L. E. O., Y. Malhi, N. Barbier, A. Lima, Y. Shimabukuro, L. Anderson, and S. Saatchi (2008), Interactions between rainfall, deforestation and fires during recent years in the Brazilian Amazonia, Philosophical Transactions of the Royal Society of London B: Biological Sciences, 363(1498), 1779-1785.

Asner, G. P., and A. Alencar (2010), Drought impacts on the Amazon forest: the remote sensing perspective, New Phytologist, 187(3), 569-578.

Avissar, R., P. S. Dias, M. S. Dias, and C. Nobre (2002), The Large-Scale Biosphere-Atmosphere Experiment in Amazonia (LBA): Insights and future research needs (DOI 10.1029/2002JD002704), Journal of Geophysical Research: Atmospheres, 107 (D20).

Babiker, I. S., M. A. A. Mohamed, T. Hiyama, K. Ikeda, and N. Kobayashi (2015), Investigating Response of Global Vegetation to ENSO Events Between 1987 and 1997 Using NDVI Data, International journal of environmental monitoring and protection, 2(5), 76-83.

Baker, I., L. Prihodko, A. Denning, M. Goulden, S. Miller, and H. Da Rocha (2008), Seasonal drought stress in the Amazon: Reconciling models and observations, Journal of Geophysical Research: Biogeosciences, 113(G1).

Baker, T. R., O. L. Phillips, Y. Malhi, S. Almeida, L. Arroyo, A. Di Fiore, T. Erwin, T. J. Killeen, S. G. Laurance, and W. F. Laurance (2004), Variation in wood density

determines spatial patterns in Amazonian forest biomass, Global Change Biology, 10(5), 545-562.

Bastos, A., S. W. Running, C. Gouveia, and R. M. Trigo (2013), The global NPP dependence on ENSO: La Niña and the extraordinary year of 2011, Journal of Geophysical Research: Biogeosciences, 118(3), 1247-1255.

Borchert, R. (1994), Soil and stem water storage determine phenology and distribution of tropical dry forest trees, Ecology, 75(5), 1437-1449.

Brando, P. M., D. C. Nepstad, E. A. Davidson, S. E. Trumbore, D. Ray, and P. Camargo (2008), Drought effects on litterfall, wood production and belowground carbon cycling in an Amazon forest: results of a throughfall reduction experiment, Philosophical Transactions of the Royal Society of London B: Biological Sciences, 363(1498), 1839-1848.

Brooks, J. R., F. C. Meinzer, R. Coulombe, and J. Gregg (2002), Hydraulic redistribution of soil water during summer drought in two contrasting Pacific Northwest coniferous forests, Tree Physiology, 22(15-16), 1107-1117.

Caldwell, M. M., and J. H. Richards (1989), Hydraulic lift: water efflux from upper roots improves effectiveness of water uptake by deep roots, Oecologia, 79(1), 1-5.

Canadell, J., R. Jackson, J. Ehleringer, H. Mooney, O. Sala, and E.-D. Schulze (1996), Maximum rooting depth of vegetation types at the global scale, Oecologia, 108(4), 583-595.

Channan, S., K. Collins, and W. Emanuel (2014), Global mosaics of the standard MODIS land cover type data, University of Maryland and the Pacific Northwest National Laboratory, College Park, Maryland, USA, 30.

Chiodi, A. M., and D. E. Harrison (2014), Comment on Qian et al. 2008: La Niña and El Niño composites of atmospheric CO 2 change, Tellus B, 66.

Costa, M. H., and J. A. Foley (1999), Trends in the hydrologic cycle of the Amazon basin, Journal of Geophysical Research: Atmospheres, 104(D12), 14189-14198.

Cox, P. M., R. A. Betts, C. D. Jones, S. A. Spall, and I. J. Totterdell (2000), Acceleration of global warming due to carbon-cycle feedbacks in a coupled climate model, Nature, 408(6809), 184-187.

Cox, P., R. Betts, M. Collins, P. Harris, C.Huntingford, and C. Jones (2004), Amazon dieback under climate-carbon cycle projections for the 21st century, Theoretical and Applied Climatology, 78, 137-156.

Cox, P. M., P. P. Harris, C. Huntingford, R. A. Betts, M. Collins, C. D. Jones, T. E. Jupp, J. A. Marengo, and C. A. Nobre (2008), Increasing risk of Amazonian drought due to decreasing aerosol pollution, Nature, 453(7192), 212-215.

Cramer, W., A. Bondeau, S. Schaphoff, W. Lucht, B. Smith, and S. Sitch (2004), Tropical forests and the global carbon cycle: impacts of atmospheric carbon dioxide, climate change and rate of deforestation, Philosophical Transactions of the Royal Society of London B: Biological Sciences, 359(1443), 331-343.

Cramer, W., A. Bondeau, F. I. Woodward, I. C. Prentice, R. A. Betts, V. Brovkin, P. M. Cox, V. Fisher, J. A. Foley, and A. D. Friend (2001), Global response of terrestrial ecosystem structure and function to CO2 and climate change: results from six dynamic global vegetation models, Global change biology, 7(4), 357-373.

da Costa, A. C. L., D. Galbraith, S. Almeida, B. T. T. Portela, M. da Costa, J. de Athaydes Silva Junior, A. P. Braga, P. H. de Gonçalves, A. A. de Oliveira, and R. Fisher (2010), Effect of 7 yr of experimental drought on vegetation dynamics and biomass storage of an eastern Amazonian rainforest, New Phytologist, 187(3), 579-591.

Da Rocha, H. R., M. L. Goulden, S. D. Miller, M. C. Menton, L. D. Pinto, and H. C. de Freitas (2004), Seasonality of water and heat fluxes over a tropical forest in eastern Amazonia, Ecological applications, 14(sp4), 22-32.

Da Rocha, H. R., A. O. Manzi, O. M. Cabral, S. D. Miller, M. L. Goulden, S. R. Saleska, N. R. Coupe, S. C. Wofsy, L. S. Borma, and P. Artaxo (2009), Patterns of water and heat flux across a biome gradient from tropical forest to savanna in Brazil, Journal of Geophysical Research: Biogeosciences, 114(G1).

Dai, A., I. Y. Fung, and A. D. Del Genio (1997), Surface observed global land precipitation variations during 1900-88, Journal of climate, 10(11), 2943-2962.

Dai, A., K. E. Trenberth, and T. R. Karl (1998), Global variations in droughts and wet spells: 1900-1995, Geophysical Research Letters, 25(17), 3367-3370.

Davidson, E. A., A. C. de Araújo, P. Artaxo, J. K. Balch, I. F. Brown, M. M. Bustamante, M. T. Coe, R. S. DeFries, M. Keller, and M. Longo (2012), The Amazon basin in transition, Nature, 481(7381), 321-328.

Dawson, T. E. (1993), Hydraulic lift and water use by plants: implications for water balance, performance and plant-plant interactions, Oecologia, 95(4), 565-574.

Duffy, P. B., P. Brando, G. P. Asner, and C. B. Field (2015), Projections of future meteorological drought and wet periods in the Amazon, Proceedings of the National Academy of Sciences, 112(43), 13172-13177.

Eckert, S. (2012), Improved forest biomass and carbon estimations using texture measures from WorldView-2 satellite data, Remote sensing, 4(4), 810-829.

Engelbrecht, B. M., and T. A. Kursar (2003), Comparative drought-resistance of seedlings of 28 species of co-occurring tropical woody plants, Oecologia, 136(3), 383-393.

Engelbrecht, B. M., L. S. Comita, R. Condit, T. A. Kursar, M. T. Tyree, B. L. Turner, and S. P. Hubbell (2007), Drought sensitivity shapes species distribution patterns in tropical forests, Nature, 447(7140), 80-82.

Erasmi, S., A. Schucknecht, M. P. Barbosa, and J. Matschullat (2014), Vegetation greenness in northeastern brazil and its relation to ENSO warm events, Remote Sensing, 6(4), 3041-3058.

Fensholt, R., and S. R. Proud (2012), Evaluation of earth observation based global long term vegetation trends—Comparing GIMMS and MODIS global NDVI time series, Remote sensing of Environment, 119, 131-147.

Figueira, A., S. Miller, C. de Sousa, M. Menton, A. Maia, H. da Rocha, and M. Goulden (2011), LBA-ECO CD-04 dendrometry, km 83 tower site, tapajos national forest, brazil. data set, edited.

Friedl, M. A., D. Sulla-Menashe, B. Tan, A. Schneider, N. Ramankutty, A. Sibley, and X. Huang (2010), MODIS Collection 5 global land cover: Algorithm refinements and characterization of new datasets, Remote Sensing of Environment, 114(1), 168-182.

Fu, R., L. Yin, W. Li, P. A. Arias, R. E. Dickinson, L. Huang, S. Chakraborty, K. Fernandes, B. Liebmann, and R. Fisher (2013), Increased dry-season length over southern Amazonia in recent decades and its implication for future climate projection, Proceedings of the National Academy of Sciences, 110(45), 18110-18115.

Gardner, W. (1965), Dynamic aspects of soil-water availability to plants, Annual review of plant physiology, 16(1), 323-342.

Gibert, D., J.-L. Le Mouël, L. Lambs, F. Nicollin, and F. Perrier (2006), Sap flow and daily electric potential variations in a tree trunk, Plant Science, 171(5), 572-584.

Gochis, D. J., E. R. Vivoni, and C. J. Watts (2010), The impact of soil depth on land surface energy and water fluxes in the North American Monsoon region, Journal of Arid Environments, 74(5), 564-571.

Goldstein, G., J. Andrade, F. Meinzer, N. Holbrook, J. Cavelier, P. Jackson, and A. Celis (1998), Stem water storage and diurnal patterns of water use in tropical forest canopy trees, Plant, Cell & Environment, 21(4), 397-406.

Goulden, M., S. Miller, and H. da Rocha (2010), LBA-ECO CD-04 Soil Moisture Data, km 83 Tower Site, Tapajos National Forest, Brazil, Oak Ridge National Laboratory Distributed Active Archive Center.

Grace, J., Y. Mahli, N. Higuchi, and P. Meir (2001), Productivity and carbon fluxes of tropical rain forest, in Global Terrestrial Productivity: Past, Present and Future, edited by H. Mooney and B. Saugier, pp. 401–426, Academic Press, San Diego.

Green, S., and B. Clothier (1995), Root water uptake by kiwifruit vines following partial wetting of the root zone, Plant and soil, 173(2), 317-328.

Green, S., B. Clothier, and D. McLeod (1997), The response of sap flow in apple roots to localised irrigation, Agricultural Water Management, 33(1), 63-78.

Groombridge, B., and M. Jenkins (2002), World atlas of biodiversity: earth's living resources in the 21st century, University of California Press.

Gu, G., and R. F. Adler (2011), Precipitation and temperature variations on the interannual time scale: Assessing the impact of ENSO and volcanic eruptions, Journal of Climate, 24(9), 2258-2270.

Guan, K., M. Pan, H. Li, A. Wolf, J. Wu, D. Medvigy, K. K. Caylor, J. Sheffield, E. F. Wood, and Y. Malhi (2015), Photosynthetic seasonality of global tropical forests constrained by hydroclimate, Nature Geoscience, 8(4), 284-289.

Hanley, D. E., M. A. Bourassa, J. J. O'Brien, S. R. Smith, and E. R. Spade (2003), A quantitative evaluation of ENSO indices, Journal of Climate, 16(8), 1249-1258.

Harper, A. B., A. S. Denning, I. T. Baker, M. D. Branson, L. Prihodko, and D. A. Randall (2010), Role of deep soil moisture in modulating climate in the Amazon rainforest, Geophysical Research Letters, 37(5).

Harris, I., P. Jones, T. Osborn, and D. Lister (2014), Updated high-resolution grids of monthly climatic observations–the CRU TS3. 10 Dataset, International Journal of Climatology, 34(3), 623-642.

Hatzis, J. J. (2010), The development of a dynamic root distribution for the Community Land Model with carbon-nitrogen interactions, M.S. thesis, Northern Illinois University, Di Kalb, 184 pp.

Haylock, M. R., T. Peterson, L. Alves, T. Ambrizzi, Y. Anunciação, J. Baez, V. Barros, M. Berlato, M. Bidegain, and G. Coronel (2006), Trends in total and extreme South American rainfall in 1960-2000 and links with sea surface temperature, Journal of climate, 19(8), 1490-1512.

Hilker, T., A. I. Lyapustin, C. J. Tucker, F. G. Hall, R. B. Myneni, Y. Wang, J. Bi, Y. M. de Moura, and P. J. Sellers (2014), Vegetation dynamics and rainfall sensitivity of the Amazon, Proceedings of the National Academy of Sciences, 111(45), 16041-16046.

Huang, B., R. Duncan, and R. Carrow (1997), Drought-resistance mechanisms of seven warm-season turfgrasses under surface soil drying: II. Root aspects, Crop Science, 37(6), 1863-1869.

Huete, A., K. Didan, T. Miura, E. P. Rodriguez, X. Gao, and L. G. Ferreira (2002), Overview of the radiometric and biophysical performance of the MODIS vegetation indices, Remote sensing of environment, 83(1), 195-213.

Huete, A. R., K. Didan, Y. E. Shimabukuro, P. Ratana, S. R. Saleska, L. R. Hutyra, W. Yang, R. R. Nemani, and R. Myneni (2006), Amazon rainforests green□up with sunlight in dry season, Geophysical research letters, 33(6).

Huffman, G. J., D. T. Bolvin, E. J. Nelkin, D. B. Wolff, R. F. Adler, G. Gu, Y. Hong, K. P. Bowman, and E. F. Stocker (2007), The TRMM multi-satellite precipitation analysis (TMPA): Quasi-global, multiyear, combined-sensor precipitation estimates at fine scales, Journal of Hydrometeorology, 8(1), 38-55.

Hultine, K. R., R. Scott, W. Cable, D. Goodrich, and D. Williams (2004), Hydraulic redistribution by a dominant, warm-desert phreatophyte: Seasonal patterns and response to precipitation pulses, Functional Ecology, 18(4), 530-538.

Huntingford, C., R. A. Fisher, L. Mercado, B. B. Booth, S. Sitch, P. P. Harris, P. M. Cox, C. D. Jones, R. A. Betts, and Y. Malhi (2008), Towards quantifying uncertainty in predictions of Amazon 'dieback', Philosophical Transactions of the Royal Society of London B: Biological Sciences, 363(1498), 1857-1864.

Jackson, R. B., H. Mooney, and E.-D. Schulze (1997), A global budget for fine root biomass, surface area, and nutrient contents, Proceedings of the National Academy of Sciences, 94(14), 7362-7366.

Jackson, R. B., J. S. Sperry, and T. E. Dawson (2000), Root water uptake and transport: using physiological processes in global predictions, Trends in plant science, 5(11), 482-488.

Jackson, R., J. Canadell, J. R. Ehleringer, H. Mooney, O. Sala, and E. Schulze (1996), A global analysis of root distributions for terrestrial biomes, Oecologia, 108(3), 389-411.

Jiang, Z., A. R. Huete, K. Didan, and T. Miura (2008), Development of a two-band enhanced vegetation index without a blue band, Remote Sensing of Environment, 112(10), 3833-3845.

Jones, C. D., P. M. Cox, R. L. Essery, D. L. Roberts, and M. J. Woodage (2003), Strong carbon cycle feedbacks in a climate model with interactive CO2 and sulphate aerosols, Geophysical Research Letters, 30(9).

Jupp, T. E., P. M. Cox, A. Rammig, K. Thonicke, W. Lucht, and W. Cramer (2010), Development of probability density functions for future South American rainfall, New Phytologist, 187(3), 682-693.

Katul, G., R. Leuning, and R. Oren (2003), Relationship between plant hydraulic and biochemical properties derived from a steady-state coupled water and carbon transport model, Plant, Cell & Environment, 26(3), 339-350.

Kim, Y., A. R. Huete, Z. Jiang, and T. Miura (2007), Multi-sensor reflectance and vegetation index comparisons of Amazon tropical forest phenology with hyperspectral Hyperion data, paper presented at Optical Engineering+ Applications, International Society for Optics and Photonics.

Kleidon, A. (2004), Global datasets of rooting zone depth inferred from inverse methods, Journal of Climate, 17(13), 2714-2722.

Kleidon, A., and M. Heimann (1998), Optimised rooting depth and its impacts on the simulated climate of an atmospheric general circulation model, Geophysical research letters, 25(3), 345-348.

Köcher, P., V. Horna, and C. Leuschner (2013), Stem water storage in five coexisting temperate broad-leaved tree species: significance, temporal dynamics and dependence on tree functional traits, Tree physiology, 33(8), 817-832.

Laio, F., P. D'Odorico, and L. Ridolfi (2006), An analytical model to relate the vertical root distribution to climate and soil properties, Geophysical Research Letters, 33(18).

Lee, J.-E., R. S. Oliveira, T. E. Dawson, and I. Fung (2005), Root functioning modifies seasonal climate, Proceedings of the National Academy of Sciences of the United States of America, 102(49), 17576-17581.

Lewis, S. L., P. M. Brando, O. L. Phillips, G. M. van der Heijden, and D. Nepstad (2011), The 2010 Amazon drought, Science, 331(6017), 554-554.

Li, W., R. Fu, R. I. N. Juarez, and K. Fernandes (2008), Observed change of the standardized precipitation index, its potential cause and implications to future climate change in the Amazon region, Philosophical Transactions of the Royal Society of London B: Biological Sciences, 363(1498), 1767-1772.

Li, W., P. Zhang, J. Ye, L. Li, and P. A. Baker (2011), Impact of two different types of El Niño events on the Amazon climate and ecosystem productivity, Journal of Plant Ecology, 4(1-2), 91-99.

Liebmann, B., and J. Marengo (2001), Interannual variability of the rainy season and rainfall in the Brazilian Amazon Basin, Journal of Climate, 14(22), 4308-4318.

Lutz, H. J., J. B. Ely, and S. Little (1937), The influence of soil profile horizons on root distribution of white pine (Pinusstrobus L.), Yale University.

Lyon, B. (2004), The strength of El Niño and the spatial extent of tropical drought, Geophysical Research Letters, 31(21).

Lyon, B., and A. G. Barnston (2005), ENSO and the spatial extent of interannual precipitation extremes in tropical land areas, Journal of Climate, 18(23), 5095-5109.

Maeght, J.-L., S. Gonkhamdee, C. Clément, S. I. N. Ayutthaya, A. Stokes, and A. Pierret (2015), Seasonal Patterns of Fine Root Production and Turnover in a Mature Rubber Tree (Hevea brasiliensis Müll. Arg.) Stand-Differentiation with Soil Depth and Implications for Soil Carbon Stocks, Frontiers in plant science, 6.

Manzoni, S., G. Vico, A. Porporato, and G. Katul (2013), Biological constraints on water transport in the soil–plant–atmosphere system, Advances in Water Resources, 51, 292-304.

Marengo, J. (2004), Inter-decadal variability and trends of rainfall across the Amazon basin, Theoretical and applied climatology, 78(1-3), 79-96.

MARengo, J. A. (2006), On the hydrological cycle of the Amazon Basin: A historical review and current state-of-the-art, Revista Brasileira de Meteorologia, 21(3), 1-19.

Marengo, J. A., and C. A. Nobre (2001), General characteristics and variability of climate in the Amazon Basin and its links to the global climate system, in The Biogeochemistry of the Amazon Basin, edited by M. E. McClain, R. L. Victoria and J. E. Richey, pp. 17-41, Oxford University Press, Oxford.

Marshall, M., E. Okuto, Y. Kang, E. Opiyo, and M. Ahmed (2016), Global assessment of Vegetation Index and Phenology Lab (VIP) and Global Inventory Modeling and Mapping Studies (GIMMS) version 3 products, Biogeosciences, 13(3), 625-639.

Mason, S. J., and L. Goddard (2001), Probabilistic precipitation anomalies associated with ENSO, Bulletin of the American Meteorological Society, 82(4), 619-638.

McDowell, N. G., R. A. Fisher, C. Xu, J. Domec, T. Hölttä, D. S. Mackay, J. S. Sperry, A. Boutz, L. Dickman, and N. Gehres (2013), Evaluating theories of drought-induced vegetation mortality using a multimodel–experiment framework, New Phytologist, 200(2), 304-321.

McElrone, A. J., W. T. Pockman, J. Martínez-Vilalta, and R. B. Jackson (2004), Variation in xylem structure and function in stems and roots of trees to 20 m depth, New Phytologist, 163(3), 507-517.

Meinzer, F., G. Goldstein, and J. Andrade (2001), Regulation of water flux through tropical forest canopy trees: do universal rules apply?, Tree Physiology, 21(1), 19-26.

Miller, S. D., M. L. Goulden, L. R. Hutyra, M. Keller, S. R. Saleska, S. C. Wofsy, A. M. S. Figueira, H. R. Da Rocha, and P. B. De Camargo (2011), Reduced impact

logging minimally alters tropical rainforest carbon and energy exchange, Proceedings of the National Academy of Sciences, 108(48), 19431-19435.

Mitchard, E. T., S. S. Saatchi, A. Baccini, G. P. Asner, S. J. Goetz, N. L. Harris, and S. Brown (2013), Uncertainty in the spatial distribution of tropical forest biomass: a comparison of pan-tropical maps, Carbon balance and management, 8(1), 1.

Mitchell, J., R. Davis, W. a. Ingram, and C. Senior (1995), On surface temperature, greenhouse gases, and aerosols: Models and observations, Journal of Climate, 8(10), 2364-2386.

Motohka, T., K. N. Nasahara, K. Murakami, and S. Nagai (2011), Evaluation of sub-pixel cloud noises on MODIS daily spectral indices based on in situ measurements, Remote Sensing, 3(8), 1644-1662.

Nepstad, D., and P. Moutinho (2008), LBA-ECO LC-14 Rainfall Exclusion Experiment, LAI, Gap Fraction, TNF, Brazil: 2000-05, Data set. [WWW document] URL http://lba. cptec. inpe. br/from LBA Data and Information System, National Institute for Space Research (INPE/CPTEC), Cachoeira Paulista, Sao Paulo, Brazil [accessed on 17 November 2012].

Nepstad, D. C., C. R. de Carvalho, E. A. Davidson, P. H. Jipp, P. A. Lefebvre, G. H. Negreiros, E. D. da Silva, T. A. Stone, S. E. Trumbore, and S. Vieira (1994), The role of deep roots in the hydrological and carbon cycles of Amazonian forests and pastures.

Nepstad, D. C., A. Verssimo, A. Alencar, C. Nobre, E. Lima, P. Lefebvre, P. Schlesinger, C. Potter, P. Moutinho, and E. Mendoza (1999), Large-scale impoverishment of Amazonian forests by logging and fire, Nature, 398(6727), 505-508.

Nepstad, D., P. Moutinho, M. Dias-Filho, E. Davidson, G. Cardinot, D. Markewitz, R. Figueiredo, N. Vianna, J. Chambers, and D. Ray (2002), The effects of partial throughfall exclusion on canopy processes, aboveground production, and biogeochemistry of an Amazon forest, Journal of Geophysical Research: Atmospheres, 107(D20).

Neumann, R. B., and Z. G. Cardon (2012), The magnitude of hydraulic redistribution by plant roots: a review and synthesis of empirical and modeling studies, New Phytologist, 194(2), 337-352.

Newman, E. (1969), Resistance to water flow in soil and plant. I. Soil resistance in relation to amounts of root: theoretical estimates, Journal of Applied Ecology, 1-12.

Oleson, K. W., D. M. Lawrence, B. Gordon, M. G. Flanner, E. Kluzek, J. Peter, S. Levis, S. C. Swenson, E. Thornton, and J. Feddema (2010), Technical description of version 4.0 of the Community Land Model (CLM).

Oliveira, R. S., T. E. Dawson, S. S. Burgess, and D. C. Nepstad (2005), Hydraulic redistribution in three Amazonian trees, Oecologia, 145(3), 354-363.

Pachauri, R. K., and A. Reisinger (2007), Climate change 2007 synthesis report: Summary for policymakers, IPCC Secretariat.

Page, Y. L., J. Pereira, R. Trigo, C. d. Camara, D. Oom, and B. Mota (2008), Global fire activity patterns (1996–2006) and climatic influence: an analysis using the World Fire Atlas, Atmospheric Chemistry and Physics, 8(7), 1911-1924.

Pan, Y., R. A. Birdsey, J. Fang, R. Houghton, P. E. Kauppi, W. A. Kurz, O. L. Phillips, A. Shvidenko, S. L. Lewis, and J. G. Canadell (2011), A large and persistent carbon sink in the world's forests, Science, 333(6045), 988-993.

Pelletier, J. D., and C. Rasmussen (2009), Geomorphically based predictive mapping of soil thickness in upland watersheds, Water Resources Research, 45(9).

Phillips, O. L., L. E. Aragão, S. L. Lewis, J. B. Fisher, J. Lloyd, G. López-González, Y. Malhi, A. Monteagudo, J. Peacock, and C. A. Quesada (2009), Drought sensitivity of the Amazon rainforest, Science, 323(5919), 1344-1347.

Pinzon, J. E., and C. J. Tucker (2014), A non-stationary 1981–2012 AVHRR NDVI3g time series, Remote Sensing, 6(8), 6929-6960.

Poveda, G., A. Jaramillo, M. M. Gil, N. Quiceno, and R. I. Mantilla (2001), Seasonally in ENSO□related precipitation, river discharges, soil moisture, and vegetation index in Colombia, Water resources research, 37(8), 2169-2178.

Powell, T. L., D. R. Galbraith, B. O. Christoffersen, A. Harper, H. Imbuzeiro, L. Rowland, S. Almeida, P. M. Brando, A. C. L. Costa, and M. H. Costa (2013), Confronting model predictions of carbon fluxes with measurements of Amazon forests subjected to experimental drought, New Phytologist, 200(2), 350-365.

Prentice, I. C., and J. Lloyd (1998), C-quest in the Amazon Basin, Nature, 396(6712), 619-620.

Prieto, I., Z. Kikvidze, and F. I. Pugnaire (2010), Hydraulic lift: soil processes and transpiration in the Mediterranean leguminous shrub Retamasphaerocarpa (L.) Boiss, Plant and Soil, 329(1-2), 447-456.

Pyke, C. R., R. Condit, S. Aguilar, and S. Lao (2001), Floristic composition across a climatic gradient in a neotropical lowland forest, Journal of vegetation science, 12(4), 553-566.

Qian, T., A. Dai, K. E. Trenberth, and K. W. Oleson (2006), Simulation of global land surface conditions from 1948 to 2004. Part I: Forcing data and evaluations, Journal of Hydrometeorology, 7(5), 953-975.

Rammig, A., T. Jupp, K. Thonicke, B. Tietjen, J. Heinke, S. Ostberg, W. Lucht, W. Cramer, and P. Cox (2010), Estimating the risk of Amazonian forest dieback, New Phytologist, 187(3), 694-706.

Richards, J. H., and M. M. Caldwell (1987), Hydraulic lift: substantial nocturnal water transport between soil layers by Artemisia tridentata roots, Oecologia, 73(4), 486-489.

Romero-Saltos, H., L. da SL Sternberg, M. Z. Moreira, and D. C. Nepstad (2005), Rainfall exclusion in an eastern Amazonian forest alters soil water movement and depth of water uptake, American Journal of Botany, 92(3), 443-455.

Ropelewski, C., and M. Halpert (1989), Precipitation patterns associated with the high index phase of the Southern Oscillation, Journal of climate, 2(3), 268-284.

Roy, J., H. A. Mooney, and B. Saugier (2001), Terrestrial global productivity, Academic Press.

Ryel, R., M. Caldwell, C. Yoder, D. Or, and A. Leffler (2002), Hydraulic redistribution in a stand of Artemisia tridentata: evaluation of benefits to transpiration assessed with a simulation model, Oecologia, 130(2), 173-184.

Saatchi, S. S., R. Houghton, R. Dos Santos Alvala, J. Soares, and Y. Yu (2007), Distribution of aboveground live biomass in the Amazon basin, Global Change Biology, 13(4), 816-837.

Saatchi, S., S. Asefi-Najafabady, Y. Malhi, L. E. Aragão, L. O. Anderson, R. B. Myneni, and R. Nemani (2013), Persistent effects of a severe drought on Amazonian forest canopy, Proceedings of the National Academy of Sciences, 110(2), 565-570.

Saatchi, S., Y. Malhi, B. Zutta, W. Buermann, L. Anderson, A. Araujo, O. Phillips, J. Peacock, H. t. Steege, and G. L. Gonzalez (2009), Mapping landscape scale variations of forest structure, biomass, and productivity in Amazonia, Biogeosciences Discussions, 6(3), 5461.

Salati, E., Dall'Olio, A., Matsui, E. and Gat, J.R., 1979. Recycling of water in the Amazon basin: an isotopic study. Water Resources Research, 15(5), pp.1250-1258.

Saleska, S. R., K. Didan, A. R. Huete, and H. R. Da Rocha (2007), Amazon forests green-up during 2005 drought, Science, 318(5850), 612-612.

Saleska, S., H. da Rocha, A. Huete, A. Nobre, P. Artaxo, and Y. Shimabukuro (2009), LBA-ECO CD-32 Brazil Flux Network Integrated Data: 1999–2006, Sao Paulo, Brazil: National Institute for Space Research (INPE/CPTEC), Cachoeira Paulista. See (http://www. daac. ornl. gov) from Oak Ridge National Laboratory Distributed Active Archive Center, Oak Ridge, Tennessee, USA and (http://lba. cptec. inpe. br/) from LBA Data and Information System.

Samanta, A., S. Ganguly, E. Vermote, R. R. Nemani, and R. B. Myneni (2012), Why is remote sensing of amazon forest greenness so challenging?, Earth Interactions, 16(7), 1-14.

Schoengart, J., W. J. Junk, M. T. F. Piedade, J. M. Ayres, A. Hüttermann, and M. Worbes (2004), Teleconnection between tree growth in the Amazonian floodplains and the El Niño–Southern Oscillation effect, Global Change Biology, 10(5), 683-692.

Scholz, F. C., S. J. Bucci, G. Goldstein, F. C. Meinzer, A. C. Franco, and F. Miralles-Wilhelm (2008), Temporal dynamics of stem expansion and contraction in savanna trees: withdrawal and recharge of stored water, Tree Physiology, 28(3), 469-480.

Sena, J. A., L. A. B. De Deus, M. A. V. Freitas, and L. Costa (2012), Extreme events of droughts and floods in Amazonia: 2005 and 2009, Water resources management, 26(6), 1665-1676.

Sheffield, J., G. Goteti, and E. F. Wood (2006), Development of a 50-year high-resolution global dataset of meteorological forcings for land surface modeling, Journal of Climate, 19(13), 3088-3111.

Silva, F. B., Y. E. Shimabukuro, L. E. Aragao, L. O. Anderson, G. Pereira, F. Cardozo, and E. Arai (2013), Large-scale heterogeneity of Amazonian phenology revealed from 26-year long AVHRR/NDVI time-series, Environmental Research Letters, 8(2), 024011.

Sitch, S., C. Huntingford, N. Gedney, P. Levy, M. Lomas, S. Piao, R. Betts, P. Ciais, P. Cox, and P. Friedlingstein (2008), Evaluation of the terrestrial carbon cycle, future plant geography and climate□carbon cycle feedbacks using five Dynamic Global Vegetation Models (DGVMs), Global Change Biology, 14(9), 2015-2039.

Song, J. and J. Hatzis (2010), Modeling the vegetation root distribution for a changed precipitation. Abstract of 2010 Washington AAG.

ter Steege, H., N. C. Pitman, D. Sabatier, C. Baraloto, R. P. Salomão, J. E. Guevara, O. L. Phillips, C. V. Castilho, W. E. Magnusson, and J.-F. Molino (2013), Hyperdominance in the Amazonian tree flora, Science, 342(6156), 1243092.

Thornton, P. E., J. F. Lamarque, N. A. Rosenbloom, and N. M. Mahowald (2007), Influence of carbon-nitrogen cycle coupling on land model response to CO2 fertilization and climate variability, Global biogeochemical cycles, 21(4).

Tian, H., J. M. Melillo, D. W. Kicklighter, A. D. McGuire, J. V. Helfrich, B. Moore, and C. J. VoÈroÈsmarty (1998), Effect of interannual climate variability on carbon storage in Amazonian ecosystems, Nature, 396(6712), 664-667.

van Marle, M., G. van der Werf, R. de Jeu, and Y. Liu (2015), Annual South American forest loss estimates based on passive microwave remote sensing (1990–2010), Biogeosciences Discussions, 12, 11499-11535.

Van Nieuwstadt, M. G., and D. Sheil (2005), Drought, fire and tree survival in a Borneo rain forest, East Kalimantan, Indonesia, Journal of Ecology, 93(1), 191-201.

van Wijk, M. T. (2011), Understanding plant rooting patterns in semi-arid systems: an integrated model analysis of climate, soil type and plant biomass, Global Ecology and Biogeography, 20(2), 331-342.

Vicente-Serrano, S. M., C. Gouveia, J. J. Camarero, S. Beguería, R. Trigo, J. I. López-Moreno, C. Azorín-Molina, E. Pasho, J. Lorenzo-Lacruz, and J. Revuelto (2013), Response of vegetation to drought time-scales across global land biomes, Proceedings of the National Academy of Sciences, 110(1), 52-57.

Victoria, R., L. Martinelli, J. Moraes, M. Ballester, A. Krusche, G. Pellegrino, R. Almeida, and J. Richey (1998), Surface air temperature variations in the Amazon region and its borders during this century, Journal of Climate, 11(5), 1105-1110.

Wang, G., C. Alo, R. Mei, and S. Sun (2011), Droughts, hydraulic redistribution, and their impact on vegetation composition in the Amazon forest, Plant Ecology, 212(4), 663-673.

Wang, H., P. Zhao, D. Hölscher, Q. Wang, P. Lu, X. A. Cai, and X. P. Zeng (2012), Nighttime sap flow of Acacia mangium and its implications for nighttime transpiration and stem water storage, Journal of Plant Ecology, 5(3), 294-304.

Wang, H.J., R.H. Zhang, J. Cole, and F. Chavez (1999), El Niño and the related phenomenon Southern Oscillation (ENSO): the largest signal in interannual climate variation, Proceedings of the National Academy of Sciences, 96(20), 11071-11072.

Weedon, G. P., G. Balsamo, N. Bellouin, S. Gomes, M. J. Best, and P. Viterbo (2014), The WFDEI meteorological forcing data set: WATCH Forcing Data methodology applied to ERA-Interim reanalysis data, Water Resources Research, 50(9), 7505-7514.

Werth, D., and R. Avissar (2002), The local and global effects of Amazon deforestation, Journal of Geophysical Research: Atmospheres, 107(D20).

White, A., M. G. Cannell, and A. D. Friend (1999), Climate change impacts on ecosystems and the terrestrial carbon sink: a new assessment, Global environmental change, 9, S21-S30.

Williamson, G. B. (1984), Gradients in wood specific gravity of trees, Bulletin of the Torrey Botanical Club, 51-55.

Williamson, G. B., W. F. Laurance, A. A. Oliveira, P. Delamônica, C. Gascon, T. E. Lovejoy, and L. Pohl (2000), Amazonian tree mortality during the 1997 El Niño drought, Conservation Biology, 14(5), 1538-1542.

Wolter, K., and M. S. Timlin (1993), Monitoring ENSO in COADS with a seasonally adjusted principal component index, paper presented at Proc. of the 17th Climate Diagnostics Workshop.

Wright, S. J., and C. P. Van Schaik (1994), Light and the phenology of tropical trees, American Naturalist, 192-199.

WWF Places: Amazon, http://www.worldwildlife.org/places/amazon, accessed on Nov. 15, 2016.

Xu, C., N. G. McDowell, S. Sevanto, and R. A. Fisher (2013), Our limited ability to predict vegetation dynamics under water stress, New Phytologist, 200(2), 298-300.

Xu, L., A. Samanta, M. H. Costa, S. Ganguly, R. R. Nemani, and R. B. Myneni (2011), Widespread decline in greenness of Amazonian vegetation due to the 2010 drought, Geophysical Research Letters, 38(7).

Xu, L., R. Myneni, F. Chapin Iii, T. Callaghan, J. Pinzon, C. Tucker, Z. Zhu, J. Bi, P. Ciais, and H. Tømmervik (2013), Temperature and vegetation seasonality diminishment over northern lands, Nature Climate Change, 3(6), 581-586.

Yan, B. and Dickinson, R.E., 2014. Modeling hydraulic redistribution and ecosystem response to droughts over the Amazon basin using Community Land Model 4.0 (CLM4). Journal of Geophysical Research: Biogeosciences, 119(11), pp.2130-2143.

Yan, D., X. Zhang, Y. Yu, and W. Guo (2016), A Comparison of Tropical Rainforest Phenology Retrieved From Geostationary (SEVIRI) and Polar-Orbiting (MODIS) Sensors Across the Congo Basin, IEEE Transactions on Geoscience and Remote Sensing, 54(8), 4867-4881.

Yeh, S.-W., J.-S. Kug, B. Dewitte, M.-H. Kwon, B. P. Kirtman, and F.-F. Jin (2009), El Niño in a changing climate, Nature, 461(7263), 511-514.

Yuan, H., Y. Dai, Z. Xiao, D. Ji, and W. Shangguan (2011), Reprocessing the MODIS Leaf Area Index products for land surface and climate modelling, Remote Sensing of Environment, 115(5), 1171-1187.

Zach, A., B. Schuldt, S. Brix, V. Horna, H. Culmsee, and C. Leuschner (2010), Vessel diameter and xylem hydraulic conductivity increase with tree height in tropical rainforest trees in Sulawesi, Indonesia, Flora-Morphology, Distribution, Functional Ecology of Plants, 205(8), 506-512.

Zeng, X. (2001), Global vegetation root distribution for land modeling, Journal of Hydrometeorology, 2(5), 525-530.

Zhang, X. (2015), Reconstruction of a complete global time series of daily vegetation index trajectory from long-term AVHRR data, Remote Sensing of Environment, 156, 457-472.

Zhang, X., B. Tan, and Y. Yu (2014), Interannual variations and trends in global land surface phenology derived from enhanced vegetation index during 1982–2010, International journal of biometeorology, 58(4), 547-564.

Zheng, Z., and G. Wang (2007), Modeling the dynamic root water uptake and its hydrological impact at the Reserva Jaru site in Amazonia, Journal of Geophysical Research: Biogeosciences, 112(G4).

Zhu, Z., J. Bi, Y. Pan, S. Ganguly, A. Anav, L. Xu, A. Samanta, S. Piao, R. R. Nemani, and R. B. Myneni (2013), Global data sets of vegetation leaf area index (LAI) 3g and Fraction of Photosynthetically Active Radiation (FPAR) 3g derived from Global Inventory Modeling and Mapping Studies (GIMMS) Normalized Difference Vegetation Index (NDVI3g) for the period 1981 to 2011, Remote Sensing, 5(2), 927-948.

Zulkafli, Z., W. Buytaert, B. Manz, C. V. Rosas, P. Willems, W. Lavado-Casimiro, J.-L. Guyot, and W. Santini (2016), Projected increases in the annual flood pulse of the Western Amazon, Environmental Research Letters, 11(1), 014013.

Zweifel, R., and R. Häsler (2001), Link between diurnal stem radius changes and tree water relations, Tree Physiology, 21(12-13), 869-877.